Technische Universität Kaiserslautern
Fachbereich Physik

Diplomarbeit

Bulk-boundary correspondence in non-equilibrium dynamics of one-dimensional topological insulators

Philipp Jaeger

May 24, 2017

carried out at

University of Manitoba
Department of Physics and Astronomy

supervised by

Prof. Dr. Sebastian Eggert[ab]

Prof. Dr. Jesko Sirker[c]

[a]Technische Universität Kaiserslautern, Kaiserslautern, Germany
[b]Landesforschungszentrum OPTIMAS, Kaiserslautern, Germany
[c]University of Manitoba, Winnipeg, MB, Canada

in partial fulfillment of the requirements for the acquisition of the academic degree “Diplom-Physiker (Dipl. Phys.)”, which is equivalent to “Magister Scientiæ (M. Sc.)”, at University of Kaiserslautern.

Abstract

Dynamical phase transitions (DPT) are receiving a rising interest. They are known to behave analogously to equilibrium phase transitions (EPT) to a large extend. However, it is easy to see that DPT can occur in finite systems, while EPT are only possible in the thermodynamic limit. So far it is not clear how far the analogy of DPT and EPT goes. It was suggested, that there is a relation between topological phase transitions (TPT) and DPT, but many open questions remain.

Typically, to study DPT, the Loschmidt echo (LE) after a quench is investigated, where DPT are visible as singularities. For one-dimensional systems, each singularity is connected to a certain critical time scale, which is given by the dispersion in the chain.

In topological free-fermion models with winding numbers 0 or 1, only the LE in periodic boundary conditions (PBC) has been investigated. In open boundary conditions (OBC), these models are characterized by symmetry protected edge modes in the topologically non-trivial phase. It is completely unclear how these modes affect DPT. We investigate systems with PBC governed by multiple time scales with a $\mathbb{Z}$ topological invariant. In OBC, we provide numerical evidence for the presence of bulk-boundary correspondence in DPT in quenches across a TPT.

Zusammenfassung

Dynamische Phasenübergänge (DP) erfreuen sich eines wachsenden Interesses. Es ist bekannt, dass sie sich analog zu Gleichgewichtsphasenübergängen (GP) verhalten. Andererseits prüft man leicht nach, dass DP im Gegensatz zu EP auch in endlichen Systemen auftreten können, während Letztere nur im thermodynamischen Limes stattfinden. Bisher ist also unklar, wie weit die zuvor erwähnte Analogie zwischen DP und GP geht. Außerdem wurde ein Zusammenhang zwischen DP und topologischen Phasenübergängen (TP) aufgezeigt, aber es sind noch viele Fragen offen.

Üblicherweise werden DP untersucht, indem man das Loschmidtecho (LE) nach einem Quench betrachtet, in welchem DP als Singularitäten sichtbar werden. In eindimensinalen Systemen kann jeder Singularität eine bestimmte kritische Zeitskala zugeordnet werden, die durch die Dispersionsrelation des Systems gegeben ist.

In topologischen freien Fermionenmodellen (FFM) mit einer Invariante in $\mathbb{Z}_2$ wurde bisher nur das LE in periodischen Randbedingungen (PRB) erforscht. Diese topologisch nichttrivialen Modelle werden in offenen Randbedingungen (ORB) durch topologiegeschützte Randmoden charakterisiert. Der Einfluss dieser Randmoden auf DP und die Zeitentwichlung des LE ist noch vollkommen unerforscht. Wir untersuchen Systeme in PRB, die aufgrund der ganzzahligen topologischen Invariante durch mehrere kritische Zeitskalen bestimmt werden. Für Systeme mit ORB erbringen wir numerische Nachweise der Existanz eines Äquivalents der holographischen Volumenrandkorrenpondenz in DP nach einem Quench über einen TP.

Contents

APPENDIX

Chapter I

Introduction

Everybody knows how water evaporates. Looking more carefully, do we really know? The answer is we do not, but in fact this does not matter. Thermodynamics is about a macroscopic description of what happens, without knowing all microscopical parameters of the system. This is the keystone to a statistical interpretation of thermodynamics, which averages over the microscopic evolution of a system to obtain macroscopic results, which in many cases are identical to the description using state functions and classical thermodynamics.

As long as a system stays in the same phase, in our example the water stays liquid, these state functions are smooth functions of certain macroscopic parameters of the system, here pressure, volume and temperature. Note, that they are not functions of time! When the system undergoes an equilibrium phase transition (EPT), the water evaporates, and the state functions become non-analytical at the transition. This means, the function itself or one of its derivatives has a jump. Another important characteristic of PT is symmetry breaking. This can for example involve the breaking of a continuous translation symmetry into a discrete one in the case of a transition into a crystalline state. In the gas to liquid transition, it means confining a particle which is free to move in a gas to a liquid phase, as in the condensation of water.

It is also common knowledge that a pot of boiling water does not evaporate suddenly but over some time. This is because of the heat transport mechanisms in liquid water, which cause it not to heat up uniformly. Boiling starts when parts of the liquid phase reach the critical temperature and evaporate, forming a bubble at the bottom of the pod. At this point, it starts getting really complicated to capture what is going on over time, and therefore, it makes sense to idealize the process by taking away the time dependency.

This works well for a system that undergoes a transition form one equilibrium state to another equilibrium state. Although there are generalizations for non-equilibrium states which are in some sense close enough to equilibrium, the framework of classical thermodynamics, which is essentially differential geometry in a parameter space, fails in general to describe time dependent processes.

Interpreting thermodynamics statistically means in the easiest case, which is known as microcanonical ensemble (MCE), essentially counting all physically possible microstates, i.e. states which have the same energy and the same number of particles. This is called the partition function $\mathcal{Z}$, out of which the

aforementioned the macroscopic properties can be derived. Generalizing this notion to states which do not have a fixed energy or particle number, but rather conserved expectation values thereof, one additionally takes into account the different probabilities for different realizations of a state, and obtains the grand canonical partition function (GCPF).

For systems whose time evolution governed by a Hamiltonian operator $\mathbf{H}$, the GCPF is a function of temperature T and chemical potential μ,

$$\mathcal{Z}(T,\mu) = \mathrm{Tr}\left\{\exp\left(\frac{1}{k_\mathrm{B}T}(\mathbf{H}+\mu\mathbf{n})\right)\right\}. \tag{I.1}$$

Here, k_B is the Boltzmann constant at $\mathbf{n}$ is the particle number operator. Often, instead of the temperature, the inverse temperature $-\beta = \frac{1}{k_\mathrm{B}T}$ is used, such that eq. (I.1) reads

$$\mathcal{Z}(\beta,\mu) = \mathrm{Tr}\left\{\mathrm{e}^{-\beta(\mathbf{H}+\mu\mathbf{n})}\right\}. \tag{I.2}$$

Close to a EPT, the GCPF becomes small. Stepping back to the MCE for a second, this would mean that the system has only one possible microstate at the critical point. While the system remains finite, $\mathcal{Z}(\beta,\mu)$ remains positive, but in the thermodynamic limit, $\mathcal{Z}(\beta,\mu)$ vanishes. The zeros of the GCPF were studied independently by Lee and Yang [68] and Fisher [34], see section II.E. For the present thesis, the latter gives the basic idea of extending the GCPF into the complex plane by allowing complex values of β.

By introducing a basis $|\phi_1\rangle, ..., |\phi_N\rangle$, the trace becomes the sum over the expectation value of the argument in all basis states, and in this notion, a boundary state can be introduced as

$$|\Psi_0\rangle = \sum_{m=1}^{N} \alpha_m |\phi_m\rangle. \tag{I.3}$$

We absorb an eventual dependency of $\mathcal{Z}$ on μ into the definition of $\mathbf{H}$ and switch from the unbounded trace operator to a bounded partition function, and obtain

$$\mathcal{Z}(z) = \mathrm{Tr}\left\{\mathrm{e}^{z\mathbf{H}}\right\} \overset{\mathsf{BC}}{\leftrightarrow} \langle\Psi_0|\,\mathrm{e}^{z\mathbf{H}}\,|\Psi_0\rangle. \tag{I.4}$$

If $z = \mathrm{i}t$ is purely imaginary, this is identical to the Loschmidt echo (LE) after a quench from an initial Hamiltonian to $\mathbf{H}$, as we will show in section II.D. If $z = -\beta$ is real, we get back the GCPF. The function $\mathcal{Z}(z)$ can however have zeros in the complex plain also for finite systems [3]. In particular, zeros on the imaginary axis are possible. Therefore we introduce, based on a study by Heyl et al. [50] the concept of dynamical phase transitions (DPT). Note that this is a different situation that for EPT, where a zero in the inverse temperature axis is only possible in the thermodynamic limit.

DPT are a very young and active field in theoretical solid state physics, which did not emerge until 2012, so many questions are still open. Two years ago, a relation between DPT and topological phase transitions (TPT) has been suggested [14; 108], which will be one of the main topics of this thesis.

TPT are phase transitions which happen without the breaking of a symmetry of the system due to the underlying topology of the wave function. Topologically nontrivial models form a completely new class of interesting materials, which was discovered in the early 1980s and since received a broad interest. For explaining the theoretical foundations of topological phases of matter, J. Michael Kosterlitz, F. Duncan M. Haldane, and David J. Thouless were awarded with the Nobel prize in physics last year [102].

To characterize topological phases, the crucial quantity is an integer closely related to the topological genus, i.e. the number of holes in a geometric object. This number is invariant under small deformations of the

wave function as long as no TPT is crossed. This quantity is known as winding number, Chern number or TKKN (Thouless, Kohmoto, Nightingale, and den Nijs) invariant [49]. We discuss this invariant in detail in section II.A. If these materials have boundaries, i.e. a finite sample faces the surrounding vacuum (or air), metallic edge modes can be observed on the surface, although the bulk remains insulating [63; 76].

These edge modes make topological states of matter, commonly known as topological insulators (TI), interesting for many kinds of applications, because they are topologically protected [114]. This means, that in principle, scattering from these modes is inhibited and therefore, a lossless transport is possible. Thus TI are theoretically ideal materials for next-level information technology, including the development of quantum computers.

Beyond solid state, TI-like behaviour was also observes in photonic crystals [88] or ultracold gases in optical lattices [36; 42; 43]. They occur as real materials in one, two and three dimensions [49], and a Weyl metal can be imagined to be the surface of a four-dimensional TI [52; 115].

In this thesis we will investigate how the presence of topological edge modes interferes with DPT by studying the non-equilibrium dynamics of a quadratic (or free) fermion (FF) system after a quench. We compute the LE, because it captures the time evolution of the entire wave function. This also means that it is a highly non-local quantity and there is no simple way to extract the contribution of one single mode. Therefore, we also study more local quantities, such as the overlap of pre-quench eigenstates with the time evolved state.

We provide a wrap-up of previous works on DPT in systems in periodic boundary conditions, i.e. where no edge modes are present, in sections II.E and III.A, and we extract the edge contribution in the LE using a purely numerical exact diagonalization (ED) algorithm in section III.B. The algorithm we use is immediately applicable to any one-dimensional FF model. Together with the observations in different quantities, see section III.C, the ED results provide a strong hint for the presence of bulk-boundary correspondence not only in equilibrium PT, but also in DPT.

Chapter II

Concepts and Models

In this chapter, we give a more detailed overview of free fermion systems in general in section II.B, and the Su-Schrieffer-Heeger (SSH) chain and the XY- or Kitaev-chain in particular, see section II.B.5. The main quantity under consideration in this work is the Lohschmidt echo, which is reviewed in section II.D. We also discuss the physical concepts of topological insulators in section II.A and non-equilibrium thermodynamics, see section II.C. The last section II.E is dedicated to the ongoing research on dynamical phase transitions (DPT) and the impact of topology on them. Finally, we will define a dynamical topological order parameter in order to discuss bulk-boundary correspondence in DPT.

II.A Topological insulators

II.A.1 History

Topological phases of matter were first predicted in the 1980's. Laudau's description of phase transitions in terms of spontaneous symmetry breaking, as described in chapter II.E.1, was challenged by the discovery of the (integer) Quantum Hall effect (IQHE) by Klitzing et al. [61] and the Fractional Quantum Hall effect (FQHE) by Laughlin [67]. These effects led to a new theory based on the topological properties of the wavefunction within the Brillouin zone [19]. In this case, the concept of topological invariance is applied to the hyperplane of equal energy in k-space.

In mathematics, two geometric objects are considered topologically equivalent if there is a smooth deformation between them, i.e. one can transform them just by squeezing and stretching. More formally, two manifolds $A \subset X$ and $B \subset Y$ are equivalent, iff[1] there is a continuous bijection $f : X \to Y$, whose inverse f^{-1} is also continuous with $\mathrm{Im}_f(A) = B$ and $\mathrm{Im}_{f^{-1}}(B) = A$. In this case, f is called a homeomorphism, and A and B are called homeomorphic to each other [57]. Thus, for example, any open interval (a, b) (with $a < b$) is homeomorphic to the real numbers $\mathbb{R}$, and a torus is homeomorphic to a cup.

II.A.1.i Quantum Hall Effects

The first topological effect to be observed was the quantisation of the Hall conductance in a two-dimensional (2D) insulator in multiples of $e^2/\hbar$. The observation of Klitzing et al. [61] triggered the examination of 2D insulating systems in the early 1980s. In 1981, Laughlin [66] showed, that the quantisation of the Hall conductance happens only due to gauge invariance and the existence of a mobility gap, in which only the metallic edge modes of the system contribute to the conductivity.

Landau Levels

To understand the various quantum Hall Effects (QHE), we examine the dynamics of an electron in a magnetic field. Let us consider the Hamiltonian of a particle in a homogeneous magnetic field. This particle is free to move in x and y direction, but constrained at $z = 0$, i.e. we consider an infinite two-dimensional sample for now. The Hamiltonian of an otherwise free particle in this field is then given by

$$\mathbf{H} = \frac{1}{2m}\left(\vec{\mathbf{p}}^2 - \frac{q}{c}\vec{A}(\vec{\mathbf{x}})\right)^2, \tag{II.A.1}$$

where $\vec{A}$ is a vector potential of the magnetic field $\vec{B} = \mathrm{rot}\,\vec{A}$. The coordinate system is chosen such, that $\vec{B}$ points in the z-direction. We ensure this choosing the vector potential to be

$$\vec{A} = B\begin{pmatrix} -y \\ 0 \\ 0 \end{pmatrix}. \tag{II.A.2}$$

[1] The abbreviation "iff" for "if and only if" is common in mathematical literature and will also be used in this work

This choice of $\vec{A}$ implements the Landau gauge $[\mathbf{p}_x, \mathbf{H}] = 0$, such that the Hamiltonian does not constrain the movement of the particle in x direction. The solutions in x direction will thererfore be plain waves. Our particular interest is to understand the behaviour of an electron in a field, thus from here forward, we set q to the electron charge, $q = -e$. Now we rewrite the Hamiltonian as

$$\mathbf{H} = \frac{1}{2m} \begin{pmatrix} \hbar k_x - \frac{eB}{c} y \\ p_y \end{pmatrix}^2 \tag{II.A.3}$$

From the x component of the above equation, we read off a characteristic length scale of the problem, the so-called *magnetic length* $l_\mathsf{m} = \sqrt{\frac{\hbar c}{eB}}$. We rescale the y direction using

$$y \to y' = \frac{y}{l_\mathsf{m}} - l_\mathsf{m} k_x \qquad \text{and} \qquad p_y \to p'_y = \frac{l_\mathsf{m}}{\hbar} p_y \tag{II.A.4}$$

and obtain the Hamiltonian in the new coordinates

$$\mathbf{H} = \hbar\omega_\mathsf{c} \left(\frac{1}{2} y'^2 + \frac{1}{2} p'^2_y \right), \tag{II.A.5}$$

which is a harmonic oscillator at the *cyclotron frequency* $\omega_\mathsf{c} = \frac{eB}{m_0 c}$. The solutions of the Schrödinger equation are then given by

$$\begin{aligned} E_n &= \left(n + \frac{1}{2} \right) \hbar\omega_\mathsf{c} \\ \Psi_{n,k} &= \frac{\mathrm{e}^{-\frac{1}{2}\left(\frac{y}{l_\mathsf{m}} - \frac{2\pi k l_\mathsf{m}}{L_x}\right)^2}}{\left(\pi 2^{2n} (n!)^2\right)^{1/4}} H_n \left(\frac{y}{l_\mathsf{m}} - \frac{2\pi k l_\mathsf{m}}{L_x} \right) \mathrm{e}^{i\frac{2\pi k}{L_x} x}. \end{aligned} \tag{II.A.6}$$

These eigenstates are called the Landau levels (LL). The quantum number k comes from applying periodic boundary conditions to the x direction with length L_x, and H_n are the Hermite polynomials. The eigenenergies do not depend on the momentum in x direction, thus the energy levels are highly degenerate. In the limit of large samples $L_x \to \infty$, $k_x = 2\pi k / L_x$ becomes continuous and the degeneracy of the energy levels becomes infinite.

Integer Quantum Hall Effect

In typical experiments, one applies a current to the sample and measures the voltage drop parallel and orthogonal to the direction of the applied current in order to determine the resistivities ρ_{xx} and ρ_{xy}, respectively. In the scheme of figure II.1, this means to measure the voltage drop in horizontal or in vertical direction, given the current is applied horizontally as well.

Remarkably, the parallel resistivity ρ_{xx} becomes zero when ρ_{xy} has a plateau. The value of ρ_{xy} at the plateaus (indexed by N) is given by

$$\rho_{xy} = \frac{h}{Ne^2}. \tag{II.A.7}$$

Both the quantisation of ρ_{xy} and the lossless transport in parallel direction can be understood using the LL picture. For zero magnetic field, all LL are degenerate, and they split for finite fields with $\Delta E \propto B$. For high fields, the higher LL start passing across the Fermi energy of the system.

We have seen that the LL energy only depends on the level index if the sample is infinite. This does however not hold in open boundary conditions. In this case, the energy of the LL becomes space dependent and

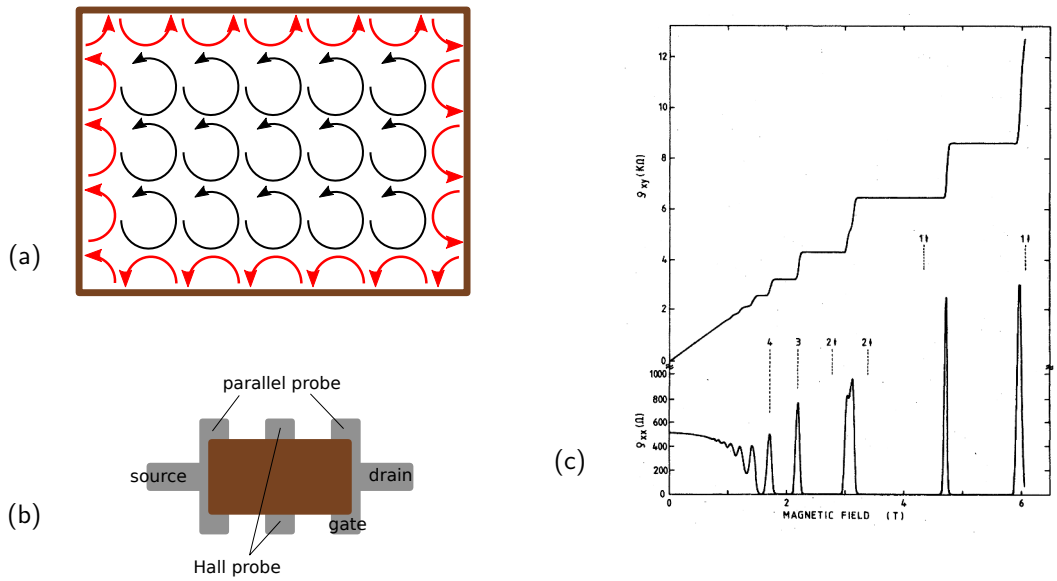

Figure II.1: (a) A schematic 2D insulator in a transversal magnetic field. Electrons in the bulk move on cyclotron trajectories (black). On the edges, they are reflected and form a metallic state (red). (b) Experimental setup. (c) Typical experimental data, reproduced from von Klitzing [110]

is shifted to higher values close to the boundary, as shown in figure II.2. In fact, if the sample would be infinitely large (i.e. there are no boundaries present), the IQHE would not be observed.

If there is a LL right at the Fermi energy, the system behaves metallic, and both resistivities are finite. If this is not the case, i.e. there is no density of states (DOS) near the Fermi energy, and there are no mobile electrons in the system. Therefore the Hall resistivity ρ_{xy} stays constant and the edge mode indicated by the red circles in figure II.1 (a) forms. Since this mode can not scatter anywhere (there is no DOS), transport in this mode becomes lossless, and the resistivity ρ_{xx} becomes zero [49]. There is one edge mode for each LL, which also explains the discrete jumps in ρ_{xy} as one LL crosses past the Fermi energy.

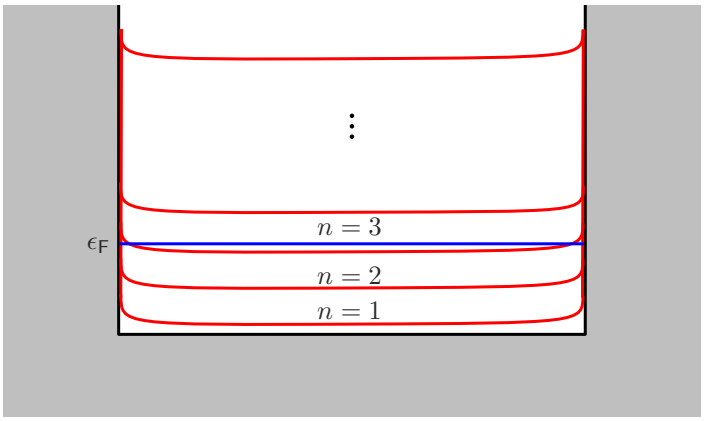

Figure II.2: Landau levels in a system with open boundary conditions. Far from the boundary, the LL are still flat and the energy of the n-th LL, E_n, is given by eq. (II.A.6). Close to the surface is shifted, and thus for certain magnetic fields, the Fermi energy has precisely two intersection points with each LL. This fact gives rise to the edge modes.

Fractional Quantum Hall Effect

Only two years after the discovery of the IQHE, in 1982, Tsui and Stormer [105] found an even more puzzling quantum state (see also figure II.3). It forms at high enough magnetic fields, when there is only one LL left below the Fermi energy. In this case, levels were observed that could not be explained by the LL picture. Laughlin [67] suggested, that electron-electron interactions might govern the properties of an electron gas in this high fields. This gives rise to a sub-structure in the band, which is explained by electron-electron interaction and leads to sharp transitions at fractional fillings

$$\nu = \frac{1}{1}, \quad \frac{1}{3}, \quad \frac{2}{3}, \quad \ldots \tag{II.A.8}$$

in the lowest LL.

Laughlin's formalism explains the occurrence of FQHE states with a fractional filling

$$\nu = \frac{1}{3}, \quad \frac{1}{5}, \quad \ldots \quad \frac{1}{m} \tag{II.A.9}$$

with m an odd integer in the lowest LL, as well as for their particle-hole counterparts

$$\nu = \frac{2}{3}, \quad \frac{4}{5}, \quad \ldots \quad \frac{m-1}{m}. \tag{II.A.10}$$

This seemed to be sufficient to explain Tsui's measurements in the first place, but as the experimental accuracy increased, also plateaus found for different fractions were observed. This lead to a generalization of Laughlin's results by Jain [56]. He introduced the concept of composite fermions, i.e. fermions with an even number $2p$ of vortices attached to them. In terms of the FQHE, one would think of an electron, which has $2p$ magnetic flux quanta attached. Then, the fractional levels are

$$\nu = \frac{m}{2pm \pm 1}. \tag{II.A.11}$$

Jain's theory explains as well the IQHE, where no composite fermions form ($p = 0$) and thus only the LL contribute, as well as the FQHE by introducing a sub-LL splitting due to a non-zero p.

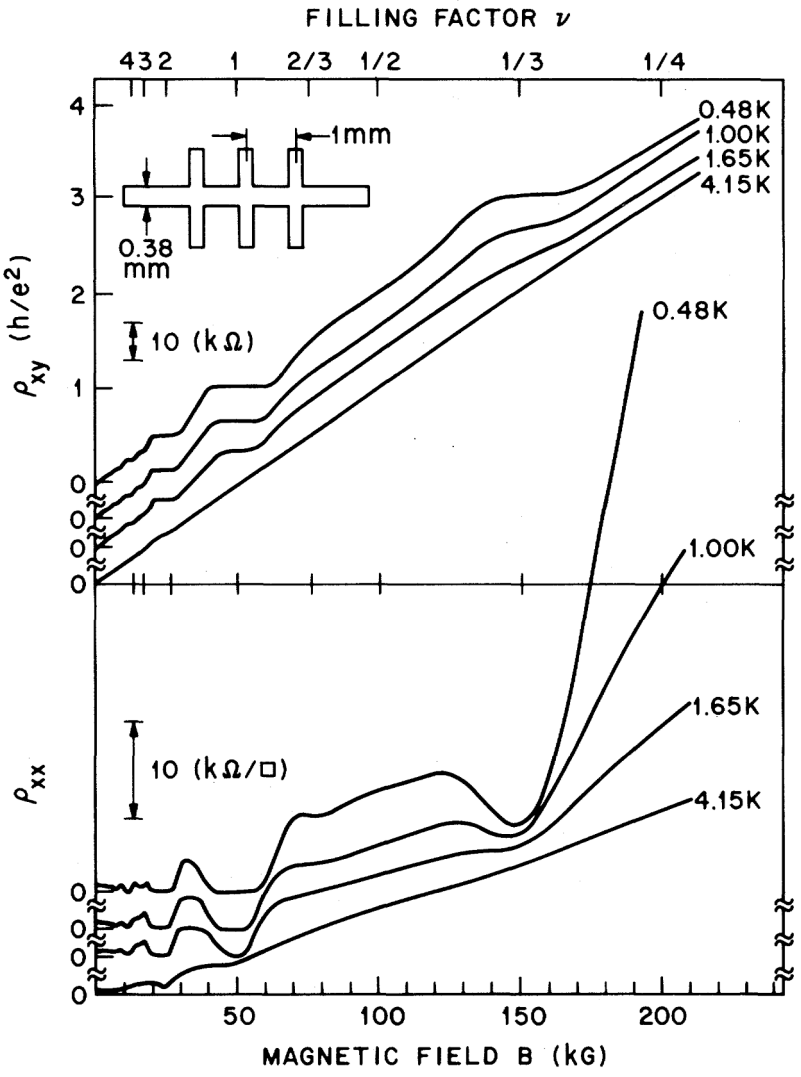

Figure II.3: Hall resistivities ρ_{xx} and ρ_{xy} in a sample of GaAs $-$ $Al_{0.3}$ $-$ $Ga_{0.7}As$ with the lowest ν LLs filled. ρ_{xy} captured at 0.48 K has a plateau around $\nu = 1/3$, whereas the corresponding parallel resistance ρ_{xx} has a minimum. This was the first observation of the FQHE. Figure adapted from [105].

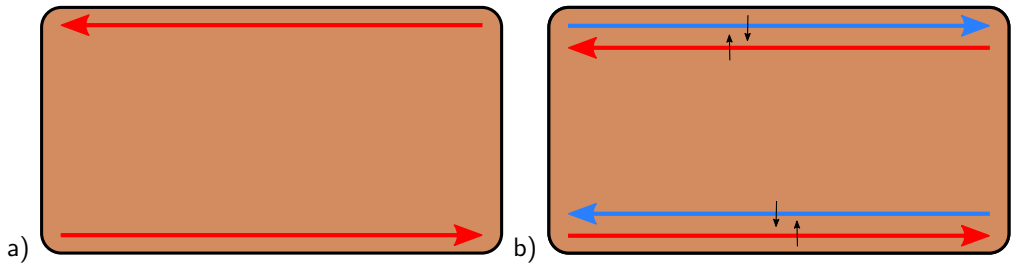

Figure II.4: (a) edge modes in a spinless QHE system (b) splitting for spin-up (red) and spin-down (blue) in QSH. The figure was inspired by [86].

Quantum Spin Hall Effect

So far, we discussed QHE in effectively spinless systems. To observe IQHE and FQHE, we have to work at very low temperatures and at fairly high magnetic fields. Both clearly limits possible applications of the QHE. In 1988, Haldane [48] found, that the presence of spin-orbit coupling can replace a strong external magnetic field in the sense, that it can lead to states similar to the QH states. These so-called *quantum spin hall (QSH)* states exhibit edge modes as well, and not necessarily require low temperatures [49; 76; 86]. However, the QSH effect has not been observed at room temperature so far. Unlike in the IQHE case, there are two edge modes in these systems. One edge mode transports only spin-up electrons e.g. from the left to the right on the top of the sample, the other one transports spin-down electrons from the right to the left, as shown in figure II.4 (b).

This state was predicted independently by Kane and Mele [58] and Bernevig et al. [10]. This state was also observed experimentally in the Molenkamp group in Würzburg, Germany in 2008 [63]. A description of the experiment is given in chapter II.A.3.

In the edge modes in these systems, scattering is still suppressed. If a particle scatters on a magnetic impurity, it gets reflected into a superposition state of the particle rotated by π and by $-\pi$. Both paths are related by time reversal symmetry (TRS). The resulting phase difference between these states is 2π, and they interfere destructively. This is alalogous to an anti-reflective coating in optics [76] Here, TRS forbids spin-flip scattering at an impurity, and therefore, the QSH state is said to be protected by TR symmetry. This does not hold for two (or in fact any even number of) edge mode pairs as it is then possible for an electron to scatter from the forward- to the backward-moving lane without reversing its spin, i.e. without perfect destructive interference. Any odd number of edge mode pairs leads to robust QSH edge states, which are synonymously referred to as *topological insulators (TI)* [86].

II.A.1.ii Chern numbers

A more profound understanding of the QHE becomes possible through the analysis of topological properties of the wave functions. The idea of characterizing geometrical object by its topology was around since the late 18th century. Major contributions in this field were made by Euler [31] and Gauss [39].

The normal vector $\vec{n}$ at a point $\vec{x}$ of a compact, regular, two-dimensional manifold M in $\mathbb{R}^3$ is always well defined, whereas the tangential vector $\vec{t}(\theta)$ may differ for different angles θ around the normal vector. More precisely, if θ is the angular coordinate on a circle in the plane perpendicular to $\vec{n}$, there is exactly one tangent vector of M in the plane $C(\theta)$ which contains both $\vec{n}$ and the point specified by θ. We refer

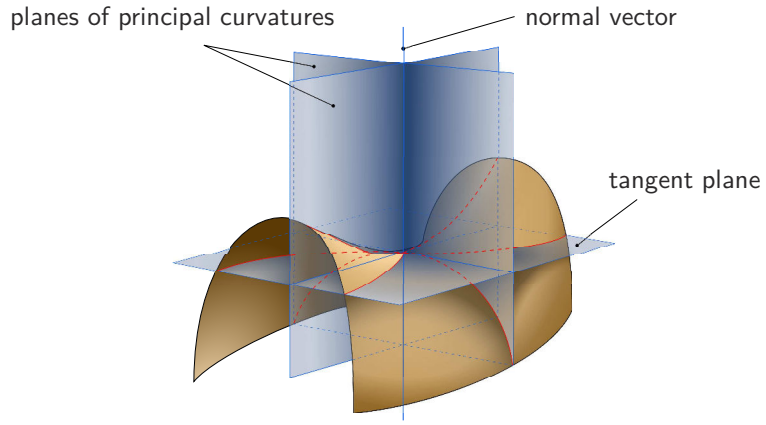

Figure II.5: Illustration of the problem of defining a curvature to a surface. The picture shows the situation where θ is chosen such that the principal curvatures are hit. Figure taken from [38].

to this vector as $\vec{t}(\theta)$, and to the geodesic curvature of the path $M \cap C(\theta)$, or *normal intersection*, in $\vec{x}$ as $k_{\vec{x}}(\theta)$.

DEFINITION II.1 *(Principal curvature)*

The principal curvatures of M in $\vec{x}$ are minimum and maximum of the curvature along all possible normal intersections.

$$\begin{aligned} k_1(\vec{x}) &= \min_{\theta\in[0,\pi]} k_{\vec{x}}(\theta) \\ k_2(\vec{x}) &= \max_{\theta\in[0,\pi]} k_{\vec{x}}(\theta) \end{aligned} \tag{II.A.12}$$

The angles $\theta_{1,2}$, at which the extremal values are taken, differ by $\pi/2$ and are called the *directions of the principal curvature*.

The principal curvatures indeed describe the local geometry of M completely. Because M is regular, the curvature along any normal intersection is given by Euler's theorem:

$$\begin{aligned} k_{\vec{x}}(\theta) &= k_1(\vec{x})\cos^2(\theta-\theta_1) + k_2(\vec{x})\cos^2(\theta-\theta_2) \\ &= k_1(\vec{x})\cos^2(\theta-\theta_1) + k_2(\vec{x})\sin^2(\theta-\theta_1). \end{aligned} \tag{II.A.13}$$

Using the principal curvatures, one can define a variety of measures of the "total" curvature of M in $\vec{x}$. The most interesting one for our purpose is the so-called Gauss curvature.

DEFINITION II.2 *(Gauss curvature)*

The Gauss curvatures of M in $\vec{x}$ is given by the product of the principal curvatures in this point,

$$\kappa(\vec{x}) = k_1(\vec{x})k_2(\vec{x}). \tag{II.A.14}$$

This quantity is directly related to the Euler characteristic of M by the Gauss-Bonnet theorem.

THEOREM II.3 *(Gauss-Bonnet theorem)*

Be M as before a compact, regular, two-dimensional manifold M in $\mathbb{R}^3$ and $\kappa(\vec{x})$ its Gaussian curvature. Further, be ∂M the boundary of M with the geodesic curvature $k_{\mathrm{g}}(\vec{x})$. Then, the Euler characteristic of M is then given by

$$\nu = \frac{1}{2\pi}\left\{\int_M \kappa(\vec{x})\mathrm{d}A + \int_{\partial M} k_{\mathrm{g}}(\vec{x})\mathrm{d}s\right\}. \tag{II.A.15}$$

it is related to the topological genus g of the manifold by $\nu = 2 - 2g$ for oriented manifolds and $\nu = 2 - g$ for non-oriented manifolds.

This is in particular also true for closed manifolds without a boundary, such as a sphere or a torus. In this case, the second term in eq. (II.A.15) vanishes and the topological genus only depends on the Gaussian curvature.

The key to the understanding of topological effects in physics is to apply this knowledge to the geometrical contribution to the phase of an adiabatically evolving wave function, the so-called *Berry phase* [11]. It can be understood as the angular mismatch of a wave function undergoing a periodical evolution when it returns to its origin, as shown in figure II.6. On a rotating sphere, like the earth, one can also think of

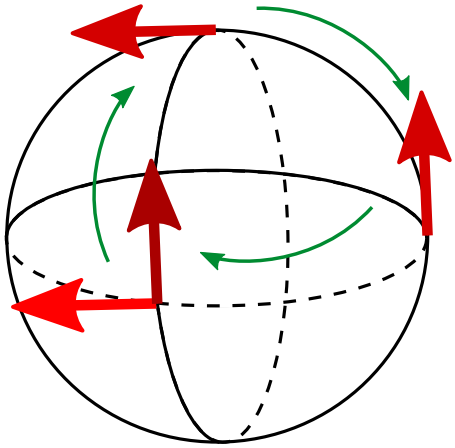

Figure II.6: Visualization of the parallel transport of a state on the surface of a (static) sphere.

a Foucault pendulum, which rotates the plane of its oscillation due to the Coriolis force with an angular speed depending on the latitude of its geographical location. This result was confirmed by a more abstract differential geometry approach [54].

Let us consider a system undergoing an adiabatic time evolution. We further assume the Hamiltonian to depend on time only implicitly by a parameter vector $\vec{r}(t)$, and its spectrum to be discrete and non-degenerate. Then, any state has a representation of the form

$$|\Psi(t)\rangle = \sum_n c_n(t)\,|\phi_n\left(\vec{r}(t)\right)\rangle\,, \tag{II.A.16}$$

where the $|\phi_n\left(\vec{r}(t)\right)\rangle$ are an orthonormal eigenbasis of the Hamiltonian the coefficients are given by

$$c_n(t) = \langle\phi_n\left(\vec{r}(t)\right)|\,\Psi(t)\rangle\,. \tag{II.A.17}$$

If the system is prepared in an eigenstate and remains there, the time evolution of the state is contained in the time evolution of the coefficients c_n:

$$\dot{c}_n(t) = \left(\frac{\partial}{\partial t}\left\langle \phi_n\left(\vec{r}(t)\right)\right|\right)\left|\Psi(t)\right\rangle + \left\langle \phi_n\left(\vec{r}(t)\right)\right|\frac{\partial}{\partial t}\left|\Psi(t)\right\rangle \tag{II.A.18}$$

To evaluate $\frac{\partial}{\partial t}\left|\Psi(t)\right\rangle$, we use the representation of thee state in the eigenbasis

$$\begin{aligned}\frac{\partial}{\partial t}\left|\Psi(t)\right\rangle &= \frac{\partial}{\partial t}\mathrm{e}^{-\mathrm{i}\mathbf{H}t}\left|\Psi(0)\right\rangle \\ &= \frac{\partial}{\partial t}\sum_m \mathrm{e}^{\mathrm{i}E_m t}c_m(0)\left|\phi_m\left(\vec{r}(0)\right)\right\rangle \\ &= -\sum_m \mathrm{i}E_m\mathrm{e}^{-\mathrm{i}E_m t}c_m(0)\left|\phi_m\left(\vec{r}(0)\right)\right\rangle \\ &= -\sum_m \mathrm{i}E_m c_m(t)\left|\phi_m\left(\vec{r}(t)\right)\right\rangle .\end{aligned} \tag{II.A.19}$$

Note, that in this and all following calculations, we set $\hbar \equiv 1$. eq. (II.A.18) then becomes

$$\begin{aligned}\dot{c}_n(t) &= \sum_m \left\langle \dot{\phi}_n\left(\vec{r}(t)\right)\right| \phi_m\left(\vec{r}(t)\right)\rangle\, c_m(t) - \mathrm{i}E_n c_n(t) \\ &= \left\langle \dot{\phi}_n\left(\vec{r}(t)\right)\right| \phi_n\left(\vec{r}(t)\right)\rangle\, c_n(t) - \mathrm{i}E_n(\vec{r}(t))c_n(t).\end{aligned} \tag{II.A.20}$$

The sum collapses, because the time evolution is adiabatic, and there is no density transferred into other eigenstates. This differential equation is easily solved by adding the boundary condition $c_n(t=0) = 1$ and integrating. Finally, we obtain

$$\begin{aligned}\left|\Psi(t)\right\rangle &= \mathrm{e}^{-\mathrm{i}\theta(t)}\left|\phi_n\left(\vec{r}(t)\right)\right\rangle, \quad \text{where} \\ \theta(t) &= \int_0^t E_n(\vec{r}(\tau))\mathrm{d}\tau - \mathrm{i}\int_0^t \left\langle \dot{\phi}_n\left(\vec{r}(\tau)\right)\right| \phi_n\left(\vec{r}(\tau)\right)\mathrm{d}\tau\rangle .\end{aligned} \tag{II.A.21}$$

We identify the first term in the above equation as the dynamic contribution and the second one as the geometric part. As the time dependency is only implicit, one can substitute the time integration by a path integral in parameter space.

DEFINITION II.4 *(Berry phase)*

The Berry phase is the geometric contribution to the phase of an adiabatically evolving state. The Berry phase along a closed path γ is given by

$$\chi = \mathrm{i}\oint_\gamma \left\langle n(\vec{r})\right| \nabla_{\vec{r}}\left|n(\vec{r})\right\rangle \mathrm{d}\vec{r}. \tag{II.A.22}$$

Analogous to classical electrodynamics, there exists a vector potential $\vec{A} = \mathrm{i}\left\langle n(\vec{r})\right| \nabla_{\vec{r}}\left|n(\vec{r})\right\rangle$ such that

$$\chi = \oint_\gamma \vec{A}\,\mathrm{d}\vec{r}, \tag{II.A.23}$$

which is given implicitly by definition II.4. As in electrodynamics, one can show that a closed-loop Berry phase is (up to multiples of 2π) invariant under gauge transformations. Thus we can use Stokes' theorem

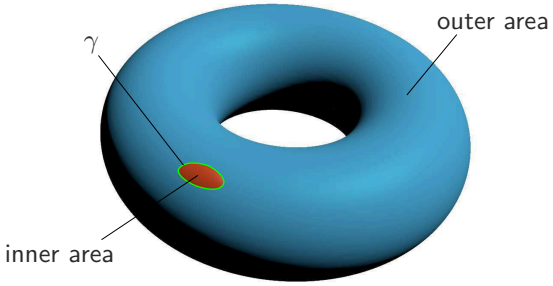

Figure II.7: A point-contractible closed curve γ on a surface divides it into an inner and an outer area.

to obtain a result of the form of the Gauss-Bonnet theorem II.3. Let Γ be a surface in the parameter space with $\partial\Gamma = \gamma$

$$\begin{aligned}\chi &= \oint_\gamma \vec{A}\,\mathrm{d}\vec{r} = \iint_\Gamma \mathrm{rot}\,\vec{A}\,\mathrm{d}F \\ &= \iint_\Gamma \nabla_{\vec{r}} \times \langle n(\vec{r})|\,\nabla_{\vec{r}}\,|n(\vec{r})\rangle\;\mathrm{d}S \\ &= \iint_\Gamma \sum_{ijk} \epsilon_{ijk}\nabla_i \langle n(\vec{r})|\;\nabla_j n(\vec{r})\rangle\,\mathrm{d}S_k.\end{aligned} \tag{II.A.24}$$

This is the Berry curvature, which we denote by

$$\vec{K} = \sum_{i,j,k} \epsilon_{ijk}\nabla_i \langle n(\vec{r})|\;\nabla_j n(\vec{r})\rangle\,\hat{e}_k. \tag{II.A.25}$$

An important difference to eq. (II.A.15) is, that the integral is not across a closed surface in this case. This problem can be solved considering the phase mismatch along a small, closed loop γ. The berry phase along this loop is - due to gauge invariance - conserved under small deformations of γ up to multiples of 2π. In fact, it must not change as long as the Berry curvature is well-defined, i.e. as long as the system is non-degenerate. When two eigenvalues come close to each other, the time evolution is no longer adiabatic, and the Berry curvature diverges.

Due to the above construction, the Berry phase must be a global feature of the parameter space topology. The parameter manifold is divided into an inner and an outer part, as illustrated in figure II.7. Because the Berry phase is well defined up to multiples of 2π, the integrals across the inner and the outer surface may only differ by $2m\pi$ with m integer. Thus, we can contract γ and obtain an again closed surface integral in the parameter space, which yields the Chern number [6].

DEFINITION II.5 *(Chern number)*

The Chern number is defined as an integral across a closed surface S in parameter space over the Berry curvature.

$$\nu_{\mathrm{Ch}} = \frac{1}{2\pi}\oint_S \vec{K}\cdot\mathrm{d}\vec{S} \tag{II.A.26}$$

The Chern number counts the number of degeneracy points in the inside of S. Each degeneracy point acts like a charge of the Berry field. When the whole band structure of the system is known, it is also

possible to calculate the Chern number as the volume integral of the divergence of the Berry field using Gauss' theorem.

With this invariant, it is possible to classify gapped Hamiltonians topologically by considering the equivalence classes of the Bloch Hamiltonian $\mathcal{H}(\vec{k})$ as described in section II.B, which can be deformed continuously into one another without closing the bulk energy gap [49]. In a system with multiple occupied bands, each band has an individual Chern number, and the total Chern number of the wave function is given by their sum,

$$\nu_{\mathsf{Ch}} = \sum_{m \text{ occupied}} \nu_{\mathsf{Ch}}^{(m)}. \tag{II.A.27}$$

In this case, Thouless et al. [103] showed, that the Chern number is identical to the integer labelling the IQHE plateaus in eq. (II.A.7).

II.A.1.iii Bulk-Boundary correspondence

In the following section, we describe a qualitative approach to understand BBC, which is inspired by more detailed reviews [22; 85]. The basic idea is, that as soon as edge modes are present, the spectrum can not be smoothly transformed to a state without edge modes, unless the bulk gap closes and thus creates a Dirac point [72; 76; 94]. In the Dirac point, the edge modes merge with (or separate from) the bulk. This gives a descriptive explanation, why the band gap has to close at a topological phase transition.

For systems in equilibrium, the presence of edge modes is known to relate to the presence of certain topological invariants in the bulk [30]. The Chern number described in the previous section is such an invariant. This phenomenon is usually referred to as *bulk-boundary correspondence (BBC)*. The IQH and QSH phases are examples for several more classes of topological insulators and superconductors, known as the *"tenfold way"* (see chapter II.B.4, and Refs. [1] and [93]) of classifying.

The Chern number can only change if the band gap closes [6] as well. We will not formally prove that both processes are equivalent in a sense that they never occur separately and only refer to the work of Essin and Gurarie [30]. They show, that BBC is a universal phenomenon in free fermion systems using Green's functions. It has also been shown that, within certain limits, BBC is also present in interacting and disordered systems [18; 20; 72].

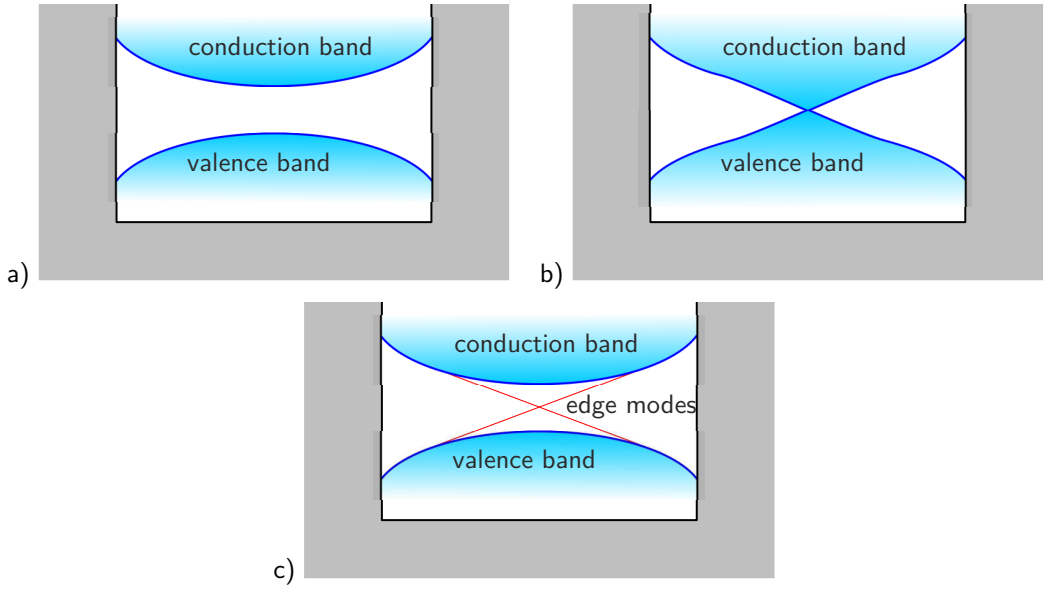

Figure II.8: Schematic of a topological phase transition. (a) Trivial (Mott) insulator without edge modes. (b) The bands touch in exactly one point, which is usually called Dirac or Weyl point. (c) Topologically non-trivial state with two edge modes. This situation is found in QSH insulators, where TR symmetry is present.

II.A.2 Symmetry protected systems

So far, we considered a phase transition to be of topological nature, if there is need of breaking some symmetry across the transition, i.e. if it can not be described within the Ginzburg-Landau picture of phase transitions, because there is no local order parameter [85]. In fact, this definition does not distinguish between two fundamentally different classes of topological phase transitions (TPT) [20].

These classes differ mainly in the stability of the TPT under perturbations. First, there is *intrinsic topological order*. These systems are stable under any kind of local perturbation. In the topologically non-trivial phase, the ground state of those systems are long-range entangled, and can not be mapped to a product state using local unitary transformations (LUT). Models in this class include (integer and fractional) QH systems, $p_x + \mathrm{i}p_y$-superconductors, and various spin liquids.

The second class has *symmetry protected topological (SPT) order*. In these systems, the presence of topological order depends on a certain symmetry, for example time-reversal symmetry in the case of QSH systems. It is possible to map the topological ground state to the topologically trivial one using general LUT. If we only allow LUT conserving the symmetry, the system has to undergo a phase transition in order to switch between the ground states. Therefore, the topologically non-trivial phases in these models are protected by the symmetry. This class contains a variety of models, such as QSH (or topological) insulators, free fermion systems, and one-dimensional spin chains.

The present work focusses on this second class of SPT systems implemented in free fermion models. A further classification of those models is discussed in section II.B.4.

II.A.3 Experimental realizations

During the last decade, various materials have been used to implement topological systems. The probably most famous experiment on TI uses a two-dimensional (2D) CdTe/HgTe/CdTe quantum well (QW) [63]. This combination of layers was predicted to show topological behaviour by Kane and Mele [58] and Bernevig et al. [10]. 3D TI have been realized in bismuth-based compounds [87; 114; 116]. Furthermore, there are realizations of TI in more artificial systems, such as ultra-cold atoms (Bose-Einstein condensate) [117] and photonic crystals [88]. In the following, we give a short introduction to the first two of the mentioned experiments.

II.A.3.i (Hg,Cd)Te quantum wells

Bernevig et al. [10] considered the band structures of the alloys HgTe and CdTe and realized, that they can be used to implement a QSH insulator. A quantum well is realized by stacking different materials with a different band structure, such that for the relevant bands, there is a potential well between the barrier material (here CdTe). The band structure of both materials is shown in figure II.9 (b). In both materials spin-orbit coupling (SOC) is present and influences the band structure.

HgTe is a semiconductor with an inverted band gap, because the s-like band Γ_6 has a lower energy than the p-like band Γ_8 in this material. Thus depending on the thickness d of the well material (here HgTe), the bound states of the potential well vary. Because of the band inversion due to SOC, the QW has bound states over a range of d, as shown in the lower panel of figure II.9 (b). At a certain critical thickness d_c, the energies of the first bound hole state $H1$ and the first bound electron state $E1$ become equal, and if $d < d_c$, the state $E1$ lies below $H1$, otherwise if $d > d_c$, the situation is opposite.

Varying d from the regime $d < d_c$ to $d > d_c$ thus represents a gap closing transition in the quantum well, and a transition from a conventional insulating state to a QSH state is expected. For the experiment by König et al. [63], a series of MBE-grown quantum wells over a range of d at low temerature $T < 30\,\mathrm{mK}$ was used. In thin enough QW, they observed the QSHE (figure II.10, left panel) for several gate voltages. Similar as in the IQH or the FQH state, the measured Hall resistance R_{xy} shows sharp plateaus which do not depend on the gate voltage. Each plateau resembles to another pair of edge modes crossing the Fermi energy, such that there are fewer states contributing to the conductivity and R_{xy} rises. The right panel of figure II.10 shows, that the gate voltage changes the intrinsic density of charge carriers linearly until a threshold, where all carriers are drawn out of the sample.

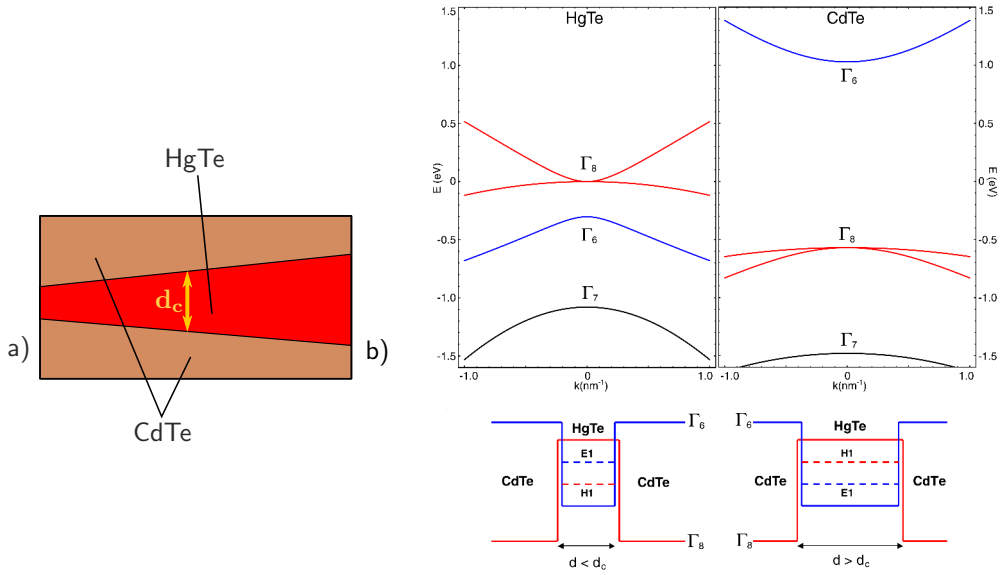

Figure II.9: Proposal for the realization of a QSH state in a (Cd,Hg)Te QW. (a) Sample structure. The thickness of the HgTe layer is varied, because the critical thickness d_c is unknown. (b) Band structure of HgTe vs. CdTe. Due to a different contribution of spin-orbit coupling, the s-like band Γ_6 has a lower energy than the p-like band Γ_8 in HgTe. Panel (b) adapted from [10]

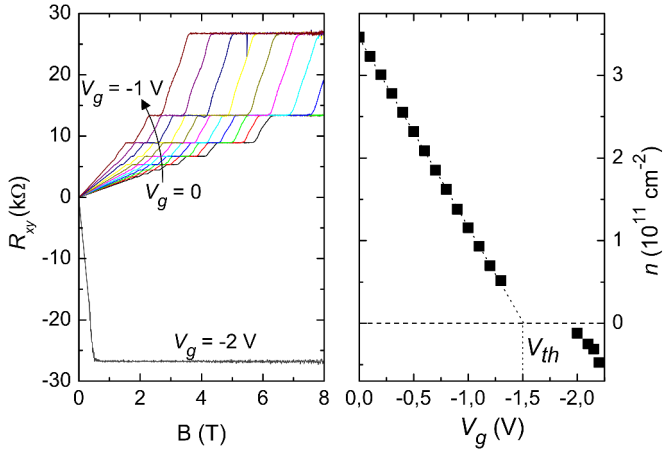

Figure II.10: Experimental data for the QSHE. Left panel: Hall resistance R_{xy} as measured for various gate voltages, indicating the transition from n-to p-conductance. Right panel: The gate-voltage dependent carrier density deduced from the Hall measurements. Figure and caption adapted from [63]

II.A.3.ii 3D topological insulators

Besides the 2D QSH system, there is a lot of interest in investigating 3D topological insulators, as they have been realized in various Bismuth based alloys, such as Bi_2Se_3, Bi_2Te_3, Sb_2Te_3, and Bi_xSb_{1-x} for a certain rage of x [87]. In the first three mentioned alloys, the band structure is simple enough to be described by an effective model [116].

Experimentally, a 3D TI is easy to be identified by its metallic surface modes, which - in terms of BBC - inherit the topological properties from the insulating bulk [76]. The presence of disorder or impurities at the surface can not affect these topological metallic states, and they never are gapped or localized, as long as the bulk stays insulating.

The wave number-dependant DOS was measured by angular resolved photo-emission spectroscopy (ARPES) in the experiment of Xia et al. [114]. In figure II.11, we show the band structure of Bi and Se in panel (a). In the rightmost column, there is a level crossing between the $p2_z^-$-band of Se and the $p1_z^+$-band of Bi, which leads to the topological state observed by ARPES. The measurement data is shown in panel (b).

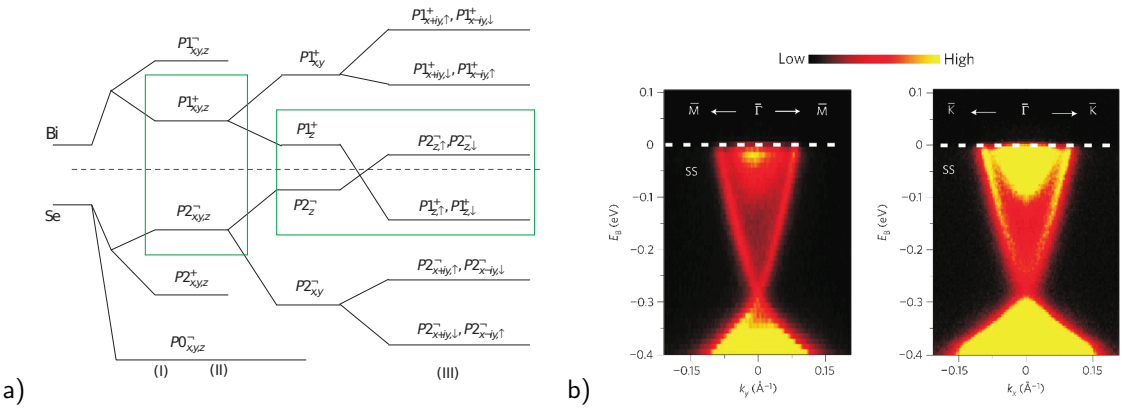

a) b)

Figure II.11: (a) Schematic diagram of the evolution from the atomic $p_{x,y,z}$ orbitals of Bi and Se into the conduction and valence bands of Bi_2Se_3 at the Γ point. The three different stages (I), (II) and (III) represent the effect of turning on chemical bonding, crystal-field splitting and SOC, respectively. The blue dashed line represents the Fermi energy. Figure and caption from [116]. (b) ARPES measurement in different directions. The yellow areas indicate a high DOS in the bulk bands, the edge modes appear in the bulk gap as distinct lines. Figure adapted from [114].

II.B Free fermion models

In the present work, we are interested in dynamical properties of free fermion (FF) systems. They are widely used in many-particle physics, as many problems are analytically solvable or one can at least do calculations for large systems using simple numerical algorithms. The following definition is possibly not the most general one, as it is rather meant to clarify what kind of systems are investigated in the present work

DEFINITION II.6 *(Free fermion model)*

Let i, j be a multi-index counting lattice sites as well as local degrees of freedom, such as spin. Further, let V_{ij} be a scalar potential which may or may not depend on the indices i and j. The Hamiltonian of a free fermion system $\mathbf{H}$ is a bilinear form in the creation and annihilation operators. In this case, the Hamilton operator takes the form

$$\mathbf{H} = \sum_{i,j} \left(\alpha_{ij} c_i^\dagger c_j + \beta_{ij} c_i^\dagger c_j^\dagger + \gamma_{ij} c_i c_j + \delta_{ij} c_i c_j^\dagger + V_{ij} \right). \tag{II.B.1}$$

II.B.1 General Properties

FF models are so easy to treat because there are no interactions involved. In terms of Feynman diagrams, this means that there are only propagators, but no vertices. This means that the many-particle states are just linear superpositions of the single-particle eigenstates of the system. For fermionic states, the Pauli principle requires all states to be totally antisymmetric under particle exchange. We introduce an antisymmetrisation operator A, which yields the totally antisymmetric superposition if applied to some input states. The following example demonstrates how to obtain a totally antisymmetric superposition of two input states.

EXAMPLE II.7 *(Two interacting particles)*

We write the two-particle state as $\phi(1,2) = \chi_1(1)\chi_2(2)$, with the single particle states $\chi_i(j)$. The antisymmetric state we need is $\psi_\mathsf{F}(1,2)$, and it must fulfil

$$\psi_\mathsf{F}(1,2) = -\psi_\mathsf{F}(2,1). \tag{II.B.2}$$

$\psi_\mathsf{F}(1,2)$ is a linear superposition of the $\phi(i,j)$ with all permutations of i and j. It is then obvious, that the superposition

$$A\phi(1,2) = \frac{1}{2}(\phi(1,2) - \phi(2,1)) = \frac{1}{2}\left(\chi_1(1)\chi_2(2) - \chi_1(2)\chi_2(1)\right) \tag{II.B.3}$$

fulfils eq. (II.B.2). One can rewrite this using a determinant of the single-particle functions,

$$\psi_\mathsf{F}(1,2) = A\phi(1,2) = \det\begin{pmatrix} \chi_1(1) & \chi_1(2) \\ \chi_2(1) & \chi_2(2) \end{pmatrix}. \tag{II.B.4}$$

This determinant in eq. (II.B.4) is called the Slater determinant. To generalize it to N "input" particles, we define A as follows:

DEFINITION II.8 *(Antisymmetrisation operator)*

Be $S(N)$ the permutation group on N elements and $\sigma : S(N) \to \pm 1$ the sign of a permutation $P \in S(N)$. The antisymmetrisation operator is then given by

$$A = \frac{1}{N!}\sum_{P\in S(N)} \sigma(P)P. \tag{II.B.5}$$

With this operator, we obtain an easy way to calculate the totally antisymmetric wave function.

THEOREM II.9 *(Slater determinant)*

For an N-particle FF system, the fully antisymmetric wave function is given by the Slater determinant

$$\psi_\mathsf{F}(1,...,N) = A\phi(1,...,N) = \det\begin{pmatrix} \chi_1(1) & \cdots & \chi_1(N) \\ \vdots & \ddots & \vdots \\ \chi_N(1) & \cdots & \chi_N(N) \end{pmatrix}. \tag{II.B.6}$$

Proof. With eq. (II.B.4) as the induction base and using definition II.8, the claim follows directly by mathematical induction. The induction step follows from the the Laplace expansion of a $(N+1)$-dimensional determinant with respect to the first row (or column). Then, the superposition parameters of χ_{N+1} and the N-particle ground state is determined analogous to eq. (II.B.3). This proof is to be found in any text book on quantum mechanics, therefore we omit a detailed discussion here. □

Thus as soon as we know which single-particle states are populated in a given state, we can write down the many-particle state immediately. In the present work we use the Slater determinant to determine the ground state of a many-particle system at half filling. As we work at zero temperature, the Fermi distribution becomes a step function

$$\rho_{\mathsf{Fermi},T=0} = \theta(-\epsilon_\mathsf{F}) \tag{II.B.7}$$

at the Fermi energy ϵ_F. If not indicated otherwise, we set $\epsilon_\mathsf{F} \equiv 0$ in this thesis. All states with $\epsilon < \epsilon_\mathsf{F}$ are populated, while those with $\epsilon > \epsilon_\mathsf{F}$ are empty. For a chain with N sites and $\frac{N}{2}$ particles, let

$$\mathbf{H}\chi_k = \epsilon_k \chi_k \tag{II.B.8}$$

be the single-particle states, with $k < l \Rightarrow \epsilon_k < \epsilon_l$. Then

$$\psi_\mathsf{G} = \det \begin{pmatrix} \chi_1(1) & \cdots & \chi_1\left(\frac{N}{2}\right) \\ \vdots & \ddots & \vdots \\ \chi_{\frac{N}{2}}(1) & \cdots & \chi_{\frac{N}{2}}\left(\frac{N}{2}\right) \end{pmatrix} \tag{II.B.9}$$

is the many-particle ground state we need.

In the following chapters, we introduce various commonly used formalisms in FF physics. The Bogoliubov-de-Gennes transformation in combination with Nambu spinors provides a very general way to switch between first and second-quantized language, i.e. between the single-particle Hilbert space and the many-particle Fock space, without using many-particle states explicitly. Thus we avoid the use of tensor products to build a many-particle state, and keep the dimension of the Fock space linear with the system size, as opposed to the exponentially large many-particle Hilbert space created by tensor products.

Later in the chapter, we discuss the Altland-Zirnbauer symmetry classes of FF models, and introduce the models which we will refer to in the remainder of this work.

II.B.2 Bogoljubov-de-Gennes transformation

For FF models which include pairing terms, it is possible to write down a first quantization representation of the Hamiltonian. This is done by a so called *Bogoljubov-de-Gennes (BdG)* transformation. Originally is was developed by Bogoljubov [12] in 1958 as a method to describe the pair creation in the BCS theory of superconductivity by generalizing the Hartree-Fock equations. In 1966, de Gennes [23] added some generalizations. The discussion in this section is based on de Gennes' work and on a lecture of Leggett [69].

The starting point is a generic Hamiltonian

$$\mathbf{H} = \mathbf{H}_0 + \mathbf{V}, \tag{II.B.10}$$

where $\mathbf{H}_0$ is the (discretized) single-particle Hamiltonian involving an electromagnetic potential and an on-site interaction, while $\mathbf{V}$ contains the interaction part

$$\mathbf{H}_0 = \sum_i \left\{ \frac{\left(\vec{p} - \frac{e\vec{A}(\vec{r})}{c}\right)^2}{2m} + U(\vec{r}_i, \sigma_i) \right\} \tag{II.B.11}$$

$$\mathbf{V} = \frac{1}{2} \sum_{i,j} V(\vec{r}_i - \vec{r}_j), \tag{II.B.12}$$

The obvious approach to this problem would be to solve the equations for the one-particle wave functions and define the creation (annihilation) operators $a^\dagger_{\vec{k},\sigma}$ ($a_{\vec{k},\sigma}$) in the usual way, where σ denotes the two spin states. Then we define a test function of BCS pairing type

$$|\phi\rangle = \prod_{\vec{k}} \left(u_{\vec{k}} + v_{\vec{k}} a^\dagger_{\vec{k},\uparrow} a^\dagger_{\vec{k},\downarrow} \right) |\mathrm{vac}\rangle \tag{II.B.13}$$

and use $|\phi\rangle$ to determine the lowest energy level.

The solution obtained from this approach does not yield the correct ground state in general. It also turns out that the minimal energy we obtain is not correct in many cases, as it can be lowered by pairing the electrons in states other than the single-particle eigenstates [23].

Bogoljubov [12] described a more powerful approach, using a different basis than the single-particle eigenstates. He defined the operators

$$\psi_{\vec{r},\sigma} = \sum_{\vec{k}} \mathrm{e}^{\mathrm{i}\vec{k}\cdot\vec{r}} a_{\vec{k},\sigma} \qquad \text{and} \tag{II.B.14}$$

$$\psi^\dagger_{\vec{r},\sigma} = \sum_{\vec{k}} \mathrm{e}^{-\mathrm{i}\vec{k}\cdot\vec{r}} a^\dagger_{\vec{k},\sigma}. \tag{II.B.15}$$

which satisfy fermionic anti-commutation rules. This is checked easily, as the commutation relations are directly inherited from the operators $a_{\vec{k},\sigma}$, $a^\dagger_{\vec{k},\sigma}$. In terms of these operators, the particle number operator becomes

$$N = \sum_{\vec{k},\sigma} a^\dagger_{\vec{k},\sigma} a_{\vec{k},\sigma} = \sum_\sigma \int \psi^\dagger_{\vec{r},\sigma} \psi_{\vec{r},\sigma} \, \mathrm{d}\vec{r}. \tag{II.B.16}$$

Equations (II.B.11) and (II.B.12) become in this basis

$$\mathbf{H}_0 = \sum_\sigma \int \psi^\dagger_{\vec{r},\sigma} \left\{ \frac{\left(\vec{p} - \frac{e\vec{A}(\vec{r})}{c}\right)^2}{2m} + U(\vec{r},\sigma) \right\} \psi_{\vec{r},\sigma} \, \mathrm{d}\vec{r} \tag{II.B.17}$$

$$\mathbf{V} = \frac{1}{2} \sum_{\sigma,\sigma'} \int \psi^\dagger_{\vec{r}\,',\sigma'} \psi^\dagger_{\vec{r},\sigma} V\left(\vec{r},\sigma;\vec{r}\,',\sigma'\right) \psi_{\vec{r},\sigma} \psi_{\vec{r}\,',\sigma'} \, \mathrm{d}\vec{r} \mathrm{d}\vec{r}\,'. \tag{II.B.18}$$

At this point, we assume for the sake of simplicity, that U does not depend on the spins, and further V is approximated by an average potential $\Delta(\vec{r})$. Further, we introduce the shorthand

$$\mathbf{H}_0 - \mu N = \sum_\sigma \int \psi^\dagger_{\vec{r},\sigma} \mathbf{H}_{\mathrm{loc}} \psi_{\vec{r},\sigma} \, \mathrm{d}\vec{r}, \tag{II.B.19}$$

where

$$\mathbf{H}_{\mathrm{loc}} = \frac{1}{2m} \left(-\mathrm{i}\nabla - \frac{e\vec{A}}{c} \right)^2 + U(\vec{r}) - \mu \tag{II.B.20}$$

is the local Hamiltonian.

Using these approximations and eq. (II.B.19), we rewrite eq. (II.B.17) and obtain an effective Hamiltonian

$$\mathbf{H}_{\mathrm{eff}} = \int \left\{ \sum_\sigma \left(\psi^\dagger_{\vec{r},\sigma} \mathbf{H}_{\mathrm{loc}} \psi_{\vec{r},\sigma} + U(\vec{r}) \psi^\dagger_{\vec{r},\sigma} \psi_{\vec{r},\sigma} \right) + \Delta(\vec{r}) \psi^\dagger_{\vec{r},\uparrow} \psi^\dagger_{\vec{r},\downarrow} + \mathrm{h.c.} \right\} \mathrm{d}\vec{r}. \tag{II.B.21}$$

The terms proportional to $\Delta(\vec{r})$ create (annihilate) two particles, such that the particle number is not conserved any more. The chemical potential μ in eq. (II.B.19) implements the change of density locally. $\Delta(\vec{r})$ is called the *pairing potential* or *pairing amplitude*.

We diagonalize the effective Hamiltonian eq. (II.B.21) using the Bogoliubov transformation

$$\begin{aligned}\psi_{\vec{r},\uparrow} &= \sum_n \left(\eta_{n\uparrow} u_n(\vec{r}) - \eta^\dagger_{n\downarrow} v^*_n(\vec{r})\right) \\ \psi_{\vec{r},\uparrow} &= \sum_n \left(\eta_{n\downarrow} u_n(\vec{r}) + \eta^\dagger_{n\uparrow} v^*_n(\vec{r})\right).\end{aligned} \tag{II.B.22}$$

The operators $\eta_{n,\sigma}$ describe normal mode fermions. The functions u and v are determined such, that the effective Hamiltonian becomes

$$\begin{aligned}\mathbf{H}_{\text{eff}} &= \frac{1}{2}\vec{\Gamma}^\dagger D \vec{\Gamma}, \quad \text{where} \quad \vec{\Gamma}^\dagger = \begin{pmatrix} \eta_1^\dagger & \cdots & \eta_N^\dagger & \eta_1 & \cdots & \eta_N \end{pmatrix} \\ &= \frac{1}{2}\sum_{k=1}^{N} \epsilon_k \left[\eta_k^\dagger \eta_k - \eta_k \eta_k^\dagger\right] \\ &= \sum_{k=1}^{N} \epsilon_k \left[\eta_k^\dagger \eta_k - \frac{1}{2}\right].\end{aligned} \tag{II.B.23}$$

II.B.3 Nambu spinors

II.B.3.i Spinless case

Aiming for a simple notation, we introduce the so-called *Nambu spinors* or *pseudospins*. Although the resulting notation resembles that of a spin Hamiltonian, we will talk about spinless systems for now. The spinor notation is thus only an algebraic tool to shorten the equations. The Nambu operators for a spinless system are defined by

$$\vec{\Psi}_j^\dagger = \begin{pmatrix} c_j^\dagger & c_j \end{pmatrix}. \tag{II.B.24}$$

The components of the Nambu operators are the usual fermionic annihilation and creation operators action on site j. In order to write down a generic, weakly interacting, spinless Hamiltonian, we introduce the vector containing the Pauli matrices $\vec{\sigma}$. In eq. (II.B.25), we only include nearest-neighbour hopping, but long-ranged hopping terms can easily be included. The actual interaction parameters are contained in $\vec{\mu}$, while the hopping and pairing amplitudes are given by $\vec{d}$.

$$\mathbf{H} = \sum_j \left\{ \vec{\Psi}_j^\dagger \left(\vec{\mu}\cdot\vec{\sigma}\right) \vec{\Psi}_j + \vec{\Psi}_j^\dagger \left(\vec{d}\cdot\vec{\sigma} - J\,\mathbb{1}\right) \vec{\Psi}_{j+1} + \text{h.c.} \right\} \tag{II.B.25}$$

As an example, we will show how to reproduce the Hamiltonian of a Kitaev chain (see also II.B.5.ii) from this notation. First, we chose

$$\vec{\mu} = \begin{pmatrix} 0 \\ 0 \\ -\mu \end{pmatrix} \qquad \text{and} \qquad \vec{d} = \begin{pmatrix} 0 \\ i\Delta \\ 0 \end{pmatrix}, \tag{II.B.26}$$

and thus the Hamiltonian becomes

$$\mathbf{H} = -\mu \sum_j \vec{\Psi}_j^\dagger \sigma^z \vec{\Psi}_j + \sum_j \left\{ \vec{\Psi}_j^\dagger \left(i\Delta\sigma^y - J\,\mathbb{1} \right) \vec{\Psi}_{j+1} + \text{h.c.} \right\}. \tag{II.B.27}$$

Evaluating this sum, one obtains all possible combinations of two creators or annihilators for neighbouring sites. To obtain an expression allowing to apply numerical methods, the Hamiltonian should become a matrix which only contains numbers. This is easily achieved by writing the Hamiltonian as a linear operator acting on a doubled Hilbert space. If the initial sum on j runs to some L, the matrix we get will be $2L \times 2L$ dimensional, and the entries are determined assuming the form

$$\mathbf{H} = \vec{\Phi}^\dagger \mathcal{H} \vec{\Phi}, \quad \text{where} \quad \vec{\Phi}^\dagger = \begin{pmatrix} c_1^\dagger & \cdots & c_N^\dagger & c_1 & \cdots & c_N \end{pmatrix}. \tag{II.B.28}$$

The matrix $\mathcal{H}$ contains any combination of creators and annihilators, and the values obtained from eq. (II.B.27) can be put in there. For the Kitaev chain, it becomes

$$\mathcal{H} = \left(\begin{array}{c|c} \left(c_i^\dagger c_j\right) & \left(c_i c_j\right) \\ \hline \left(c_i^\dagger c_j^\dagger\right) & \left(c_i c_j^\dagger\right) \end{array} \right) = \frac{1}{2} \begin{pmatrix} -\mu & J & 0 & \cdots & 0 & 0 & -\Delta & 0 & \cdots & 0 \\ J & \ddots & \ddots & \ddots & \vdots & \Delta & \ddots & \ddots & \ddots & \vdots \\ 0 & \ddots & & \ddots & 0 & 0 & \ddots & & \ddots & 0 \\ \vdots & \ddots & \ddots & \ddots & J & \vdots & \ddots & \ddots & \ddots & -\Delta \\ 0 & \cdots & 0 & J & -\mu & 0 & \cdots & 0 & \Delta & 0 \\ 0 & \Delta & 0 & \cdots & 0 & \mu & -J & 0 & \cdots & 0 \\ -\Delta & \ddots & \ddots & \ddots & \vdots & -J & \ddots & \ddots & \ddots & \vdots \\ 0 & \ddots & & \ddots & 0 & 0 & \ddots & & \ddots & 0 \\ \vdots & \ddots & \ddots & \ddots & \Delta & \vdots & \ddots & \ddots & \ddots & -J \\ 0 & \cdots & 0 & -\Delta & 0 & 0 & \cdots & 0 & -J & \mu \end{pmatrix}. \tag{II.B.29}$$

Thus we define a map $\xi : \mathbf{H} \to \mathcal{H}$, which maps the second-quantized operator $\mathbf{H}$ to its first quantized equivalent $\mathcal{H}$. The underlying transformation a Bogoljubov-de-Gennes transformation as describes in section II.B.2.

II.B.3.ii Enlarged unit cells

The above representation fails as soon as there is more than one degree of freedom per lattice site. It is still possible to define Nambu spinors, but they will have 2^N entries for N degrees of freedom. Common cases where this generalisation is necessary are spinfull fermions or systems with enlarged unit cells. Thus eq. (II.B.24) becomes for one additional degree of freedom

$$\vec{\Psi}_j^\dagger = \begin{pmatrix} c_{j,A}^\dagger & c_{j,B}^\dagger & c_{j,A} & c_{j,B} \end{pmatrix}. \tag{II.B.30}$$

This can represent a model with two lattice sites per unit cell, i.e. with sub-lattices A and B, such as the Su-Schrieffer-Heeger model (chapter II.B.5.i). If one identifies $A \equiv\uparrow$ and $B \equiv\downarrow$, the spinors describe a chain of spin-$\frac{1}{2}$-particle or a qubit.

II.B.4 The tenfold way

The physics of free fermion (FF) models strongly depends on the symmetries of the individual model. Wigner and Dyson assumed, that FF systems can be grouped in three major symmetry classes, unitary, orthogonal and symplectic. The discovery of TI and superconductors (SC) challenged that picture, as these new phases fit in neither of those classes. Symmetry protected topological (SPT) order can not be caused by all possible symmetries. In this section, we give a short overview of SPT symmetry classes.

Altland and Zirnbauer proposed a generalized and completed set of precisely ten classes in 1997 [1], which is based on Cartan's classification of Lie groups [15; 16]. The Cartan labels are a mathematical, more general framework, whereas Altland and Zirnbauer take into account fundamental restrictions of physics, and therefore reduce the set of possible classes to ten. A comprehensive review on the topic was presented by Ryu et al. [93] in 2010. This section is mostly based on this article.

The classification of TI and SC in terms of symmetries aims at the most generic symmetry properties of a concrete system. Ryu points out, that this does not refer to unitary symmetries which commute with the Hamilton operator. For example, mirroring a (spinless) system is such an "ordinary" symmetry operation, and it will always be possible to write the Hamiltonian of this system in a basis where the two subsystems are decoupled, i.e. in a block-diagonal form. In that sense, the Hamiltonian is "reducible" and the mirror symmetry is not eligible to be one of the most generic symmetries a Hamiltonian can have. This argument applies similarly to translational and rotational symmetries, spin rotation symmetry, and many more.

We are interested in the symmetry features, which are possible in an in that notion irreducible Hamiltonian. In fact, the only two symmetries which play a role in this classification are time reversal symmetry (TRS) and charge-conjugation or particle hole symmetry (PHS).

II.B.4.i Possible symmetry classes

The systems we consider are all of the BdG form, and their Hamiltonian in Nambu representation looks like

$$\mathbf{H} = \sum_{A,B} \Psi_A^\dagger \mathcal{H} \Psi_B, \tag{II.B.31}$$

where A and B are multi-indices labelling the lattice sites and if necessary any additional quantum number, such as spin. $\mathcal{H}$ is then a $N^d \times N^d$ matrix, if N is the system size and d the dimension of the local Hilbert space, i.e. the number of possible combinations of quantum numbers other from the lattice site.

Applying a TRS operation to this Hamiltonian then yields its complex conjugate, up to a unitary rotation

$$\mathcal{T}\mathcal{H} = U_\mathcal{T}^\dagger \mathcal{H}^* U_\mathcal{T}. \tag{II.B.32}$$

A similar equation holds for PHS [94]:

$$\mathcal{C}\mathcal{H} = -U_\mathcal{C}^\dagger \mathcal{H}^* U_\mathcal{C}. \tag{II.B.33}$$

These two symmetries are enough to construct the ten possible symmetry classes. Other than the "ordinary" symmetries mentioned earlier, TRS and PHS "are not unitary symmetries, but rather reality conditions on the Hamiltonian $\mathcal{H}$ modulo unitary rotations" [93].

In a second quantized language, eq. (II.B.32) and eq. (II.B.33) become

$$\begin{aligned} \mathbf{H} &= \mathcal{T}\mathbf{H}\mathcal{T}^{-1} \qquad \text{and} \\ \mathbf{H} &= \mathcal{C}\mathbf{H}\mathcal{C}^{-1}. \end{aligned} \tag{II.B.34}$$

Applying $\mathcal{T}$ and $\mathcal{C}$ to a first-quantized state, one finds, that while $\mathcal{C}$ is unitary, $\mathcal{T}$ is anti-unitary $\mathcal{T}\mathrm{i}\mathcal{T}^{-1} = -\mathrm{i}$.

Further, we consider the possible products of $\mathcal{T}$ and $\mathcal{C}$. Therefore we apply each operator twice to a given state $\Psi_A(t)$, we find

$$\mathcal{T}\Psi_A(t)\mathcal{T}^{-1} = \mathcal{T}\mathrm{e}^{\mathrm{i}\mathbf{H}t}\Psi_A(t)\mathrm{e}^{-\mathrm{i}\mathbf{H}t}\mathcal{T}^{-1} = \sum_B (U_T)_{A,B}\,\Psi_B(-t) \tag{II.B.35}$$

due to eq. (II.B.34) for a single TRS operation and

$$\mathcal{T}^2\Psi_A\mathcal{T}^{-2} = \sum_B (U_\mathcal{T}^* U_\mathcal{T})_{A,B}\,\Psi_B \tag{II.B.36}$$

for double time reversal. Since $U_\mathcal{T}$ is unitary, $U_\mathcal{T}^* U_\mathcal{T} = \pm\mathbb{1}$. Thus $\mathcal{T}$ can square to plus or minus the identity. This also holds for $\mathcal{C}$, as one can go through the above calculation just as well for double charge conjugation.

The case we haven't considered yet is the product $\mathcal{S} = \mathcal{T}\mathcal{C}$, where there is no trivial solution, because the product of the unitary rotations is not necessarily $\pm\mathbb{1}$ any more. The product of the TRS and the PHS operator is another symmetry that may or may not be present. We will refer to $\mathcal{S}$ as "chiral" or "sub-lattice" symmetry (SLS).

II.B.4.ii A "periodic table" for FF models

With this result, it is straight-forward to write down the ten possible symmetry classes. Both $\mathcal{T}$ and $\mathcal{C}$ can occur in the kind that squares to $+\mathbb{1}$ or $-\mathbb{1}$, or they are absent at all, which makes $3 \times 3 = 9$ possible combinations. As soon as either $\mathcal{T}$ or $\mathcal{C}$ are present, the behaviour of $\mathcal{S}$ is determined, but if both $\mathcal{T}$ and $\mathcal{C}$ are absent, $\mathcal{S}$ can be present or absent. The different classes are shown in table II.1

Table II.1: An overview of the symmetry classes, involving Cartan labels, the symmetry of the Hamiltonian and the corresponding generic symmetries. For TRS and PHS, the square of the operator is given (or 0 if the symmetry is absent), whereas for SLS 1 and 0 refers to present and absent, respectively. Table and caption adapted from [93]

System	Cartan label	TRS	PHS	SLS	Hamiltonian
standard	A (unitary)	0	0	0	U(N)
(Wigner-Dyson)	AI (orthogonal)	$+1$	0	0	U(N)/O(N)
	AII (symplectic)	-1	0	0	U(2N)/Sp(2N)
chiral	AIII (ch. unit.)	0	0	1	$\mathrm{U(N+M)/U(N)\times U(M)}$
(sublattice)	BDI (ch. orthog.)	$+1$	$+1$	1	$\mathrm{SO(N+M)/SO(N)\times SO(M)}$
	CII (ch. sympl.)	-1	-1	1	$\mathrm{Sp(2N+2M)/Sp(2N)\times Sp(2M)}$
BdG	D	0	$+1$	0	SO(2N)
	DIII	-1	$+1$	1	SO(2N)/U(N)
	C	0	-1	0	Sp(2N)
	CI	$+1$	-1	1	Sp(2N)/U(N)

II.B.5 Models

We will investigate one-dimensional free fermion (FF) systems which have topologically non-trivial phases, where the Chern number ν_{Ch} is different from zero. For those models we consider the behaviour after a quench from an initial Hamiltonian $\mathbf{H}^{\mathsf{i}}$ to a final Hamiltonian $\mathbf{H}^{\mathsf{f}}$. We assume the system to be prepared in the ground state of $\mathbf{H}^{\mathsf{i}}$. After the quench, it is in a non-thermal state far away from equilibrium. Thus it is possible to investigate the non-equilibrium dynamics and the thermalization of the system. In the last few years, the concept of dynamical phase transitions (see chapter II.E) was introduced and developed [14; 50; 96; 106; 108]. We investigate their interplay with topologically non-trivial states.

II.B.5.i Su-Schrieffer-Heeger model

The Su-Schrieffer-Heeger (SSH) model was initially introduced to describe simple polymers such as Polyacetylene [101]. The physical representation of this molecule is a one-dimensional chain with two sublattices causing a staggered hopping amplitude. In the topologically trivial phase, the intra-cell hopping amplitude w is larger that the inter-cell hopping amplitude v, as sketched in figure II.12 (b). The SSH model is one of the few topologically non-trivial systems where analytic or semi-analytic solutions are available. This makes it very interesting for proof of principle calculations. Numerical methods can be immediately checked by doing the same calculation using the semi-analytical solution. For the sake of simple notation, we introduce the hopping amplitude

$$J = \frac{v+w}{2} \tag{II.B.37}$$

and the dimerization strength

$$\delta = \frac{v-w}{2J}. \tag{II.B.38}$$

We then have the intra-cell (inter-cell) hopping

$$w = J(1-\delta) \quad \text{and} \quad v = J(1+\delta), \tag{II.B.39}$$

respectively. Thus the Hamiltonian of the system becomes

$$\mathbf{H} = -J \sum_{i=1}^{N-1} \left[(1+(-1)^j \delta) c_j^\dagger c_{j+1} + \text{h.c.} \right]. \tag{II.B.40}$$

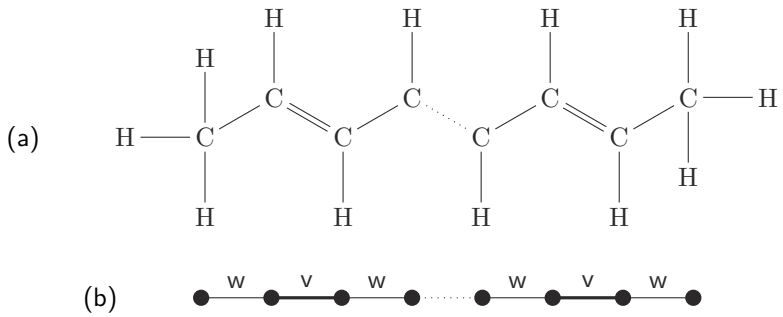

Figure II.12: (a) Polyacetylene with single bonds at the edges. This configuration is described by the topological phase of the SSH model. (b) Physical representation of this molecule.

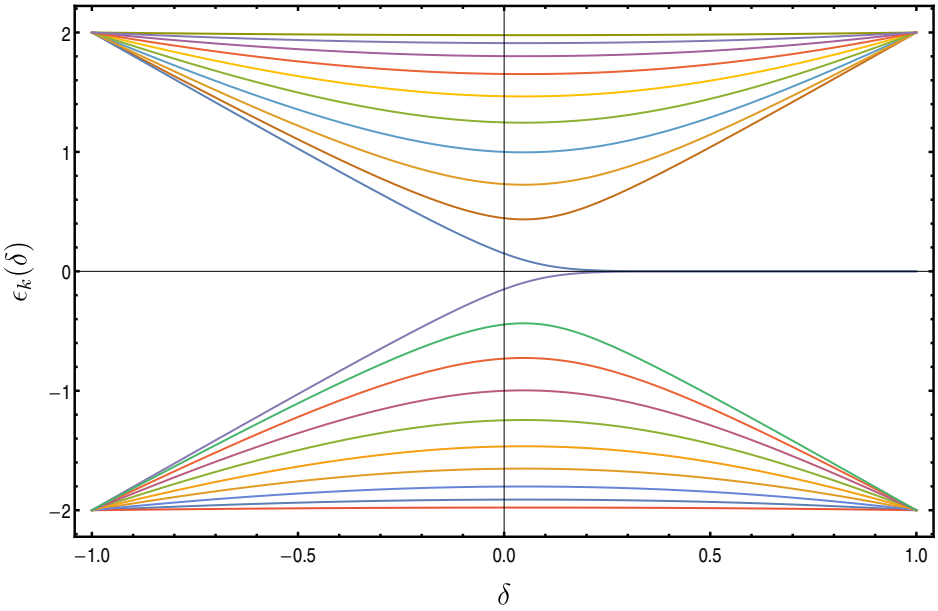

Figure II.13: The spectrum of a SSH chain with $L = 20$ sites in open boundary conditions (OBC). For $\delta < 0$ the system is gapped and the chain is insulating, but for $\delta > 0$ edge modes are present. These modes have an energy very close to zero, which makes it difficult to exactly diagonalize the Hamiltonian. For reasonably big systems, this requires multi-precision arithmetics.

In Nambu representation with enlarged unit cells, the SSH Hamiltonian becomes

$$\mathbf{H} = \vec{\Psi_k}^\dagger \mathcal{H}_k \vec{\Psi}_k. \tag{II.B.41}$$

Here, $\vec{\Psi}_k^\dagger = (c_{k,1}^\dagger \; c_{k,2}^\dagger)$, the $c_{k,j}^\dagger$ being the creators in sublattice mode (k, j), and $\mathcal{H}_k = \vec{d}_k \cdot \vec{\sigma}$ with

$$\vec{d}_k = -2J \begin{pmatrix} \cos(k) \\ \delta \sin(k) \\ 0 \end{pmatrix}. \tag{II.B.42}$$

With these definitions, $w > v$ if $\delta < 0$. In this case, there are dimers at the edges of the chain, and the system is in the topologically trivial phase. For $\delta > 0$, the edge sites have a weak bond to the neighbouring site, as shown in figure II.12. This gives rise to localized modes at the edges, and the system is in the topologically non-trivial phase. The hopping amplitude J is a constant which rescales the spectrum of eq. (II.B.40) and therefore the time evolution. Most of the time, we will ignore this factor in the calculations (i.e. set it to one), although we put it back in the results.

Note that the edge modes are only present in open boundary conditions (OBC), see figure II.13. In the case of periodic boundary conditions (PBC), the spectrum is symmetric in δ, as shown in figure II.14. The sum in eq. (II.B.40) runs to N in the periodic case, and a sign change in delta is the same as re-labelling the lattice sites $j \to j + 1$.

The SSH model is analytically solvable. In PBC, closed expressions for both eigenvectors and eigenvalues are known, while in OBC, the eigenvectors are known exactly, but the eigenvalues are only given in terms

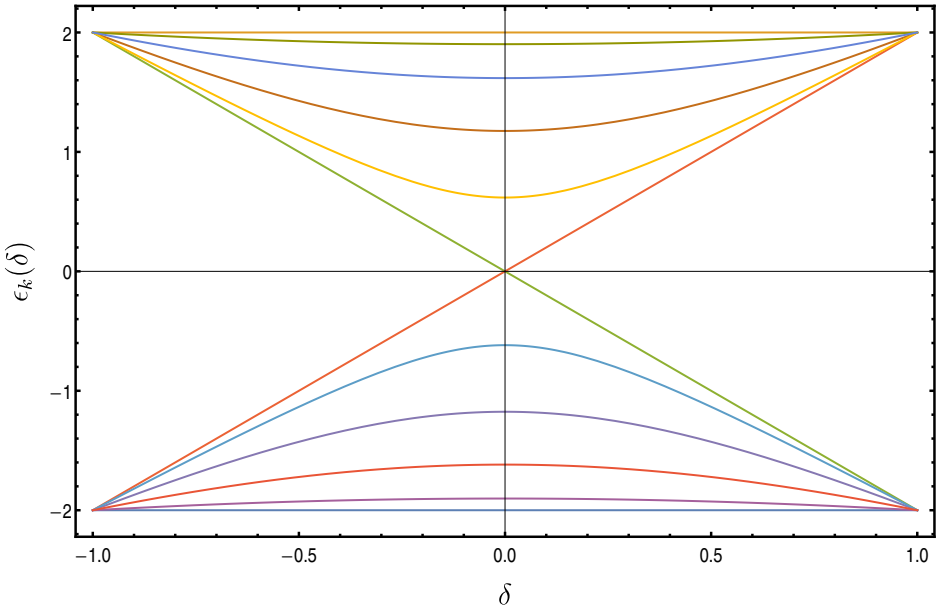

Figure II.14: The spectrum of a SSH chain with $L = 20$ sites in periodic boundary conditions (PBC). In this case, the spectrum is always gapped, and all but the constant states are twofold degenerate.

of an implicit equation, which has to be solved numerically [99]. We mostly use the SSH model as a test model, where we can check that the numerical algorithms are working correctly.

II.B.5.ii Kitaev chain

In this section we discuss a one-dimensional (1D) toy model introduced in 2000 by Kitaev [60]. Essentially, it represents a XY-chain. The model involves a spinless tight-binding fermion chain with an additional superconducting term,

$$\mathbf{H} = -\mu \sum_{j}^{N} c_j^\dagger c_j + \sum_{j}^{N-1} \left(-J c_j^\dagger c_{j+1} + \Delta c_j^\dagger c_{j+1}^\dagger \right) + \text{h.c.}. \tag{II.B.43}$$

In terms of Nambu spinors, this Hamiltonian reads

$$\mathbf{H} = -\frac{\mu}{2} \sum_{j} \vec{\Psi}_j^\dagger \sigma^z \vec{\Psi}_j + \frac{1}{2} \sum_{j} \left\{ \vec{\Psi}_j^\dagger \left(i\Delta\sigma^y - J\sigma^z \right) \vec{\Psi}_{j+1} + \text{h.c.} \right\}, \tag{II.B.44}$$

as shown in eq. (II.B.27) and eq. (II.B.29), with the Nambu operators $\vec{\Psi}$ defined as in section II.B.3. Note we omitted the constant term $\frac{\mu}{2}$, which remains from the anticommutator $[c_j^\dagger, c_j]_+ = 1$. We will mostly use the Nambu representation in this work. The topological properties of this model become visible in the basis of Majorana fermions (MF).

DEFINITION II.10 *(Majorana fermions)*

Let $c_j^\dagger$ (c_j) be the fermionic creation (annihilation) operators at lattice site j. The Majorana fermions are then defined as

$$\begin{aligned} \gamma_{j,1} &= \frac{1}{\sqrt{2}} \left(c_j^\dagger + c_j \right) \qquad \text{and} \\ \gamma_{j,2} &= \frac{\mathrm{i}}{\sqrt{2}} \left(c_j^\dagger - c_j \right). \end{aligned} \tag{II.B.45}$$

One easily checks that the anti-commutation relation

$$[\gamma_{i,\alpha}, \gamma_{j,\beta}]_+ = \delta_{ij}\delta_{\alpha\beta} \tag{II.B.46}$$

holds for MF. Further, MF are their own anti-particles, i.e. the Majorana creators and annihilators are identical,

$$\gamma_{j,\alpha} = \gamma_{j,\alpha}^\dagger. \tag{II.B.47}$$

Writing the Hamiltonian eq. (II.B.43) (for simplicity we set $\Delta = J$ here, and again negelct constant diagonal terms) in terms of MF yields [41]

$$\mathbf{H} = \mathrm{i}\mu \sum_{j}^{N} \gamma_{j,1}\gamma_{j,2} - \mathrm{i}J \sum_{j}^{N-1} \left(\gamma_{j+1,1}\gamma_{j,2} + \gamma_{j,1}\gamma_{j+1,2} \right). \tag{II.B.48}$$

Swiching to the MF basis means to introduce a second sub-lattice, such that there are two MF on each lattice site j, which introduces a sub-lattice. The apperance of topological modes follows a similar scheme as for the SSH chain, depending on how the MF are coupled together, as shown in figure II.15.

One finds that the chain behaves topologically non-trivially if $\Delta \neq 0$ and $0 < \mu < 2|J|$, and trivially otherwise. At $\Delta = 0$, there is topological phase boundary, which separates phases with winding numbers ± 1 [96].

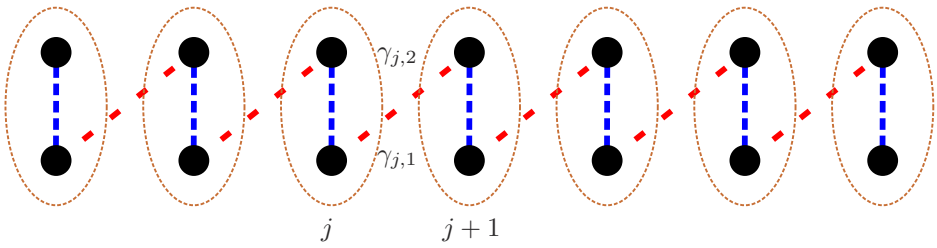

Figure II.15: Majorana pairs $\gamma_{j,\alpha}$ on each lattice site j. In the topologically trivial phase, blue dashed lines indicate the strong, intra-cell bonds, while red dashed lines indicate the weak, inter-cell bonds. This situation is switched in the topologically non-trivial phase, where the inter-cell bonds are stronger than the intra-cell bonds, and thus there are unpaired MF at the edges.

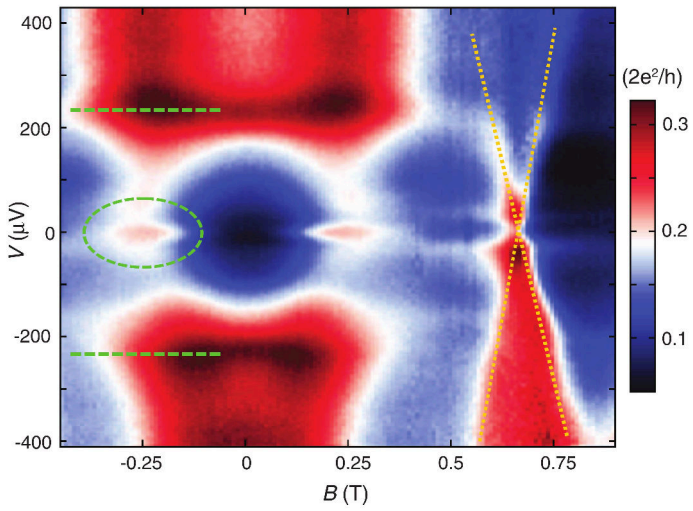

Figure II.16: Spectra of the edges of a InSb quantum wire, dependent on the external magnetic field strength $B = |\vec{B}|$. The green circle highlights a peak at zero energy, which is assumed to be due to unpaired MF. The dashed yellow lines are an artefact from the electrodes. Figure taken from [77]

This system was realized experimentally by placing a InSb quantum wire on an s-wave superconductor (SC) [77]. In their implementation, they used a magnetic field $\vec{B}$ to tune the chemical potential μ of the Kitaev chain and measured resulting spectra for a range of $\vec{B}$. The results are shown in figure II.16. The authors consider various other effects to explain the zero-energy peaks, like the Kondo effect or the presence of IQH-like Andreev states, but conclude that they "are not aware of any mechanism that could explain our observations, besides the conjecture of a MF".

II.B.5.iii Long-ranged Kitaev chain

The long-range (LR) Kitaev chain is a generalization of the Kitaev chain discussed in the section before. It allows longer ranged hopping terms up to a maximal distance $|i-j|$, and thus allows integer winding numbers. The Hamiltonian of this model in Nambu representation is

$$H = \frac{1}{2}\sum_{i,j}\left[\Psi_i^\dagger\left(\mathrm{i}\Delta_{|i-j|}\sigma^y - J_{|i-j|}\sigma^z\right)\Psi_{j+1} + \text{h.c.} - \delta_{ij}\Psi_j^\dagger\mu\sigma^z\Psi_j\right] . \tag{II.B.49}$$

In this form, the model is still part of the BDI symmetry class. Allowing complex pairing fields $\Delta_i = |\Delta_i| e^{i\theta_i}$ with $\theta_i \neq \theta_j$ breaks time reversal symmetry and changes the symmetry class of the model to D [96]. The edge modes of the LR Kitaev chain were investigated using a CFT-based approach by Vodola et al. [109]. We pick up their idea to study the behaviour of the system after a quench (see chapter II.C.2).

II.C Non-equilibrium dynamics

Both classical thermodynamics and statistical mechanics mostly apply to equilibrium systems. In equilibrium, a system does not change macroscopically over time, unless a (generalized) force acts on it. As soon as there is such a generalized force, such as a pressure, or a change in temperature, the state functions of the system are functions of this force, but not of time, and the system is described in a quasi-static, non-physical way.

The state variables in the non-equilibrium case should then have a continuous time dependency and still be related to each other in a similar way as in equilibrium. While this works for many applications where the considered states are close enough to thermal equilibrium, there are strong restrictions outside this range [37; 47].

II.C.1 Beyond equilibrium

Statistical mechanics assumes particles to be distributed in microstates according to some probability distribution. In equilibrium, this is a thermal distribution, i.e. the Maxwell-Boltzmann distribution for a classical particle or the Bose or the Fermi distribution for bosons or fermions, respectively [37]. To address dynamical problems, it is however necessary to understand the behaviour of a system out of equilibrium. For certain states "close enough" to equilibrium, there are extensions to classical thermodynamics, where the state functions also are functions of time. Systems far out of equilibrium can not be addressed with this approach, and are most commonly investigated using quantum quenches.

II.C.2 Quench dynamics

In the last 15 years, many studies use quantum quenches to investigate non-equilibrium systems. During a quench, the spectrum of the system undergoes a sudden change. In theory, this is usually implemented by turning on some interaction or changing a parameter of the Hamiltonian. Experimentally, quenches are usually investigated in ultra-cold gases setups. The sudden (non-adiabatic) change of the spectrum causes the density from the initial state to be projected on any state which has a non-zero overlap with it, regardless the energy of the (final) eigenstates. Thus, on short time scales after the quench, also high energy eigenstates are populated, and dynamics far from equilibrium can be studied.

We will here shortly present the first experiment on quenches conducted by Greiner et al. [44] in 2002, in which the Mott to superfluid (SF) transition of three-dimensional (3D) Bose-Hubbard (BH) lattice was

observed. The Hamiltonian of this system is given by

$$\mathbf{H} = -J \sum_j \left(b_j^\dagger b_{j+1} + \text{h.c.} \right) + \frac{V}{2} \sum_i n_i \left(n_i - 1 \right) - \mu \sum_i n_i. \tag{II.C.1}$$

Here, $b_j^\dagger$ (b_j) creates (annihilates) a boson at site j, and $n_j = b_j^\dagger b_j$ is the occupation number operator at site j. This transition was predicted by Fisher et al. [35]. At zero temperature, the BH lattice is SF at high hopping amplitudes J/V, but becomes Mott-insulating at small hopping amplitudes for most chemical potentials μ/V (figure II.17 (a)).

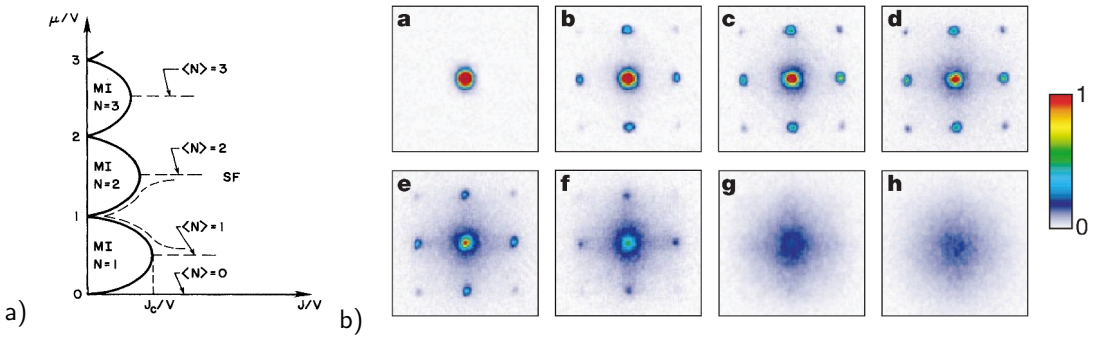

Figure II.17: (a) Phase diagram of a BH lattice, as predicted by Fisher et al. [35]. (b) Absorption images of matter waves interference patterns at different potential depths $V = 0, 3, 7, 10, 13, 14, 16,$ and $20\, E_\text{r}$ (left to right, top to bottom). Figure and caption adapted from [44].

Greiner et al. [44] used a Bose-Einstein condensate (BEC) in an optical trap with a variable depth V to observer this phase transition. The potential depth is measured in units of the recoil energy E_r. In figure II.17 (b), there is a single BEC peak for $V = 0$. A crystalline structure is present in the SF phase ($V = 3, 7, 10, 13, 14\, E_\text{r}$, panels (a)-(f)), while the interference pattern vanishes completely in the Mott phase ($V = 16, 20\, E_\text{r}$, panels (g) and (h)), and the absorption images show only an incoherent blob of atoms.

In a second part of their experiment, they investigated the relaxation behaviour of the lattice when it is quenched from the Mott phase to the SF phase. To archive the quench, they suddenly changed the potential depth from $V = 22\, E_\text{r}$ to $V = 9\, E_\text{r}$, and measured the width of the main peak over time (figure II.18).

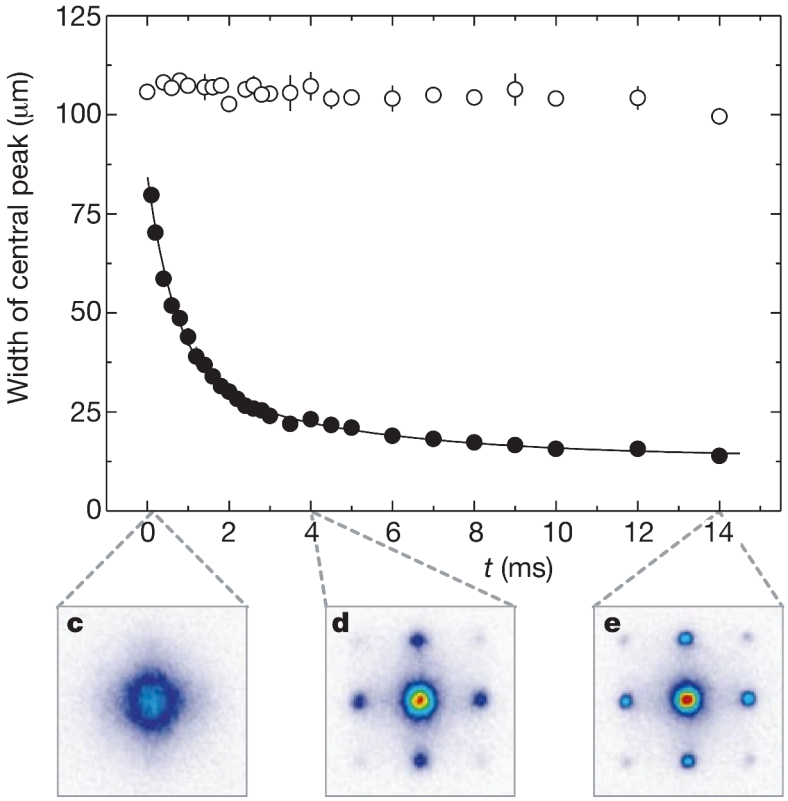

Figure II.18: Width of the central peak when quenching from a Mott state with $V = 22\,E_\mathrm{r}$ to a SF state with $V = 9\,E_\mathrm{r}$. The filled circles show the evolution of a coherent initial state, the empty circles show the behaviour of an initially incoherent state. In the latter case, no interference pattern is observed also for larger than the shown times. In the bottom panel, the interference patterns for wait times t of 0.1 ms, 4 ms, and 14 ms are shown. Figure and caption adapted from [44].

II.C.3 Alternative approaches

Quantum mechanical time evolution of non-equilibrium systems is also investigated using a variety of different techniques. In the following section, we introduce some of them, but without going into details.

Experimentally, it is possible to generate non-equilibrium states using parametrically driven systems. In order to have a well-defined and reproducible state, one excites the system periodically and waits for a dynamical quasi-equilibrium state to form, which does again not change over time. In these states, the average occupation of the microstates is static, but does not follow the aforementioned thermal distributions. Instead, the distribution depends on dynamical properties of the system and the parametric excitation, and out-of-equilibrium dynamics become accessible.

From a theoretical point of view, the problem of generating a non-equilibrium state does not exist, because we are free to choose any initial state. The only requirement to meet is reality, i.e. we make sure that the chosen initial state can in principle be realized in the system. Then, there are many methods to study the system both numerically and analytically. On the numerical side, there were progresses using renormalization group algorithms, like the density matrix renormalization group [3; 4; 8; 100]. Analytically, non-equilibrium systems are accessible for example by dynamical mean field theory [5] or Greens functions [71; 74]. Further, analytical renormalization group approaches can be used [9; 75; 111; 112].

II.C.4 Thermalization

In classical thermodynamics, a non-thermal (or non-equilibrium) in a non-integrable state will always relax to a state in which all energetically accessible areas of the phase space are actually populated. Initially, Boltzmann assumed, that any trajectory would reach any (energetically possible) point in phase space. This statement became known as the *ergodic hypothesis*. In this form, the hypothesis does in general not hold. Instead, a weaker formulation holds and is one of the basic assumptions of statistical mechanics [95].

THEOREM II.11 *(Quasi-ergodic hypothesis)*

Any physical trajectory of a particle comes arbitrarily close to any point in the phase space $\mathcal{P}$, such that averaging a function $f : \mathcal{P} \to \mathbb{R}$ over time is the same as averaging over the ensemble for sufficiently large times. This is equivalent to

$$\lim_{t\to\infty} \frac{1}{t} \int_0^t f\left(\vec{q}(\tau), \vec{p}(\tau)\right) \mathrm{d}\tau = \frac{1}{\Omega(E)} \int_{\mathcal{P}} f\left(\vec{q}, \vec{p}\right) \mathrm{d}\Gamma, \tag{II.C.2}$$

where $\Omega(E)$ is the number of possible realizations of the energy state E. Systems where this is true are called ergodic.

Integrable classical system are non-ergodic, as one easily checks for the free harmonic oscillator. Without any perturbations, its trajectory in the phase space is a circle around the origin with a radius given by the energy of the oscillator, which is obviously not dense in $\mathbb{R}^2$. Instead, the Kolmogorov-Arnold-Moser

(KAM) theorem II.12 completely describes the motion of any classical integrable system.

THEOREM II.12 *(Kolmogorov-Arnold-Moser theorem)*

Let $H = H(\vec{p}, \vec{q})$ be a Hamiltonian on a phase space $\mathcal{P}$ of dimension $2n$, depending on the canonical variables $\vec{p} = (p_1, ..., p_n)$ and $\vec{q} = (q_1, ..., q_n)$, with initial conditions $p(0), q(0)$. Then, there exists a d-dimensional torus $\mathcal{T}^d \subset \mathcal{P}$, such that

$$H(\vec{p}(0), \vec{q}(0)) \in \mathcal{T}^d \Rightarrow \forall t \in \mathbb{R} : H(\vec{p}(t), \vec{q}(t)) \in \mathcal{T}^d. \tag{II.C.3}$$

This torus is called a maximal KAM-torus for the Hamiltonian H. Its dimension $2 \leq d \leq n$ depend on the details of H.

The thermalization of classical systems is well understood, but for quantum mechanical systems, the situation is more complex. To classify the various behaviours known from quantum systems, we introduce the notion of *(Liouville) integrability*.

DEFINITION II.13

A system is called *(Liouville) integrable*, if there is a maximal set of local conserved quantities

$$Q = \int_{\mathcal{P}} q(x) \mathrm{d}\Gamma, \tag{II.C.4}$$

in a phase space $\mathcal{P}$ of dimension $2N$. Such quantities commute with its Hamiltonian, i.e. $[Q, H] = 0$.

An alternative interpretation of integrability is closer related to interactions in a quantum field theory setting. In many-particle physics, a free particle problem can always be reduced to a single-particle problem, which we use extensively throughout this work. Similarly, an integrable problem can always be reduced to a two-particle problem [64].

While non-integrable systems usually return to a thermal equilibrium without memory of the initial state [7; 104], many integrable models are known to keep some information from the initial state also for $t \to \infty$ [3; 45; 118]. An open question in this context receiving a lot of attention is, if and how the concept of thermalization can be generalized on integrable systems. A promising approach is to describe the a state of the system by its integrals of motion. This is realized for example in a generalized Gibbs ensemble [7; 78; 91; 90].

There is also evidence, that non-integrable systems, such as the Bose-Hubbard model [62], return to thermal equilibrium under certain conditions. One possible way to "break" integrability is, to introduce a strong enough disorder potential [83; 90]. Thermalization might be generalized to integrable systems through the *eigenstate thermalization hypothesis*, which was established by Deutsch [25] in 1991. Although some results support this hypothesis, there is no general theoretical argument supporting it so far. It would also be interesting to find or to neglect a quantum equivalent of the KAM theorem.

II.D Loschmidt echo

In the present work, we are not interested in the behaviour of a systems at long times, which would be given by the behaviour in the limit of infinite time, and the thermalization or the formation of a non-equilibrium steady state. Instead, we investigate the behaviour of the system at short time scales after a quench, when the system is far from equilibrium. In this section, we will give a motivation and a definition of the Loschmidt echo (LE). Later on, we describe different algorithms to calculate the LE in free fermion (FF) systems with either open or periodic boundary conditions (OBC or PBC).

In quantum mechanics, the time evolution under a hermitian Hamilton operator $\mathbf{H}$ is represented by a unitary linear operator

$$U(t) = \mathrm{e}^{-\mathrm{i}\mathbf{H}t}. \tag{II.D.1}$$

As it is unitary, the inverse operator $U^{-1}(t)$ exists and is equal to $U(-t)$. Once the time evolution of a system is known, it is natural to ask how stable it behaves with respect to small perturbations in the Hamiltonian. Then, applying first $U(t)U(-t)\,|\psi\rangle \equiv |\psi\rangle$ for all times. The original idea behind the LE was to do a "forward" time evolution under an initial Hamiltonian $\mathbf{H}^{\mathrm{i}}$ and a "backward" time evolution under a perturbed Hamiltonian $\mathbf{H}^{\mathrm{f}}$, as shown in figure II.19.

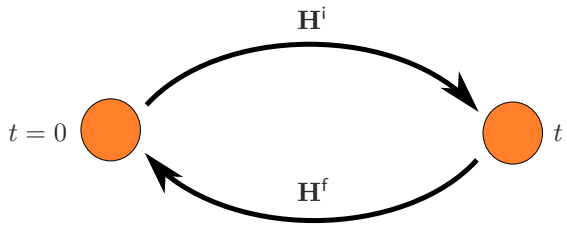

Figure II.19: Definition of LE

Historically, this idea goes back to a discussion between Boltzmann [13] and Loschmidt [73]. Loschmidt argued, that it should be possible to exploit the classical time reversal symmetry in order to create a thermodynamic system with a decreasing entropy and in contradiction to the second law of thermodynamics. He proposed creating such a state by inverting the velocities of every particle in the system. However, this does not agree with the statistical interpretation of thermodynamics, and is also not possible for macroscopic, gas-like systems: as soon as one fixes the initial conditions on each particle by reversing its velocity at a given time, statistical mechanics does not longer apply [113].

II.D.1 Definition

Although the LE was initially developed using the notion of time evolved states under different Hamiltonians, it can also be viewed in a more general scope. Therefore, we note that the time evolution operators

are unitary, and thus their product is unitary as well.

DEFINITION II.14 *(Loschmidt echo)*

Let U be an arbitrary unitary transformation. The quantity

$$G(U) = \langle\psi_0| U |\psi_0\rangle \tag{II.D.2}$$

is called Loschmidt echo (or Loschmidt amplitude). It measures the overlap between an initial wave function $|\psi_0\rangle$ with its image under U.

In the literature, the LE is sometimes defined as the absolute value $|G(t)|$ of this quantity, but in this context, we will refer to the complex quantity $G(U)$, unless stated otherwise. This is slightly more general, since one does not require the unitary operators to represent a time evolution. Despite this possibility, in this work we will only consider the case where both operators do have the same form as in eq. (II.D.1), and $U = U(t)$. In this case, the LE becomes

$$G(t) = \langle\psi_0| \mathrm{e}^{\mathrm{i}\mathbf{H}^{\mathrm{i}}t}\mathrm{e}^{-\mathrm{i}\mathbf{H}^{\mathrm{f}}t} |\psi_0\rangle . \tag{II.D.3}$$

II.D.2 LE in many-particle physics

In the study of quenched many-particle systems, the LE can be used to set up an experimentally realizable framework. One prepares a given system in its ground state $|\Psi_{\mathrm{G}}\rangle$ with respect to an initial Hamiltonian $\mathbf{H}^{\mathrm{i}}$. Then, at $t = 0$, the system is quenched to a final Hamiltonian $\mathbf{H}^{\mathrm{f}}$. In this case, the backward time evolution part of the LE becomes trivial, as it only adds a phase. If the Schrödinger equation

$$\mathbf{H}^{\mathrm{i}}\Psi_{\mathrm{G}} = E_{\mathrm{G}}\Psi_{\mathrm{G}} \tag{II.D.4}$$

is fulfilled, omitting the time evolution under the initial Hamiltonian only means multiplying $G(t)$ by $\mathrm{e}^{-\mathrm{i}E_{\mathrm{G}}t}$. E_{G} denotes the ground state energy. It is convenient to introduce the polar representation of the LE

$$G(t) = \prod_k g_k(t) = \prod_k r_k(t)\mathrm{e}^{\mathrm{i}\phi_k(t)}, \tag{II.D.5}$$

where $r_k : \mathbb{R}_{\geq 0} \to \mathbb{R}_{\geq 0}$ and $\phi_k : \mathbb{R}_{\geq 0} \to [0, 2\pi)$ take real values. In fact, all the analysis performed on the LE depends only on either on the radius $r_k(t)$ or on a partial derivative $\left.\frac{\partial\phi_k(t)}{\partial k}\right|_t$ at fixed times.

In a many-particle system, even small changes to the initial state $|\Psi\rangle$ cause the LE to vanish, as

$$\langle\Psi|\,\tilde{\Psi}\rangle \propto \mathrm{e}^{-N}, \tag{II.D.6}$$

if N is the number of particles in the system. This was dubbed Anderson orthogonality catastrophe [2; 40; 70]. A simple solution to this problem to define the Loschmidt return rate (LRR)

$$l(t) = -\frac{1}{N}\log(|G(t)|). \tag{II.D.7}$$

II.D.3 Mathematical prerequisites

The LE is defined as an expectation value of a product of two exponential functions (see definition II.14). Evaluating the LE is trivial when the arguments A and B of the exponentials in eq. (II.D.8) commute. This means, there is a basis in which both A and B are diagonal,

$$\mathrm{e}^{A}\mathrm{e}^{B} = \mathrm{e}^{AB}, \quad \text{iff} \quad [A,B] = 0. \tag{II.D.8}$$

In this case, it is physically not very interesting to evaluate the LE, because the eigenstates of the two Hamiltonians are identical, and the perturbation of the system is only given by a shift in the energy levels. Thus the LE is smooth and just reflects the formation of a steady state after the quench. A general rule how to evaluate expressions of this type is obtained from the Baker-Campbell-Hausdorff (BCH) theorem.

THEOREM II.15 *(Baker-Campbell-Hausdorff)*

Let $\mathfrak{g}$ be a Lie algebra and $A, B \in \mathfrak{g}$ and $\exp$ the exponential map and $\log$ its inverse. Then there exists a formal expression $C(A,B)$ such that $\exp\{C\} = \exp\{A\}\exp\{B\}$. If $C \in \mathfrak{g}$, we write $C = \log\{\exp\{A\}\exp\{B\}\}$

The proof of this theorem would exceed the scope of this work. It is available in many textbooks on advanced linear algebra or Lie theory. Strictly speaking, the claim is that C is a primitive element of $\mathfrak{g}$, and thus can be written as an infinite sum over elements of the Lie algebra generated by A and B. This sum does not necessarily converge, but for the physically relevant Lie algebras, it usually does.

COROLLARY II.16

Let A and B be linear operators. Then, there is an operator $C \in \mathrm{GL}(N)$ such that

$$\exp\{C\} = \exp\{A\}\exp\{B\}. \tag{II.D.9}$$

Proof. Due to theorem II.15, $C = \log(\exp\{A\}\exp\{B\})$ is an element of the underlying Lie algebra and thus its exponential $\exp\{C\}$ is in the Lie group. The group properties then also ensure, that $\exp\{C\}$ is unique. □

An explicit formula for C was developed by Dynkin [26]. The following theorem lists the first few terms of the infinite series.

THEOREM II.17 *(Dynkin's Formula)*

The matrix C from corollary II.16 can be written as an infinite sum over continued commutators

$$\begin{aligned} C &= \log(\exp\{A\}\exp\{B\}) \\ &= A + B + \frac{1}{2}[A,B] + \frac{1}{12}\left([A,[A,B]] + [B,[B,A]]\right) + \cdots \end{aligned} \tag{II.D.10}$$

This formula can also be derived without the BCH theorem. One simply writes down the first few terms of the exponential series for $\exp\{A\}\cdot\exp\{B\}$, and $\exp\{A+B\}$ expands the product and reorders the terms by their order in A and B. The additional terms in the first expression have then to be entered in the form above, such that the second expression reads $\exp\left\{A + B + \frac{1}{2}[A,B]\right\} + \cdots$ up to some maximum order of nested commutators.

In principle, one finds an expression of this form for any finite order. Dynkin's original work gives also an explicit expression for the infinite series [26], resulting in a general combinatorial formula. We do not repeat the lengthy calculations here.

With this formula, we can evaluate the LE semi-analytically in PBC in terms of the parameter vectors before and after the quench, because momentum is a good quantum number and we have independent modes. Therefore, we finally obtain a product over all momenta.

In the OBC case, we have to evaluate the LE numerically, because we can not decouple the modes analytically. Therefore, we write

$$G(t) = \langle\Psi_{\mathsf{G}}|\, \mathrm{e}^{\mathrm{i}\mathbf{H}^{\mathrm{i}}t}\mathrm{e}^{-\mathrm{i}\mathbf{H}^{\mathrm{f}}t}\, |\Psi_{\mathsf{G}}\rangle = \mathrm{Tr}\left\{|\Psi_{\mathsf{G}}\rangle\langle\Psi_{\mathsf{G}}|\, \mathrm{e}^{\mathrm{i}\mathbf{H}^{\mathrm{i}}t}\mathrm{e}^{-\mathrm{i}\mathbf{H}^{\mathrm{f}}t}\right\} = \mathrm{Tr}\left\{\rho_{\mathsf{G}}\mathrm{e}^{\mathrm{i}\mathbf{H}^{\mathrm{i}}t}\mathrm{e}^{-\mathrm{i}\mathbf{H}^{\mathrm{f}}t}\right\}. \tag{II.D.11}$$

This trace is transformed in a determinant using Levitov's formula [70]. In order to give a derivation, we first define a representation of a single-particle operator in the Fock space.

DEFINITION II.18 *(Fock space representation)*

Let O be a linear operator on a Hilbert space $\mathfrak{H}$. Treating a free fermion (FF) system in second quantization, the single particle space $\mathfrak{H}$ is becomes the Fock space $\mathfrak{F}$ and the representation of O is

$$\Gamma(O) = \sum_{i,j} \langle i|\, O\, |j\rangle\, a_i^\dagger a_j. \tag{II.D.12}$$

The creation and annihilation operators satisfy $a_j a_i^\dagger - \xi a_i^\dagger a_j = \delta_{ij}$, thus for $\xi = 1$ the particles behave like bosons, and for $\xi = -1$ like fermions. It is easy to check, that definition eq. (II.18) conserves the commutators between operators.

LEMMA II.19 *(Conservation of Commutators)*

Let A and B be linear operators, $\Gamma(A), \Gamma(B)$ their representations in Fock space, and $c_j^\dagger$ (c_j) the operators creating (annihilating) a fermion at site j. Then

$$[\Gamma(A), \Gamma(B)] = \Gamma\left([A, B]\right) \tag{II.D.13}$$

Proof. Let $\{|i\rangle\} \hookrightarrow \left\{c_i^\dagger\, |\mathrm{vac}\rangle\right\}$ be a orthonormal basis of the single-particle space and of the Fock space, respectively. We start using the definition II.18 to calculate the commutator in the Fock space.

$$\begin{aligned}
[\Gamma(A), \Gamma(B)] &= \sum_{i,j} \langle i|\, A\, |j\rangle\, c_i^\dagger c_j \sum_{k,l} \langle k|\, B\, |l\rangle\, c_k^\dagger c_l - \sum_{k,l} \langle k|\, B\, |l\rangle\, c_k^\dagger c_l \sum_{i,j} \langle i|\, A\, |j\rangle\, c_i^\dagger c_j \\
&= \sum_{i,j,k,l} \langle i|\, A\, |j\rangle\, \langle k|\, B\, |l\rangle\, c_i^\dagger c_j c_k^\dagger c_l - \sum_{i,j,k,l} \langle k|\, B\, |l\rangle\, \langle i|\, A\, |j\rangle\, c_k^\dagger c_l c_i^\dagger c_j \\
&= \sum_{i,j,k,l} \langle i|\, A\, |j\rangle\, \langle k|\, B\, |l\rangle \left(c_i^\dagger c_j c_k^\dagger c_l - c_k^\dagger c_l c_i^\dagger c_j\right).
\end{aligned} \tag{II.D.14}$$

We use the anti-commutation relations

$$\begin{aligned}
[c_i^\dagger, c_j]_+ &= \delta_{ij} \qquad \text{and} \\
[c_i, c_j]_+ &= 0,
\end{aligned} \tag{II.D.15}$$

where $[\cdot,\cdot]_+$ denotes the anti-commutator. We rewrite the second term inside the bracket as

$$\begin{aligned} c_k^\dagger c_l c_i^\dagger c_j &= c_k^\dagger(\delta_{il} - c_i^\dagger c_l)c_j \\ &= \delta_{il}c_k^\dagger c_j - c_k^\dagger c_i^\dagger c_j c_l \\ &= \delta_{il}c_k^\dagger c_j - c_i^\dagger(\delta_{kj} - c_j c_k^\dagger)c_l \\ &= \delta_{il}c_j^\dagger c_k - \delta_{kj}c_i^\dagger c_l + c_i^\dagger c_j c_k^\dagger c_l. \end{aligned} \tag{II.D.16}$$

Substituting this into eq. (II.D.14), we obtain

$$\begin{aligned} [\Gamma(A),\Gamma(B)] &= \sum_{i,j,k,l} \langle i|\, A\,|j\rangle \langle k|\, B\,|l\rangle \left(c_i^\dagger c_j c_k^\dagger c_l - \delta_{il}c_j^\dagger c_k + \delta_{kj}c_i^\dagger c_l - c_i^\dagger c_j c_k^\dagger c_l\right) \\ &= \sum_{i,j,k,l} \langle i|\, A\,|j\rangle \langle k|\, B\,|l\rangle \left(\delta_{kj}c_i^\dagger c_l - \delta_{il}c_j^\dagger c_k\right) \\ &= \sum_{i,l} \langle i|\, AB\,|l\rangle\, c_i^\dagger c_l - \sum_{kj} \langle k|\, BA\,|j\rangle\, c_k^\dagger c_j \\ &= \sum_{i,j} \left(\langle i|\, AB\,|j\rangle - \langle i|\, BA\,|j\rangle\right) c_i^\dagger c_j \\ &= \sum_{i,j} \langle i|\, [A,B]\,|j\rangle\, c_i^\dagger c_j \quad = \quad \Gamma\left([A,B]\right). \end{aligned} \tag{II.D.17}$$

□

In the bosonic case, the proof is analogous up to the switched sign as they commutate instead of the anti-commutate. Also the following theorem holds in the bosonic case, but here, we restrict ourselves to fermions.

Calculating (partial) traces in the Fock space is necessary in many fields in many-particle physics. It was addressed systematically by Levitov et al. [70], who investigated transport properties of solids. He derived a formula to transform the trace operator into a determinant. Instead of calculating the trace directly (which is often non-trivial), Levitov uses the following theorem to relate the trace operator in the Fock space to a determinant in the single-particle space. The proof as shown here was formalized by Kilch [59].

THEOREM II.20 *(Levitov's Formula)*

Be A and B linear operators and $\Gamma(A),\Gamma(B)$ their representations in Fock space. Then holds

$$\mathrm{Tr}\left\{\mathrm{e}^{\Gamma(A)}\mathrm{e}^{\Gamma(B)}\right\} = \det\left(1 + \mathrm{e}^{A}\mathrm{e}^{B}\right). \tag{II.D.18}$$

Proof. By corollary II.16 there exists a matrix C such that $\mathrm{e}^C = \mathrm{e}^A\mathrm{e}^B$, which can be written as an infinite sum of continued commutators. Thus, by lemma II.19, it is

$$\mathrm{e}^C = \mathrm{e}^A\mathrm{e}^B \mapsto \mathrm{e}^{\Gamma(C)} = \mathrm{e}^{\Gamma(A)}\mathrm{e}^{\Gamma(B)}. \tag{II.D.19}$$

We now evaluate $\mathrm{Tr}\left\{\mathrm{e}^{\Gamma(C)}\right\}$ using the Jordan normal form of C. Switching to Jordan basis, C becomes $\mathrm{diag}(\mu_1,...,\mu_n) + K$ with K upper triagular. By construction, K is nilpotent and does not contribute to the trace. Then,

$$\mathrm{Tr}\left\{\mathrm{e}^{\Gamma(C)}\right\} = \mathrm{Tr}\left\{\mathrm{e}^{\Gamma(\mathsf{diag}(\mu_1,\ldots,\mu_n))+\Gamma(K)}\right\}$$

$$= \mathrm{Tr}\left\{\mathrm{e}^{\Gamma(\mathsf{diag}(\mu_1,\ldots,\mu_n))}\right\} = \mathrm{Tr}\left\{\prod_i \mathrm{e}^{\mu_i a_i^\dagger a_i}\right\}$$
$$= \prod_i (1+\mathrm{e}^{\mu_i}) = \det\left(1+\mathrm{e}^{C}\right),$$

and by corollary II.16, we have

$$\mathrm{Tr}\left\{\mathrm{e}^{\Gamma(A)}\mathrm{e}^{\Gamma(B)}\right\} = \mathrm{Tr}\left\{\mathrm{e}^{\Gamma(C)}\right\} = \det\left(1+\mathrm{e}^{C}\right) = \det\left(1+\mathrm{e}^{A}\mathrm{e}^{B}\right). \tag{II.D.20}$$

□

In the present work, we evaluate this determinant numerically. Determinants of the Form

$$\det(\mathbb{1}+A), \tag{II.D.21}$$

where A is some square matrix, are known as Fredholm determinants [98]. This type of derterminants in known to occur regularly in Bethe ansatz [46] and random matrix calculations [29], and there are various methods to treat them analytically as well [32; 65].

II.D.4 Periodic boundary conditions

In periodic boundary conditions (PBC), a free fermion (FF) system is diagonal in the momentum basis. Consider the Nambu spinor $\vec{\Psi}_{\vec{k}}^\dagger = \{c_{\vec{k}}^\dagger, c_{\vec{k}}\}$ containing the creation and annihilation operators for a fermion at momentum $\vec{k}$. As we are addressing one-dimensional (1D) systems, $\vec{k}$ has only one entry and degenerates to a number k. For PBC, k is a good quantum number, and all momentum modes can be considered a two-level system, because there is no scattering to different modes. Therefore, the LE can be calculated per mode, and one obtains the following semi-analytic formula.

THEOREM II.21 *(Bulk Loschmidt echo)*

In a FF system with PBC, the LE can be written as

$$G(t) = \prod_k \left[\cos(\epsilon_k^{\mathsf{f}} t) + \mathsf{i}\,\hat{d}_k^{\mathsf{i}} \cdot \hat{d}_k^{\mathsf{f}} \sin(\epsilon_k^{\mathsf{f}} t)\right]. \tag{II.D.22}$$

Proof. In FF systems, the Hamiltonian takes the form

$$\mathbf{H}^{\mathsf{i,f}} = \sum_{\vec{k}} \vec{\Psi}_{\vec{k}}^\dagger \mathcal{H}_{\vec{k}}^{\mathsf{i,f}} \vec{\Psi}_{\vec{k}}, \qquad \mathcal{H}_{\vec{k}} = \vec{d}_{\vec{k}}^{\,\mathsf{i,f}} \cdot \vec{\sigma}. \tag{II.D.23}$$

The ground state, and therefore the LE, can then be obtained from the Bogoljubov-de-Gennes (BdG) normal mode fermions created (annihilated) by $\eta_k^\dagger$ (η_k). as given in eq. (II.B.23) [107]. In the models we consider (see chapter II.B.5), $\vec{d}_k^{\,\mathsf{i,f}}$ always lie in the yz-plane, and if the Hamiltonian is diagonal,

$$\mathcal{H}_k = \epsilon_k \sigma^z, \qquad \text{or} \qquad \vec{d}_k = \begin{pmatrix} 0 \\ 0 \\ \epsilon_k \end{pmatrix} = \epsilon_k \hat{e}_z. \tag{II.D.24}$$

For arbitrary Hamiltonians restricted to the yz-plane, the Bogoljubov transformation "rotates" the vector $\vec{d}_k$ describing the model to the z-direction, and one easily checks that the Bogoljubov angle is related to the angle between $\vec{d}_k^{\,\mathsf{i}}$ and $\vec{d}_k^{\,\mathsf{f}}$ by

$$2\theta_k = \sphericalangle\left(\vec{d}_k, \hat{e}_z\right). \tag{II.D.25}$$

The factor 2 is due to the fact, that we are considering only half the Brillouin zone. To calculate the LE from definition II.14, we need to know the ground state $|\Psi_\mathsf{G}\rangle$ of $\mathbf{H}^\mathsf{i}$, which is given by a Slater determinant (theorem II.9), and the time evolution operators $U(t) = \mathrm{e}^{-\mathrm{i}\mathbf{H}^{\mathsf{i},\mathsf{f}}t}$. The ground state of the initial Hamiltonian is given by the BdG transfiormation

$$|\Psi_\mathsf{G}\rangle = \prod_k \left(\cos(\theta_k) - \sin(\theta_k)\eta_k^\dagger \eta_{-k}^\dagger\right)|\mathsf{vac}\rangle \qquad \text{and} \tag{II.D.26}$$

$$\begin{aligned}\mathrm{e}^{-\mathrm{i}\mathbf{H}^\mathsf{f}t} &= \prod_{k,-k} \eta_k^\dagger \eta_k \mathrm{e}^{\mathrm{i}\epsilon_k^\mathsf{f} t} \\ &= \prod_{k,-k} \eta_k^\dagger \eta_k \left(\cos(\epsilon_k t) + \mathrm{i}\,\sin(\epsilon_k^\mathsf{f} t)\right).\end{aligned} \tag{II.D.27}$$

Inserting equations (II.D.22) and (II.D.26) into definition II.14 and using the geometric definition of the cosine, $\cos(2\theta_k^\mathsf{f} - 2\theta_k^\mathsf{i}) = \hat{d}_k^\mathsf{i} \cdot \hat{d}_k^\mathsf{f}$, we obtain

$$\begin{aligned}G(t) &= \langle\Psi_\mathsf{G}|\,\mathrm{e}^{\mathrm{i}\mathbf{H}^\mathsf{i}t}\mathrm{e}^{-\mathrm{i}\mathbf{H}^\mathsf{f}t}\,|\Psi_\mathsf{G}\rangle \\ &= \prod_k \left(\cos(\epsilon_k^\mathsf{f} t) - \mathrm{i}\,\cos(\theta_k^\mathsf{i} - \theta_k^\mathsf{f})\sin(\epsilon_k^\mathsf{f} t)\right) \\ &= \prod_k \left(\cos(\epsilon_k^\mathsf{f} t) - \mathrm{i}\hat{d}_k^\mathsf{i} \cdot \hat{d}_k^\mathsf{f}\sin(\epsilon_k^\mathsf{f} t)\right).\end{aligned} \tag{II.D.28}$$

□

II.D.5 Open boundary conditions

As soon as a topological system is considered in open boundary condition (OBC)s, metallic edge modes form, see section II.A.1.iii. These modes are not extended throughout the system, but, as the name suggests, they are localized near the edges of the chain in the 1D case. Further, applying a Fourier transformation to the Hamiltonian does not diagonalize it any longer, and thus k is no good quantum number. Therefore, the analytical solution eq. (II.D.22) does not hold, and it is not known how to calculate the LE analytically.

It is possible though to use a numerical approach, which was developed by Rossini et al. [92] and Levitov et al. [70]. Levitov's idea was to express a trace of an operator by a determinant (theorem II.20). This was wrapped up and put into a nice form by Kilch [59] and Levitov et al. [71]. The following derivation is mainly based on their works.

II.D.5.i Numerical calculation of the LE

To start, let us consider the two Hamiltonians $\mathbf{H}^{\mathsf{i,f}}$ before and after the quench, respectively. In either case, there is a unitary transformation U^ν such that

$$U^\nu \mathbf{H}^\nu U^{\nu\dagger} = \tilde{\mathbf{H}}^\nu = \mathsf{diag}(\lambda_1^\nu, \cdots, \lambda_N^\nu) \tag{II.D.29}$$

is a diagonal matrix, where $\nu = \mathsf{i}, \mathsf{f}$. Without loss of generality we choose $\lambda_i \leq \lambda_j$ for any $i \leq j$. Then, $c_m^{\nu\dagger}$ (c_m^ν) are the creation (annihilation) operators in the m-th single particle state. The corresponding real space creators are then $U^{\nu\dagger} c_m^{\nu\dagger}$. The many-particle ground state is then simply the Slater determinant of the $L/2$ lowest eigenstates of $\mathbf{H}^{\mathsf{i}}$,

$$|\Psi_{\mathsf{G}}\rangle = |\phi_1\rangle \otimes |\phi_2\rangle \otimes \cdots \otimes \left|\phi_{\frac{N}{2}}\right\rangle = \prod_{m=1}^{\frac{N}{2}} c_i^\dagger |\mathsf{vac}\rangle \,. \tag{II.D.30}$$

THEOREM II.22 *(Determinant formula for the Loschmidt echo)*

Let R be the correlation martix $R = (\langle \phi_i | \, \phi_j \rangle)_{ij}$. The LE can be evaluated by calculating

$$G(t) = \left| \det \left(\mathbb{1} - R + R \cdot \mathrm{e}^{-\mathrm{i}\mathbf{H}^{\mathsf{f}} t} \right) \right| \tag{II.D.31}$$

Proof. We use theorem II.20 to evaluate the LE. First, we rewrite the definition II.14, as we need a trace of exponential functions. As mentioned in section II.D.1, the time evolution under the initial Hamiltonian acts on the ground state of $\mathbf{H}^{\mathsf{i}}$ and therefore only adds a phase factor. We are only interested in the Loschmidt return rate (LRR) which only depends on the absolute value of $G(t)$. In this case, we omit this time evolution.

$$G(t) = \langle \Psi_{\mathsf{G}} | \, \mathrm{e}^{-i\mathbf{H}^{\mathsf{f}} t} \, |\Psi_{\mathsf{G}}\rangle = \mathrm{Tr}\left\{ \rho_{\mathsf{G}} \mathrm{e}^{-\mathrm{i}\mathbf{H}^{\mathsf{f}} t} \right\}, \tag{II.D.32}$$

where $|\Psi_{\mathsf{G}}\rangle \langle \Psi_{\mathsf{G}}| = \rho_G$ is the density matrix in the many-particle ground state. The density matrix can also be written as

$$\rho_{\mathsf{G}} = \frac{1}{\mathcal{Z}} \mathrm{e}^{-\beta \Gamma(\mathbf{H}^{\mathsf{i}})} \tag{II.D.33}$$

with the partition function

$$\mathcal{Z} = \mathrm{Tr}\left\{ \mathrm{e}^{-\beta \Gamma(\mathbf{H}^{\mathsf{i}})} \right\} = \det\left(1 + \mathrm{e}^{\beta \mathbf{H}^{\mathsf{i}}}\right). \tag{II.D.34}$$

The LE then becomes

$$\begin{aligned} G(t) &= \frac{1}{\mathcal{Z}} \mathrm{Tr}\left\{ \mathrm{e}^{-\beta \Gamma(\mathbf{H}^{\mathsf{i}})} \mathrm{e}^{-\mathrm{i}\Gamma(\mathbf{H}^{\mathsf{f}}) t} \right\} \\ &= \frac{1}{\mathcal{Z}} \det\left(1 + \mathrm{e}^{-\beta \mathbf{H}^{\mathsf{i}}} \mathrm{e}^{-\mathrm{i}\hat{\mathbf{H}}^{\mathsf{f}} t}\right) \\ &= \frac{1}{\mathcal{Z}} \det\left(1 + \mathrm{e}^{-\beta \mathbf{H}^{\mathsf{i}}} - \mathrm{e}^{-\beta \mathbf{H}^{\mathsf{i}}} + \mathrm{e}^{-\beta \mathbf{H}^{\mathsf{i}}} \mathrm{e}^{-\mathrm{i}\hat{\mathbf{H}}^{\mathsf{f}} t}\right) \\ &= \det\left(\frac{1 + \mathrm{e}^{-\beta \mathbf{H}^{\mathsf{i}}}}{1 + \mathrm{e}^{-\beta \mathbf{H}^{\mathsf{i}}}} - \frac{\mathrm{e}^{-\beta \mathbf{H}^{\mathsf{i}}}}{1 + \mathrm{e}^{-\beta \mathbf{H}^{\mathsf{i}}}} - \frac{\mathrm{e}^{-\beta \mathbf{H}^{\mathsf{i}}} \mathrm{e}^{-\mathrm{i}\hat{\mathbf{H}}^{\mathsf{f}} t}}{1 + \mathrm{e}^{-\beta \mathbf{H}^{\mathsf{i}}}} \right) \\ &= \det\left(1 - n + n \mathrm{e}^{-\mathrm{i}\hat{\mathbf{H}}^{\mathsf{f}} t}\right). \end{aligned} \tag{II.D.35}$$

We introduced the shorthand $\hat{\mathbf{H}}^{\mathsf{f}} = U^{\mathsf{i}}\mathbf{H}^{\mathsf{f}}U^{\mathsf{i}\dagger}$ and the fermion number operator in the single-particle space

$$n = \frac{\mathrm{e}^{-\beta\mathbf{H}^{\mathsf{i}}}}{1+\mathrm{e}^{-\beta\mathbf{H}^{\mathsf{i}}}}. \tag{II.D.36}$$

This is the LE in the energy basis. Note, that this basis may change during the quench! We now need to transform this formula into the real space basis. Because $\det(U) = 1$ for any unitary operator U and $\det(AB) = \det(A)\det(B)$ for any operators A, B, we only need to multiply the determinant with an eligible combination of the operators U^{i} (U^{f}) diagonalizing the initial (final) Hamiltonian and their inverses.

$$\begin{aligned} G(t) &= \det(U^{\mathsf{i}\dagger})\det\left(1-n+n\mathrm{e}^{-\mathrm{i}\tilde{\mathbf{H}}^{\mathsf{f}}t}\right)\det(U^{\mathsf{i}}) \\ &= \det\left(U^{\mathsf{i}\dagger}U^{\mathsf{i}} - U^{\mathsf{i}\dagger}nU^{\mathsf{i}} + U^{\mathsf{i}\dagger}nU^{\mathsf{i}}U^{\mathsf{i}\dagger}\mathrm{e}^{-\mathrm{i}\hat{\mathbf{H}}^{\mathsf{f}}t}U^{\mathsf{i}}\right) \\ &= \det\left(1-R+R\mathrm{e}^{-\mathrm{i}\mathbf{H}^{\mathsf{f}}t}\right). \end{aligned} \tag{II.D.37}$$

In the last line, we resubstituted $\hat{\mathbf{H}}^{\mathsf{f}}$. R denotes the correlation matrix of the ground state. Using the fact that n represents the ground state of $\mathbf{H}^{\mathsf{i}}$ and that U^{i} contains its eigenvectors ϕ_j, one finds that

$$\begin{aligned} U^{\mathsf{i}}nU^{\mathsf{i}\dagger} &= \begin{pmatrix} \phi_1^\dagger & \cdots & \phi_N^\dagger \end{pmatrix} \left(\begin{array}{c|c} \mathbb{1}_{\frac{N}{2}} & 0 \\ \hline 0 & 0 \end{array}\right) \begin{pmatrix} \phi_1 \\ \vdots \\ \phi_N \end{pmatrix} \\ &= \begin{pmatrix} \phi_1^\dagger & \cdots & \phi_{\frac{N}{2}}^\dagger \end{pmatrix} \begin{pmatrix} \phi_1 \\ \vdots \\ \phi_{\frac{N}{2}} \end{pmatrix} \\ &= \left(\sum_{m=1}^{\frac{N}{2}} \bar{\phi}_m(i)\phi_m(j)\right)_{ij} \equiv R, \end{aligned} \tag{II.D.38}$$

where $\phi_l(k)$ denotes the k-th component of the l-th eigenvector. □

II.D.5.ii Simplification for the SSH model

Here R is the correlation matrix in the ground state of $\mathbf{H}^{\mathsf{i}}$. Since $\mathbf{H}^{\mathsf{i}}$ is quadratic one can rewrite the matrix elements of R in terms of components of the eigenvectors of $\mathbf{H}^{\mathsf{i}}$, that are populated in the ground state $|\Psi_{\mathsf{G}}\rangle$. Starting with the usual definition of a two-point correlation function, the $R_{i,j}$ is defined as

$$\begin{aligned} R_{ij} &= \langle\Psi_{\mathsf{G}}|\, c_i^\dagger c_j \,|\Psi_{\mathsf{G}}\rangle \\ &= \langle\phi_1|\,\langle\phi_2|\cdots\left\langle\phi_{\frac{N}{2}}\right|\, c_i^\dagger c_j \left|\phi_{\frac{N}{2}}\right\rangle\cdots|\phi_2\rangle\,|\phi_1\rangle \\ &= \sum_m \langle\phi_m|\, c_i^\dagger c_j \,|\phi_m\rangle\,. \end{aligned} \tag{II.D.39}$$

Here, the fact that the eigenvectors of $\mathbf{H}^{\mathsf{i}}$, $|\phi_m\rangle$ form a complete basis of the Hilbert space is exploited. Now, the eigenvectors can be created from the vacuum by applying the fermionic creation operators on

each lattice site.

$$\begin{aligned} R_{ij} &= \sum_m \sum_{l,l'} \bar{\phi}_m(l)\phi_m(l') \langle 0| c_l c_i^\dagger c_j c_{l'}^\dagger |0\rangle \\ &= \sum_m \bar{\phi}_m(i)\phi_m(j). \end{aligned} \tag{II.D.40}$$

The sum on l collapses since $c_l c_i^\dagger = \delta_{l,i}$ and a similar argument applies on l'. The next step is to write this sum over eigenvector components as a matrix product. Since only the lowest $\frac{N}{2}$ eigenvalues are involved, we need to introduce a selector matrix

$$A = \left(\begin{array}{c|c} \mathbb{1}_{\frac{N}{2}} & 0 \\ \hline 0 & 0 \end{array}\right). \tag{II.D.41}$$

If now

$$U^{\mathsf{i}}\mathbf{H}^{\mathsf{i}}U^{\mathsf{i}\dagger} = \tilde{\mathbf{H}}^{\mathsf{i}} = \begin{pmatrix} E_1 & & 0 \\ & \ddots & \\ 0 & & E_n \end{pmatrix} \tag{II.D.42}$$

is diagonal and U^{i} is a unitary matrix and $i < j \Rightarrow E_i \leq E_j$ are sorted,

$$A \cdot U^{\mathsf{i}} = \left(\begin{array}{c} U^{\mathsf{i}}_{1,1\cdots N} \\ \vdots \\ \hline U^{\mathsf{i}}_{\frac{N}{2},1\cdots N} \\ \hline 0 \end{array}\right) \tag{II.D.43}$$

will contain the $\frac{N}{2}$ lowest eigenvectors of $\mathbf{H}^{\mathsf{i}}$. Using the above notation, eq. (II.D.40) becomes

$$R_{ij} = (AU^{\mathsf{i}})^\dagger AU^{\mathsf{i}} = U^{\mathsf{i}\dagger}AU^{\mathsf{i}}, \tag{II.D.44}$$

since $A^\dagger A \equiv A$. In order to calculate the LE from eq. (II.D.31), we use this representation of R together with the fact, that U^{i} is unitary and thus $\det U^{\mathsf{i}} \det U^{\mathsf{i}\dagger} \equiv 1$. This means we can rewrite eq. (II.D.31) as

$$\begin{aligned} G(t) &= \left|\det\left(U^{\mathsf{i}}\right) \det\left(\mathbb{1} - R + R \cdot \mathrm{e}^{-\mathrm{i}\mathbf{H}^{\mathsf{f}}t}\right) \det\left(U^{\mathsf{i}^\dagger}\right)\right| \\ &= \left|\det\left(\mathbb{1} - A + AU^{\mathsf{i}}U^{\mathsf{f}}\mathrm{e}^{-\mathrm{i}\tilde{\mathbf{H}}^{\mathsf{f}}t}U^{\mathsf{f}\dagger}U^{\mathsf{i}\dagger}\right)\right|, \end{aligned} \tag{II.D.45}$$

where $\tilde{\mathbf{H}}^{\mathsf{f}} = U^{\mathsf{f}}\mathbf{H}^{\mathsf{f}}U^{\mathsf{f}\dagger}$ is diagonal. The argument of the determinant is block triangular and consists $\frac{N}{2}$ rows of numbers (we will split these rows in two quadratic matrices of dimension $\frac{N}{2} \times \frac{N}{2}$, C_{left} and C_{right}) and zeros and the unity matrix in the lower half, such that the argument becomes

$$\mathbb{1} - A + AU^{\mathsf{i}}U^{\mathsf{f}}\mathrm{e}^{-\mathrm{i}\tilde{\mathbf{H}}^{\mathsf{f}}t}U^{\mathsf{f}\dagger}U^{\mathsf{i}\dagger} = \left(\begin{array}{c|c} C & D \\ \hline 0 & \mathbb{1}_{\frac{N}{2}} \end{array}\right). \tag{II.D.46}$$

We evaluate this using the Laplace decomposition on the lowest row $\frac{N}{2}$ times. This yields up to a sign (which is absorbed by the absolute value)

$$G(t) = |\det(C)| \tag{II.D.47}$$

which with the definition $A' = \left(\mathbb{1}_{\frac{N}{2}}|0\right)$ can be written as

$$C = A'U^{\mathsf{i}}U^{\mathsf{f}}\mathrm{e}^{-\mathrm{i}\tilde{\mathbf{H}}^{\mathsf{f}}t}U^{\mathsf{f}\dagger}U^{\mathsf{i}\dagger}A'^{T}. \tag{II.D.48}$$

This result reduces the computation of the Lohschmidt echo to the evaluation on a $\frac{N}{2} \times \frac{N}{2}$ determinant instead of a $N \times N$ determinant. In terms of computation complexity, the determinant scales as $\mathcal{O}(n^3)$ when using the LU decomposition. Therefore, the total computation time is reduced by a factor of up to 8 with this formula.

II.D.5.iii Generic bilinear Hamiltonians

In the previous section, we discussed an algorithm to calculate the LE in open systems in the case when the first-quantized Hamiltonian becomes

$$\mathbf{H} = \vec{\Phi}^\dagger \mathcal{H} \vec{\Phi}, \quad \text{where} \quad \vec{\Phi}^\dagger = \begin{pmatrix} c_1^\dagger & \cdots & c_N^\dagger \end{pmatrix} \tag{II.D.49}$$

in terms of the Nambu spinors. The derivation shown in the following is similar to ref. [92], except that for the Kitaev chain, the additional degree of freedom is given by unit-cell doubling in the Majorana basis as opposed to a spin degree of freedom in [92]. This does not cover those cases where eq. (II.B.28) contains correlations of the type $c_i^\dagger c_j^\dagger$ or $c_i c_j$. To address these systems, like for example the Kitaev chain, an additional Bogoljubov-de-Gennes (BdG) transformation is required. We introduce the normal mode fermions

$$\begin{pmatrix} \eta_1 \\ \vdots \\ \eta_N \end{pmatrix} \equiv \vec{\Gamma} = V\vec{\Phi} + W\vec{\Phi^\dagger} \tag{II.D.50}$$

which are created (annihilated) by $\eta_k^\dagger$ (η_k). In this notation, the vectors $\vec{\Phi}^\dagger(\vec{\Phi})$ contain the creators (annihilators) in the Fock space. We will show, that the matrices V and W are made up from entries of the matrix which diagonalizes the Hamiltonian later on. The operators η_k are the BdG normal mode fermions from eq. (II.B.23).

Here, we used the anti-commutation relation of $\eta_k^\dagger$ and η_k. We define D as the diagonal matrix which contains the positive (negative) eigenvalues of $\mathbf{H}$ in descending (ascending) order,

$$D = \begin{pmatrix} \epsilon_1 & & & & & \\ & \ddots & & & 0 & \\ & & \epsilon_N & & & \\ & & & -\epsilon_1 & & \\ & 0 & & & \ddots & \\ & & & & & -\epsilon_N \end{pmatrix}. \tag{II.D.51}$$

with $i < j \Rightarrow \epsilon_i \geq \epsilon_j > 0$. According to eq. (II.B.28), it is also

$$\begin{aligned} \mathbf{H} &= \vec{\Phi}^\dagger \mathcal{H} \vec{\Phi} \\ &= \frac{1}{2} \vec{\Gamma}^\dagger U \mathcal{H} U^\dagger \vec{\Gamma}, \end{aligned} \tag{II.D.52}$$

i.e. U diagonalizes the (first quantized) Hamiltonian $U\mathcal{H}U^\dagger = D$. Sorting the eigenvectors in the above mentioned way and comparing eq. (II.D.52) to eq. (II.D.50) then yields

$$U = \left(\begin{array}{c|c} V & W \\ \hline W & V \end{array}\right) \tag{II.D.53}$$

Because the eigenvalues $\pm\epsilon_k$ of $\mathcal{H}$ are real, also the entries of V and W can be chosen real. Inverting eq. (II.D.50) gives

$$\vec{\Phi} = V^T\vec{\Gamma} + W^T\vec{\Gamma}^\dagger, \tag{II.D.54}$$

and thus the correlation matrix is

$$R = \left(\begin{array}{c|c} W^TW & W^TV \\ \hline V^TW & V^TV \end{array}\right). \tag{II.D.55}$$

The LE is then given by theorem II.20.

II.E Dynamical phase transitions

The purpose of this work to investigate *dynamical phase transitions (DPT)* in free fermion (FF) systems. The concept of DPT was introduced by Heyl et al. [50] in 2012. In literature, there are different definitions of DPT, but we will use the one according to ref. [50]. This section gives an introduction in the physical background of DPT, as well as an overview of the "state of the art".

In the first place, we review equilibrium phase transitions (EPT) in terms of Landau theory. Then, we discuss properties of a generalized partition function such as *Fisher zeros* [34] or *Lee-Yang zeros* [68]. The last few sections are dedicated to the interplay of topologically non-trivial phases and dynamical phase transitions and the definition of a *dynamical topological order parameter (DTOP)* as proposed by Budich and Heyl [14] in 2015.

II.E.1 Phase transitions

The following review of this theory is mostly based on chapter 7 in ref. [95] and chapter 39 and 40 in ref. [37]. In thermodynamics, phase transitions are characterized by non-analyticities of an applicable thermodynamic potential as functions of an order parameter. For example, at constant pressure $p = p_0$, water evaporates at a certain critical temperature T_c. The resulting gas has a much larger volume that the liquid, i.e. at constant pressure, the volume $V = V(T)$ changes non-analytically as a function of temperature. In this case, volume is the *order parameter* of the EPT. Note, that in equilibrium thermodynamics, the potential V is not a function of time.

Note that the choice of the order parameter is not unique: If $V = V_0$ instead of p is kept constant, p becomes the order parameter. If neither are fixed, any can be chosen as the order parameter. Here we assume that the potential in question is the free energy, but it can be another potential if the model requires that. Ehrenfest introduced a phenomenological classification of phase transitions by the nature of the non-analyticities.

At these non-analyticities, there is a transition from an ordered to an unordered state, because the free energies of both phases intersect, and due to the principle of the least action, the system chooses to change its phase in order to lower its free energy. This process is called *spontaneous symmetry breaking*. When a (unordered) molten metal cools down, it solidifies to a (ordered) crystal, in which (continuous) translation symmetry is broken into a lattice translation symmetry.

DEFINITION II.23 *(phase transition of n-th order, according to Ehrenfest)*

Let $f = f(\phi_1, \ldots, \phi_N)$ be a thermodynamic potential dependent on N parameters $\phi_1, \ldots, \phi_N$. A phase transition is of order n, iff $\forall l \in \mathbb{N} : 0 < l < n$ the derivatives

$$\left(\prod_{k=1}^{l} \frac{\partial}{\partial \phi_{i_k}} \right) f \qquad \forall k \in \{1, \ldots, l\} : i_k \in \{1, \ldots, N\} \tag{II.E.1}$$

exist and are continuous, but at least one of the derivatives

$$\left(\prod_{k=1}^{n} \frac{\partial}{\partial \phi_{i_k}} \right) f \tag{II.E.2}$$

is singular at the critical point.

Landau theory focusses on first and second order phase transitions. Its main idea is, that the relevant thermodynamic potential (usually the free energy) is approximated by a series expansion near the critical value of the order parameter. For simplicity, we assume that there is $n = 1$ order parameter, although in reality, there is often more than one. In the ferromagnetic to paramagnetic transition, the order parameter is the magnetization $\vec{M}$, which is a three-component vector, i.e. $n = 3$.

Landau's initial ansatz was to write the free energy for $|T - T_\mathrm{c}| \ll T_\mathrm{c}$ as

$$f(T, h, \phi) = F_0(T) + V \left(a \left(T - T_\mathrm{c} \right) \phi^2 + u\phi^4 - h\phi \right). \tag{II.E.3}$$

Here, $u > 0$, because otherwise, no global minimum of the energy would exist. Depending on the signs of a and h, this equation can describe both first and second order EPT. Let for example $a < 0$ and $h = 0$. In this case, one obtains the minimum of f with respect to ϕ, which is the equilibrium value of the free energy $\bar{\phi}_0$. One finds $\bar{\phi}_0 = 0$ for $T \geq T_\mathrm{c}$, while for $T < T_\mathrm{c}$,

$$\bar{\phi}_0 = \sqrt{\frac{a}{2u}(T_\mathrm{c} - T)}. \tag{II.E.4}$$

Thus Landau theory reproduces the usual second-order behaviour, such as the Curie curve for the ferromagnetic-paramagnetic transition, as shown in figure II.20.

On the other hand, thermodynamic quantities can be calculated using a statistical mechanics approach based on the partition function

$$\mathcal{Z} = \mathrm{Tr} \left\{ \mathrm{e}^{-\beta \mathbf{H}} \right\}. \tag{II.E.5}$$

In this equation, we added the boundary state $|\Psi_0\rangle$ in the second equality, the superscript indicating that this equality only holds in this boundary. The free energy is related to the partition function by

$$f = -k_\mathrm{B} T \log(\mathcal{Z}). \tag{II.E.6}$$

It is $\mathcal{Z}(T, h, \phi) \geq 1$, and therefore $f(T, h, \phi) \leq 0$ for real parameters. Nonetheless that $\mathcal{Z}$ may have zeros in the complex plane, which are discussed in the following section.

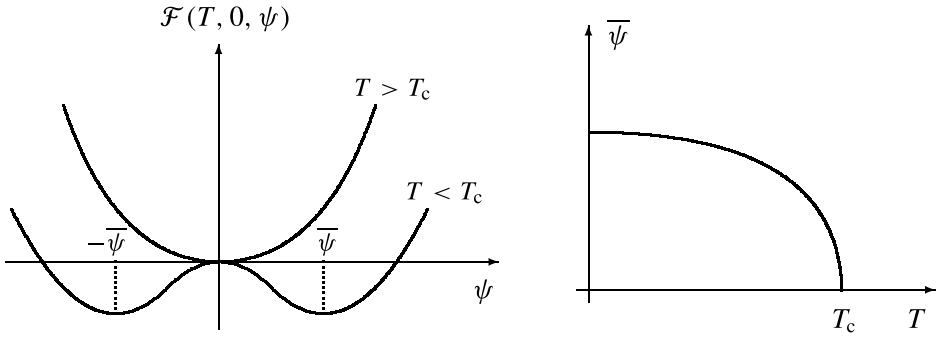

Figure II.20: Illustration of the bifurcation in the solution of Landau's ansatz eq. (II.E.3). For $T \geq T_c$, the contribution of the quadratic term is not important, while it creates a double minimum for $T < T_c$. Picture taken from [37]

.

II.E.2 Lee-Yang- and Fisher zeros

Formally, the Loschmidt echo (LE) from definition II.14 resembles to a partition function with fixed boundaries

$$\mathcal{Z} = \mathrm{Tr}\left\{\mathrm{e}^{-\beta \mathbf{H}}\right\} \overset{\mathsf{BC}}{\leftrightarrow} \langle \Psi_0 | \, \mathrm{e}^{-\beta \mathbf{H}} \, | \Psi_0 \rangle \, . \tag{II.E.7}$$

With this background, the idea of viewing the partition function (or the Lohschmidt echo (LE)) as a function of a complex parameter is not far. It was addressed independently and with slightly different approaches by Lee and Yang [68] and Fisher [34].

Lee and Yang stared from the grand canonical ensemble, where the partition function is a function of the chemical potential μ and inverse temperature $-\beta = \frac{1}{k_B T}$,

$$\mathcal{Z}(\mu, \beta) = \mathrm{Tr}\left\{\mathrm{e}^{-\beta(\mathbf{H}+\mu N)}\right\}. \tag{II.E.8}$$

In this case, the relevant potential is no longer the free energy, but the grand canonical potential. They allowed complex values for μ and found, that the partition function becomes a polynomial in μ of degree N,

$$\mathcal{Z}(z, \beta) = \mathcal{P}\left[\mathrm{e}^{-\beta \mathbf{H}}\right] \qquad \text{with} \tag{II.E.9}$$

$$\mathcal{P}(\xi) = \sum_{n=0}^{N} p_n \xi^n. \tag{II.E.10}$$

The main result of their work is the following theorem.

THEOREM II.24 *(Lee-Yang theorem)*

Assume a two-dimensional (2D) lattice gas model (e.g. Ising model). Let the interaction between two particles at sites i and j be

$$u_{ij} = \begin{cases} \infty & i = j \\ f(i,j) \leq 0 & i \neq j \end{cases} \tag{II.E.11}$$

for some negative-valued function f. The Hamiltonian is $\mathbf{H} = \sum_{i,j} u_{ij} c_i^\dagger c_j$. Then, all the roots of $\mathcal{P}(\xi)$ lie on the unit circle in the complex plane.

Fisher [34] started from a canonical ensemble and chose β as the complex parameter. In this case, the zeros of the resulting function

$$\mathcal{Z}(z) = \mathrm{Tr}\left\{\mathrm{e}^{-z\mathbf{H}}\right\} \tag{II.E.12}$$

are not simple functions, but can show a very odd behaviour, such as filling whole areas in $\mathbb{C}$ densely [106].

For $z = \beta \in \mathbb{R}$, eq. (II.E.12) is the partition function, while for $z = \mathrm{i}t \in \mathbb{I} \equiv \mathrm{i}\mathbb{R}$, it is similar to the LE, except for the missing boundary state $|\psi_0\rangle$. As shown in the proof of theorem II.20,

$$\langle\psi_0|\,\mathrm{e}^{-z\mathbf{H}}\,|\psi_0\rangle \overset{\mathsf{BC}}{\leftrightarrow} \mathrm{Tr}\left\{\rho_{\psi_0}\mathrm{e}^{-z\mathbf{H}}\right\}. \tag{II.E.13}$$

The left-hand side of eq. (II.E.13) corresponds to the partition function of the system in boundaries seperated by z [50]. The boundary state $|\psi_0\rangle$ was chosen to be the ground state of the system, and thus in the real space basis at half filling, $\rho_{\psi_0} = |\psi_0\rangle\langle\psi_0| = \frac{1}{2}\mathbb{1}$.

It is straight-forward to define a function

$$f(z) = -\lim_{N\to\infty} \frac{1}{N} \log \mathcal{Z}(z). \tag{II.E.14}$$

Along the real axis, $f(z)$ resembles to the free energy (up to a factor $k_\mathrm{B}T$) and is strictly positive. It is therefore called *dynamical free energy*. Generally, negative values are possible, and thus zeros can occur in the complex plane. In particular, zeros are possible even for finite N on the imaginary axis, i.e. for real times. This means, that we have to distinguish two possible cases in which DPT may occur [3]:

1. The dynamical free energy is non-zero at a given $z = \mathrm{i}t$, but it becomes zero in the limit $N \to \infty$. This case is analogous to EPT.
2. $\mathcal{Z}(\mathrm{i}t) = 0$ at finite N. This type of zeros does not occur on the real (inverse temperature) axis, and has no analogue in equilibrium.

Introducing an eigenbasis of $\mathbf{H}$, eq. (II.E.12) becomes a sum over exponentials of numbers, which are holomorphic, and therefore also $\mathcal{Z}(z)$ must be holomorphic. By the Weierstrass factorization theorem [89], it can be written as

$$\mathcal{Z}(z) = \mathrm{e}^{h(z)} \prod_j \left(1 - \frac{z}{z_j}\right) \tag{II.E.15}$$

with $\forall j:\ \mathcal{Z}(z_j) = 0$, and $h(z)$ an entire function. $f(z)$ then becomes

$$f(z) = -\lim_{N\to\infty} \frac{1}{N} \left\{ h(z) + \sum_j \log\left(1 - \frac{z}{z_j}\right) \right\}. \tag{II.E.16}$$

The singularities of this function are then only determined by the solutions z_j of $\mathcal{Z}(z) = 0$. If $z_j \in \mathbb{I}$ for certain j, the LE shows singularities, and the system undergoes *dynamical phase transitions (DPT)*. Analogously with the definition of thermal phase transitions on the real axis, one might understand these zeros as DPT. It should be noticed that this is a fundamental difference to EPT which are generally only possible in the thermodynamic limit. The interpretation as DPT is supported by analytical results for the one-dimensional transverse Ising model showing that the Fisher zeros form lines in the complex plane which cross the imaginary axis $z = \mathrm{i}t$ only if the quench leads across the equilibrium quantum critical point [50].

II.E.3 DPT and topology

In this section, we give a wrap-up of the current state of the field of dynamical phase transitions (DPT). We review the latest results, but we mostly discuss open questions in the field.

Originally, DPT have been discussed in the transverse field Ising model [84]. In this specific system, a direct connection between the quantum phase transition from the paramagnetic to the ferromagnetic phase and the occurrence of singularities in the Loschmidt echo (LE) was established [50].

Since, DPT have been shown to occur in a variety of systems [36; 51; 53; 97]. It is however not clear, how general the analogy between DPT and EPT is. There is also interest in the interplay of topological phase transitions (TPT) and DPT, because in this case, there is no symmetry breaking involved, and the details of this relation seem to be more subtle [3; 106]. The impact of topological edge modes on non-equilibrium dynamics is also completely unknown so far.

For quadratic Hamiltonians, it has been shown that crossing a TPT will cause DPT to occur [108]. In those models, the Hamiltonian takes the form of eq. (II.B.1), or when it is diagonalized using a Bogoljubov-de-Gennes (BdG) transformation, it reads (c.f. eq. (II.D.23))

$$\mathbf{H} = \sum_k \vec{\Psi}_k^\dagger \mathcal{H}_k \vec{\Psi}_k, \qquad \text{where} \qquad \mathcal{H}_k = \vec{d}_k \cdot \vec{\sigma}. \tag{II.E.17}$$

The LE can be obtained from theorem II.21

$$G(t) = \prod_k \left[\cos(\epsilon_k^{\mathsf{f}} t) + \mathrm{i}\, \hat{d}_k^{\mathsf{i}} \cdot \hat{d}_k^{\mathsf{f}} \sin(\epsilon_k^{\mathsf{f}} t) \right], \tag{II.E.18}$$

and the Fisher zeros are given by [108]

$$z_n(k) = \frac{\mathrm{i}\pi}{\epsilon_k^{\mathsf{f}}} \left(n + \frac{1}{2} \right) - \frac{1}{\epsilon_k^{\mathsf{f}}} \mathrm{arth} \left(\hat{d}_k^{\mathsf{i}} \cdot \hat{d}_k^{\mathsf{f}} \right), \tag{II.E.19}$$

where arth is the hyperbolic arc tangent function. In section II.E.2, we showed that DPT occur if $G(t) = 0$. From eq. (II.E.18), we immediately find the eligible condition

$$G(t) = 0 \quad \Rightarrow \quad \exists k = k_{\mathsf{c}} : \hat{d}_{k_{\mathsf{c}}}^{\mathsf{i}} \cdot \hat{d}_{k_{\mathsf{c}}}^{\mathsf{f}} = 0, \tag{II.E.20}$$

because sine and cosine are never both zero for the same argument. We call $k = k_{\mathsf{c}}$ a critical momentum.

These momenta yield time scales on which DPT occur, because

$$G(t) = \cos(\epsilon^{\mathrm{f}}_{k_\mathrm{c}} t) \times \prod_{k \neq k_\mathrm{c}} \left[\cos(\epsilon^{\mathrm{f}}_k t) + \mathrm{i}\, \hat{d}^{\mathrm{i}}_k \cdot \hat{d}^{\mathrm{f}}_k \sin(\epsilon^{\mathrm{f}}_k t) \right] \tag{II.E.21}$$

obviously has zeros at $\epsilon^{\mathrm{f}}_{k_\mathrm{c}} t = \left(n + \frac{1}{2}\right) \pi$, or

$$t^{(n)}_\mathrm{c} = \frac{\pi}{\epsilon^{\mathrm{f}}_{k_\mathrm{c}}} (2n+1) \tag{II.E.22}$$

with $n \in \mathbb{Z}$. This result is consistent with refs. [14; 108; 96], although the notation may differ.

II.E.3.i Vajna-Dóra theorem

So far, we have shown that DPT occur at times $t^{(n)}_\mathrm{c}$, iff we find a critical momentum k_c such that $\hat{d}^{\mathrm{i}}_{k_\mathrm{c}} \cdot \hat{d}^{\mathrm{f}}_{k_\mathrm{c}} = 0$, and so far this conclusion is indeed an equivalence, as one easily checks. More interesting is the *Vajna-Dóra (VD) theorem*, because it provides a link to a different class of transitions. The proof given in ref. [108] includes one-dimensional (1D) and 2D models. Here, we only give the proof for the 1D case.

THEOREM II.25 *(Vajna-Dóra theorem)*

If a 1D FF system is quenched across a TPT, DTP will occur.

Proof. We prove the theorem in two steps.

1. *The vectors $\vec{d}^{\mathrm{i}}_k$ and $\vec{d}^{\mathrm{f}}_k$ are restricted to a plane.*
   Consider a quench in a 1D topological FF model from an initial Hamiltonian defined by $\vec{d}^{\mathrm{i}}_k$ to the final Hamiltonian $\vec{d}^{\mathrm{f}}_k$. In this case, the possible symmetry classes are AIII (chiral) BDI (chiral and particle-hole symmetric) [1]. For the Hamiltonians in BdG form, the time reversal (TRS) and the particle-hole symmetry (PHS) are then given by (see eq. (II.B.32), eq. (II.B.33), and ref. [93])

   $$\begin{aligned} \mathcal{T}: &\quad \mathcal{H} = U^\dagger_\mathcal{T} \mathcal{H}^* U_\mathcal{T} \\ \mathcal{C}: &\quad \mathcal{H} = -U^\dagger_\mathcal{C} \mathcal{H}^* U_\mathcal{C} \end{aligned} \tag{II.E.23}$$

   with $\mathcal{H}^{\mathrm{i,f}} = \vec{d}^{\mathrm{i,f}}_k \cdot \vec{\sigma}$. In this case, the x- and y-components of the $\vec{d}$s are odd functions of k, while the z component is even. At $k = 0 \equiv \pi$, the vectors therefore point in the z direction. In the SSH model and the Kitaev chain, $d^x_k = 0$ and thus, $\vec{d}^{\,\mathrm{i,f}}$ lie in the yz-plane.

2. *If the winding numbers of $\vec{d}^{\mathrm{i}}_k$ and $\vec{d}^{\mathrm{f}}_k$ differ, $\hat{d}^{\mathrm{i}}_k \cdot \hat{d}^{\mathrm{f}}_k$ at least one has a zero*
   The winding numbers are calculated as integrals of the curvature of the trajectory of $\vec{d}^{\,\mathrm{i,f}}_k$ in parameter space,

   $$\begin{aligned} \nu &= \frac{1}{2\pi} \oint \left(\vec{d}_k \times \left(\frac{\partial \vec{d}_k}{\partial k} \right) \right) \mathrm{d}k \\ &= \frac{1}{2\pi} \oint \left(d^z_k \left(\frac{\partial d^y_k}{\partial k} \right) - d^y_k \left(\frac{\partial d^z_k}{\partial k} \right) \right) \mathrm{d}k. \end{aligned} \tag{II.E.24}$$

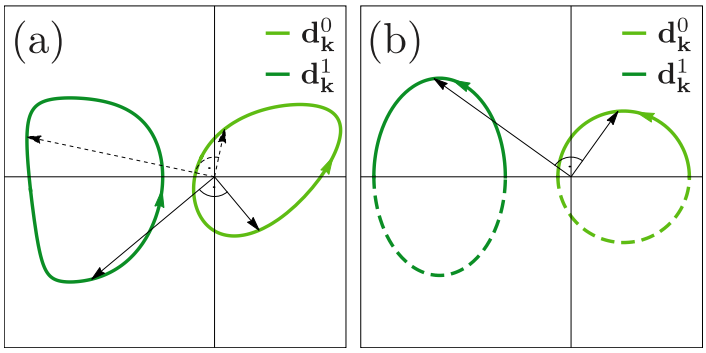

Figure II.21: Illustration of the existence of perpendicular vectors if the quench connects different topological phases. The plots show the situation for TI in the symmetry classes (a) AIII and (b) BDI. Picture adapted from [108]

This number counts, how often the parameter vector winds around the origin. In figure II.21, the situations for both symmetry classes are shown, and in both cases, for the left circle, $\nu = 0$, while on the right, $\nu = 1$. Then, because one of the vectors "moves ahead" of the other, because when sweeping the whole Brillouin zone, they must collect a "phase difference" of 2π. The vectors only move in a plane, therefore there must exist a k_c such that which implies the occurrence of a DPT.

□

II.E.3.ii Dynamical topological order parameter

Having a connection between TPT and DPT established, a straight-forward question is if there is some equivalent to the Berry curvature, or the Chern number. Such a quantity, called *dynamical topological order parameter (DTOP)*, was proposed in 2015 by Budich and Heyl [14]. Another naturally arising question is, if one considers topological FF with open boundary conditions, whether or not there is some sort of bulk-boundary correspondence (BBC). This topic was to the best of our knowledge not addressed so far.

In order to define the DTOP, we consider the LE (eq. (II.E.18)) in polar coordinates,

$$G(t) = \prod_k r_k(t) \mathrm{e}^{\mathrm{i}\phi_k(t)}. \tag{II.E.25}$$

Instead of the radius $r_k(t)$, we are now interested in the phase $\phi_k(t)$. For the equilibrium case, the total phase of a time evolved wave function is a sum of a dynamical and a geometrical contribution, the latter being the Berry phase (see section II.A.1.ii). A similar geometric contribution in a generalized interference setting [80] and is known as the *Pancharatnam geometric phase (PGP)*. There is no obvious way to do a similar calculation in the dynamical case to obtain a closed expression for the geometrical phase, but numerically, we can calculate it because we know the dynamical phase. Therefore, we define

$$\phi^\mathsf{G}_k(t) = \phi_k(t) - \phi^\mathsf{dyn}_k(t) = \phi_k(t) - \epsilon^\mathsf{f}_k \left(\hat{d}^\mathsf{i}_k \cdot \hat{d}^\mathsf{f}_k\right) t, \tag{II.E.26}$$

and we assume all the above mentioned phases to be defined on the interval $(-\pi, \pi]$. The reality condition $\phi_\pi(t) - \phi_0(t) = n2\pi \equiv 0$ ensures that $\phi^\mathsf{G}_0(t) = \phi^\mathsf{G}_\pi(t) = m2\pi \equiv 0$ for $n, m \in \mathbb{Z}$. This is due to the aide lemma in the proof of theorem II.25.

The DTOP should count, how often the geometric phase wraps around the unit circle as k sweeps through the Brillouin zone, i.e. how often it wraps the interval $(-\pi, \pi]$. According to Budich and Heyl [14], we give the following definition:

DEFINITION II.26 *(Dynamical topological order parameter)*

Let ϕ_k^{G} be the PGP of the LE. The *dynamical topological order parameter (DTOP)* is given by

$$\nu_D(t) = \frac{1}{2\pi} \oint_{\mathsf{BZ}} \left(\frac{\partial \phi_k^{\mathsf{G}}(t)}{\partial k} \right). \tag{II.E.27}$$

As we will explain in section III.A this means nothing else than counting the jumps of the geometric phase including their signs, as k sweeps through the Brillouin zone.

Chapter III

Results

III.A Loschmidt echo and DTOP in periodic boundary conditions

The Loschmidt echo (LE) for free fermion (FF) models with periodic boundary conditions (PBC) was investigated in many works [14; 36; 51; 106]. In PBC, the LE is given by eq. (III.A.1) for any FF model, because the Hamiltonian of a FF model in PBC is diagonal in momentum space.

However, in PBC, we learn nothing about the edge modes in systems in topologically non-trivial phases, because all states look like bulk states. Edge modes are only present at boundaries between subsystems with different Chern numbers. This is known as bulk boundary correspondence (see II.A.1.iii). Most studies consider a boundary between an topological insulator (TI) and the vacuum, which means that the TI has to be considered in open boundary conditions (OBC).

The LE in OBC can be calculated for example using theorem II.20, which applies an exact diagonalization (ED) approach. We do not go into further detail on diagonalization algorithms we use to find the eigensystems of the initial and the final Hamiltonian, respectively, as all the functionality we need is

included in any linear algebra library. While for the SSH model, we use an arbitrary precision approach using GMP and the LAPACK [24] implementation MPACK [79] to solve large systems. For sufficiently small systems and for the Kitaev chains we implemented the simulation in double precision in Mathematica [55].

III.A.1 Tests on the ED algorithm

The SSH chain is exactly solvable, and Nicholas Sedlmayr wrote a Mathematica script which calculates both the LRR and the edge contribution to the LRR from the semi-analytic solution. The results of this work is going to be published in ref. [96]. For other models, like the Kitaev chain, it is no longer possible to determine the eigensystem analytically, thus an ED approach is required. The SSH model is an ideal testing model because one can compare analytical and numerical results easily, see figure III.1. We also generalized the ED algorithm for generic bilinear Hamiltonians, see II.D.5. In this case, the eigensystem is only known numerically for open boundary conditions (OBC), thus we can only compare the ED results with the solution for periodic boundary conditions (PBC).

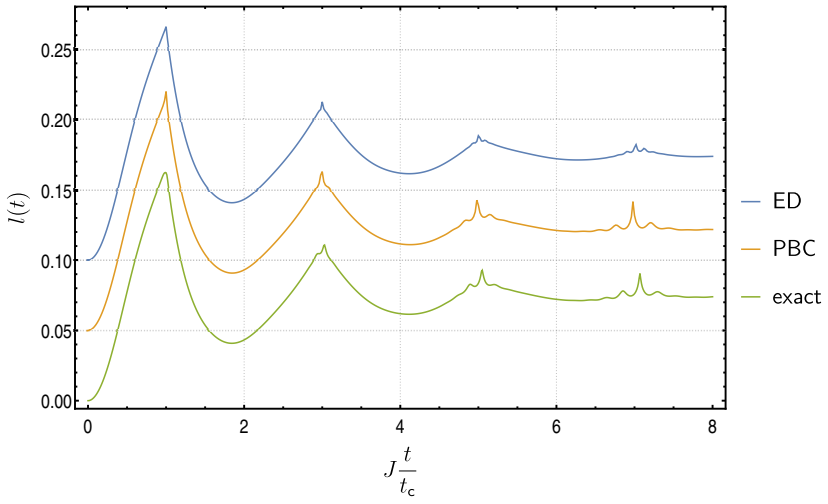

Figure III.1: Comparison of different algorithms to calculate the LRR. The plots for the ED and the PBC results are offset for clarity. The exact solution was calculated using the analytical eigensystem of the Hamiltonian, and we used eq. (III.A.1) to calulate the LRR in PBC. We show data for a symmetric quench from the topological to the topologically trivial phase at $\delta = 0.3$ for a chain of $N = 300$ sites. Therefore, we observe finite size effects at relatively small times, which are different for each algorithm.

III.A.2 Numerical calculation of the DTOP

Momentum is a good quantum number in PBC. The LE can be written as

$$G(t) = \prod_k g_k(t) = \prod_k \left[\cos(\epsilon_k^{\mathsf{f}} t) + \mathrm{i}\, \hat{d}_k^{\mathsf{i}} \cdot \hat{d}_k^{\mathsf{f}} \sin(\epsilon_k^{\mathsf{f}} t)\right], \tag{III.A.1}$$

and each individual k mode can be understood as a separate two-level system. A more detailed derivation of this formula is given in the proof of theorem II.21, and in refs. [106; 107]. We denote the contribution of each mode by $g_k(t)$.

We are interested in the points where the Loschmidt return rate (LRR) $l(t) = -\frac{1}{N}\log(G(t))$ is singular, which is the case iff $G(t) = 0$. It is sufficient that $g_k(t) = 0$ for a certain k, which we call the critical momentum k_{c}. At the critical momentum,

$$\hat{\vec{d}}_{k_{\mathsf{c}}}^{\mathsf{i}} \cdot \hat{\vec{d}}_{k_{\mathsf{c}}}^{\mathsf{f}} \stackrel{!}{=} 0 \tag{III.A.2}$$

and thereby $g_k(t)$ is real, as only the cosine term is left. This term then causes zeros in $G(t)$ at the critical times

$$t_c^{(n)} = \frac{\pi}{\epsilon_{k_{\mathsf{c}}}^{\mathsf{f}}}(2n+1), \tag{III.A.3}$$

where $n \in \mathbb{N}_0$. Dynamical phase transitions (DPT) occur at every odd multiple of t_{c}. The solutions of eq. (III.A.2) and the normalized dispersion ϵ_k^{f} for a symmetric quench in the SSH model with $|\delta| = 0.3$. The red line marks the critical momentum k_c, at which the factor of eq. (III.A.1) becomes 0. For a given k_c, one finds a set of critical times $t_c^{(n)}$. Because the inner product is symmetric, there is no difference in the critical momenta. However, the LRR drastically changes when one changes the direction of the quench. The topologically non-trivial phase of the SSH model corresponds to the polarized situation in ref. [107], because of the half unit cell at the edge.

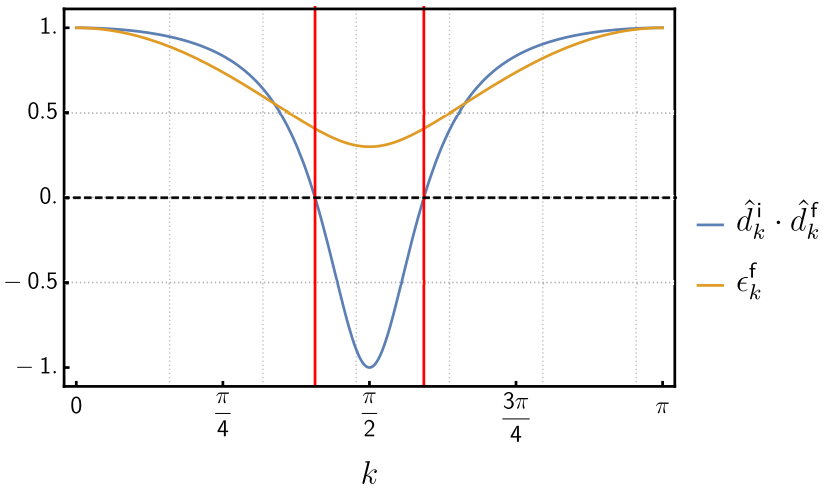

Figure III.2: The cosine of the Bogoljubov angle and the energy dispersion in the SSH model. The system undergoes a symmetric quench at $|\delta| = 0.3$.

Based on the discussion in the previous section, we extract the Pancharatnam geometric phase (PGP) by defining the geometric contribution as

$$\phi_k^{\mathsf{G}}(t) = \phi_k(t) - \phi_k^{\mathsf{dyn}}(t) = \phi_k(t) - \epsilon_k^{\mathsf{f}}\left(\hat{d}_k^{\mathsf{i}} \cdot \hat{d}_k^{\mathsf{f}}\right) t. \tag{III.A.4}$$

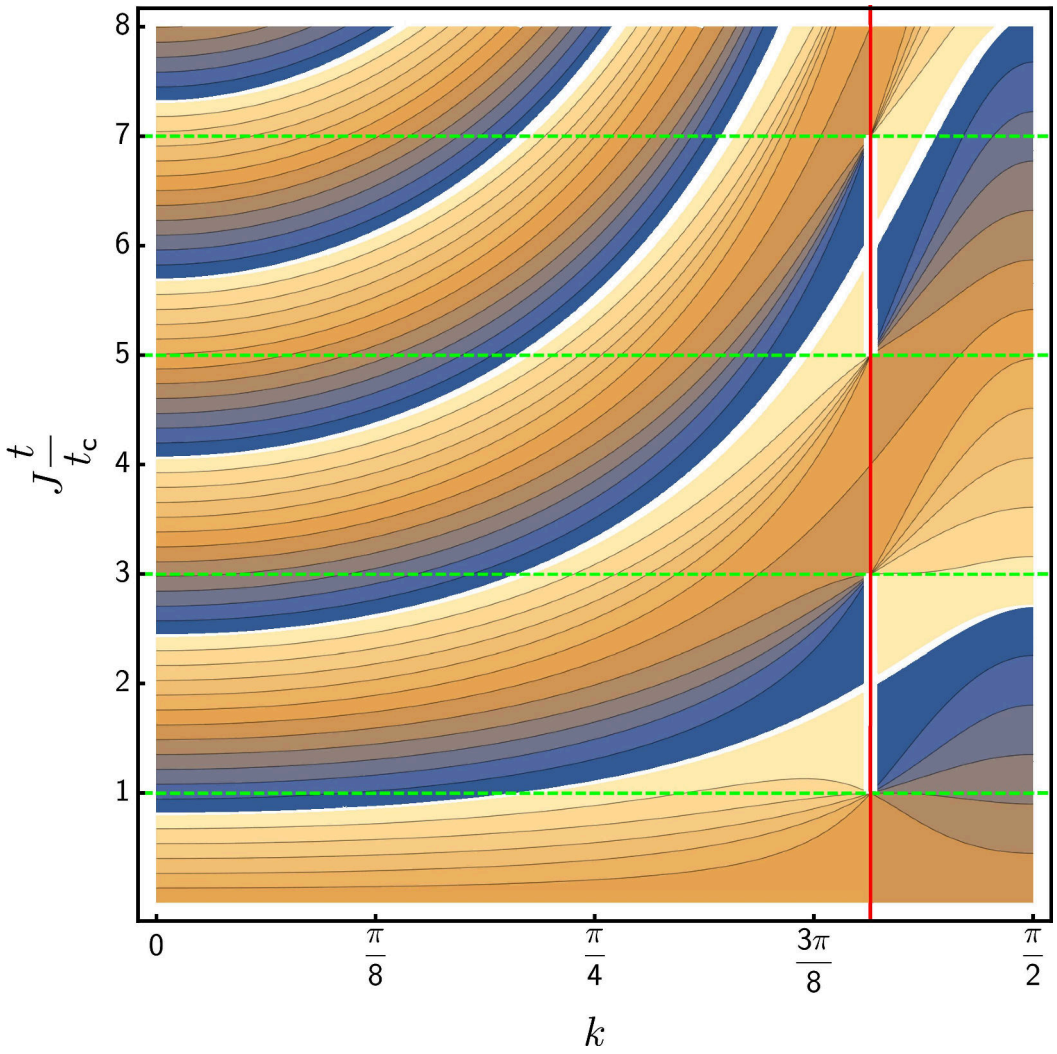

Figure III.3: Contour plot of the total phase $\phi_k(t) = \phi_k^{\mathsf{G}}(t) + \phi_k^{\mathsf{dyn}}(t) \in (-\pi, \pi)$ of the LE. Blue color indicates negative values. For momenta far away from the critical momentum (red line), the phase of the LE rises nearly linearly except for the jumps from $\frac{\pi}{2}$ to $-\frac{\pi}{2}$, due to the dynamical contribution. As k gets closer to k_{c}, the behaviour is no longer purely linear, and at k_{c}, it becomes singular at the critical times $t_c^{(n)}$ (green dashed lines).

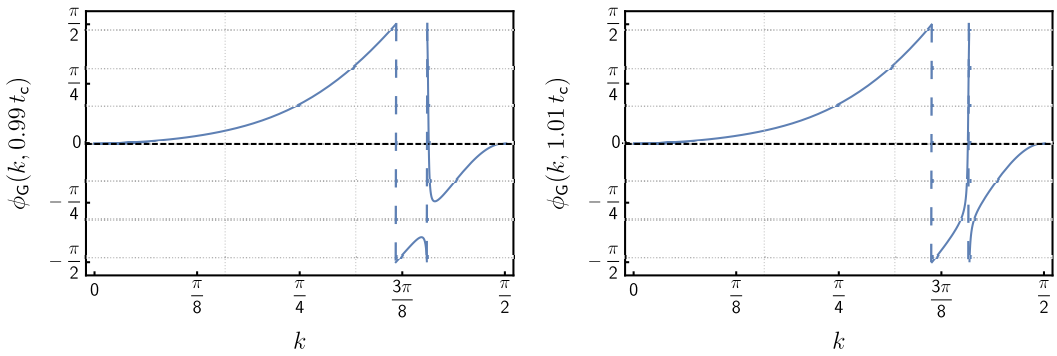

Figure III.4: PGP at fixed t slightly below (left panel) and above (right panel) the first critical time $t_c^{(1)}$. Evaluating the integral eq. (II.E.27), one finds that the DTOP counts the jumps of those functions, including their sign. In the picture on the left, there is one jump from $\frac{\pi}{2}$ to $-\frac{\pi}{2}$ and one from $-\frac{\pi}{2}$ to $\frac{\pi}{2}$, which gives a total of zero jumps. This changes at the critical time, where the second jump changes its sign. This situation is shown in the right panel, where one counts a total of two jumps, and the integral becomes equal to 2π, and thus $\nu_D = 1$

In the SSH model, it is enough to investigate the behaviour of the phase contributions on the interval $k \in \left[0, \frac{\pi}{2}\right)$, because the a function $f(k)$ defined in $k \in [0, \frac{\pi}{2})$ is given in the rest of the Brillouin zone is then given by

$$f(k) = f(\pi - k) \tag{III.A.5}$$

due to time reversal symmetry (TRS). We check this behaviour with the Bogoljubov angle and energy dispersion given in figure III.2. In the SSH model, the unit cells are doubled, and therefore the first Brillouin zone is given by $k \in \left[0, \frac{\pi}{2}\right)$.

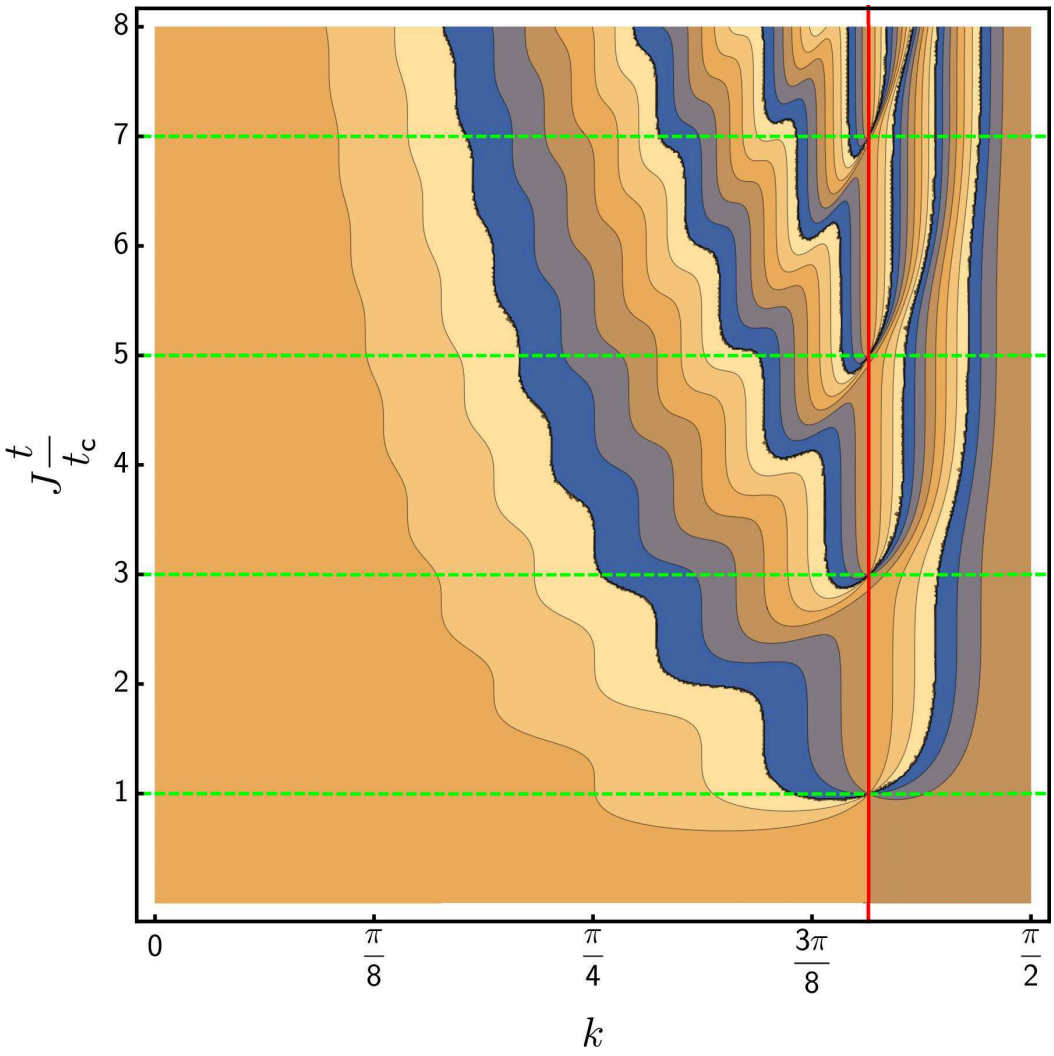

Figure III.5: Contour plot of the geometric contribution to the phase of the LE $\phi^{\mathsf{G}}(t)_k$. The DTOP is defined as an integral of the derivative of this phase (see eq. (II.E.27)), which means to calculate the DTOP, one essentially sums the differences of adjacent points along a horizontal line. It is easy to see, that the DTOP has to change for all critical times.

III.A.3 Comparison to previous works

The idea of defining a dynamical topological order parameter (DTOP) goes back to a recent work of Budich and Heyl [14]. As a proof of concept, the DTOP was calculated for a quench in the Kitaev chain (see section II.B.5.ii)

$$\mathbf{H} = -\mu \sum_j c_j^\dagger c_j + \sum_j \left(-J c_j^\dagger c_{j+1} + \Delta c_j^\dagger c_{j+1}^\dagger \right) + \text{h.c.}. \tag{III.A.6}$$

with $J = \Delta = 1$ and from $\mu = 0$ to $\mu = 3$.

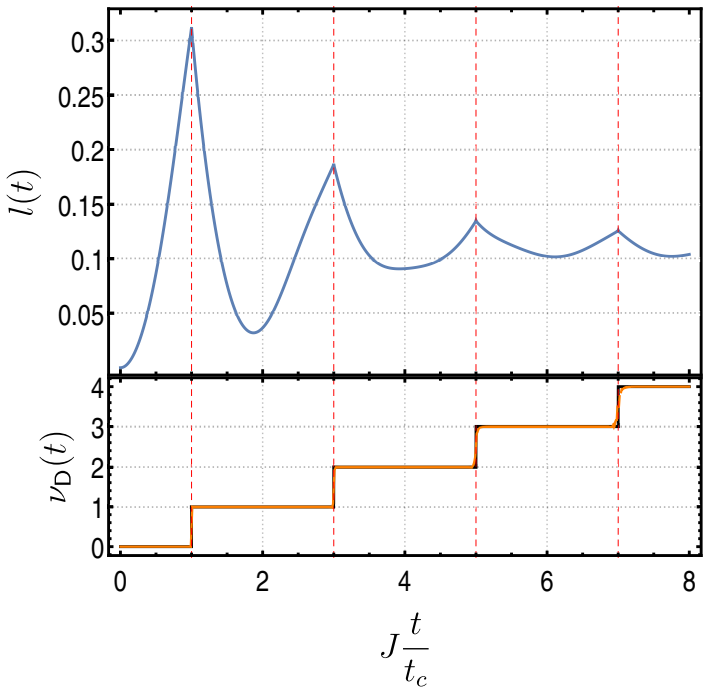

Figure III.6: Reproduced data from Budich and Heyl [14]. In the referenced study, the DTOP has an additional negative sign, because we defined the momenta k sightly different in this work for the sake of a more general notation. The underlying physics however is not affected. The DTOP is derived from a phase, and therefore, its sign does not have any physical meaning. Top panel: Lohschmidt return rate (LRR). Bottom panel: DTOP, as calculated by evaluation the defining integral (see definition II.26) numerically (orange line), and by the local slope of the Bogoljubov angle eq. (III.A.7)

The DTOP can be simplified eq. (III.A.7). This result is obtained by convincing oneself that the PGP is pinned at momenta $k = 0, \pi$ such that $g_k(t) \in \mathbb{R}$ for all times. One expands $\partial_k \phi_k^{\mathsf{G}}$ to the leading order and obtains eq. (III.A.7) immediately. For more details, see ref. [14].

$$\begin{aligned} \Delta\nu_{\mathsf{D}}(t_c) &= \text{sgn}\left(\frac{\partial}{\partial k} \left(1 - \hat{d}_k^{\mathsf{i}} \cdot \hat{d}_k^{\mathsf{f}} \right) \Big|_{k=k_c} \right) \\ &= -\text{sgn}\left(\frac{\partial}{\partial k} \hat{d}_k^{\mathsf{i}} \cdot \hat{d}_k^{\mathsf{f}} \Big|_{k=k_c} \right) \end{aligned} \tag{III.A.7}$$

Instead of the integration eq. (II.E.27), this formula essentially counts, how often the geometric phase wraps around the Brillouin zone.

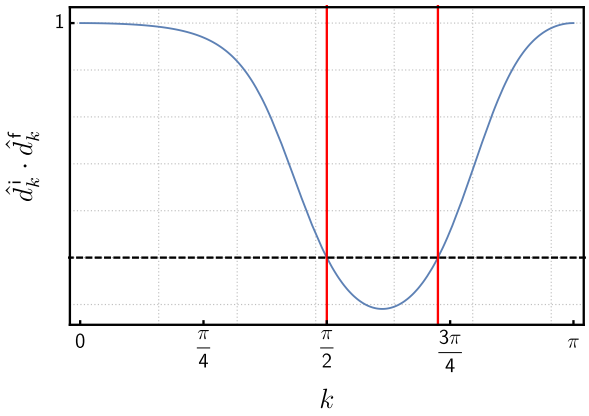

Figure III.7: Critical times of a Kitaev chain which also includes a next-nearest neighbour hopping term. The parameter vectors of this model are given in eq. (III.A.8). For this set of parameters, the quench does not change the topological phase of the system [14].

III.A.4 DTOP in models with integer Chern number

So far, to the best of our knowledge, no coherent analysis of the DTOP in systems with integer Chern number, such as the long-range Kitaev chain, has been done. Ref. [14] only gives one example for a rather obscure quench with parameter vectors

$$\vec{d}_k^{\,\mathrm{i}} = \begin{pmatrix} 0 \\ 0 \\ 1 \end{pmatrix} \quad \text{and} \quad \vec{d}_k^{\,\mathrm{f}} = \begin{pmatrix} 0 \\ \sin(k) \\ 1 + \cos(2k) + \lambda \cos(k) \end{pmatrix} \tag{III.A.8}$$

with $\lambda = 1.3$. Here, the initial state is simply a free particle, because it has no dependence on k at all. By construction, this model has two critical time scales, as shown in figure III.7. It should be noted that this is an example where no topological phase is changed. The winding number of a Hamiltonian given by a parameter vector is

$$\nu_{\mathrm{Ch}} = \frac{1}{2\pi} \int_{\mathrm{BZ}} \left(\hat{d}_k^y \frac{\partial}{\partial k} \hat{d}_k^z - \hat{d}_k^z \frac{\partial}{\partial k} \hat{d}_k^y \right) \mathrm{d}k, \tag{III.A.9}$$

if the parameter vector is restricted to the yz plane [106]. The initial Hamiltonian has the winding number $\nu_{\mathrm{Ch}} = 0$. For the final Hamiltonian, the winding number vanishes if $0 < \lambda < 2$ [14].

For this model, the DTOP is a non-monotonous function, because $\hat{d}_k^{\mathrm{i}} \cdot \hat{d}_k^{\mathrm{f}}$crosses zero once with a positive and once with a negative slope. Due to eq. (III.A.7), this means that one critical time causes a jump by $+1$, and the other by -1.

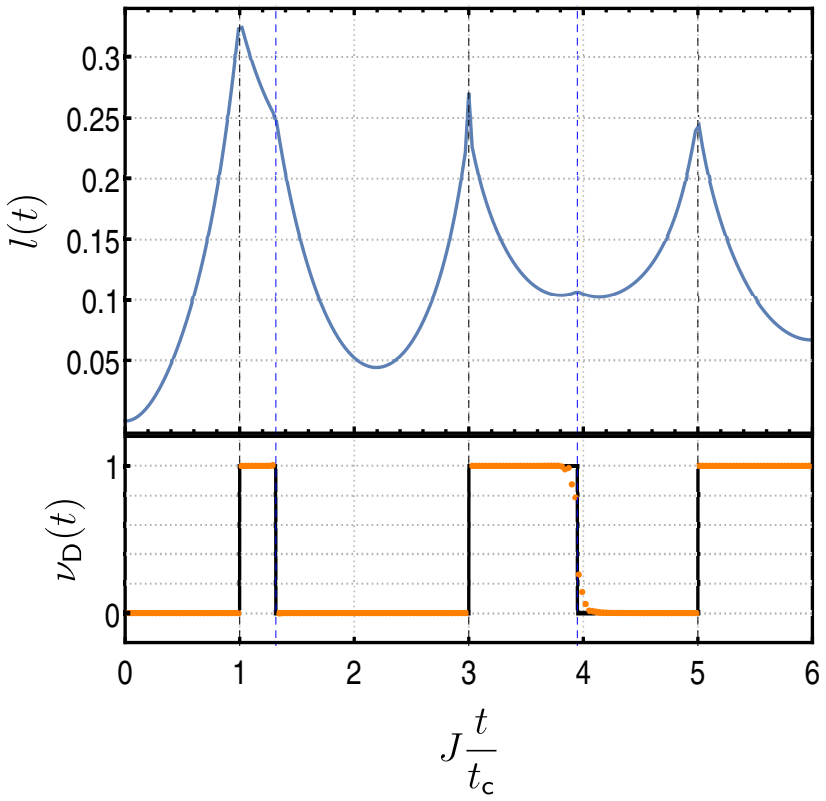

Figure III.8: LE and DTOP for the model with two critical times. The DTOP is no longer monotonous in this case. As the quench does not change the topological invariant of the model, this proves that DPT can happen without crossing a TPT in models with integer Chern number.

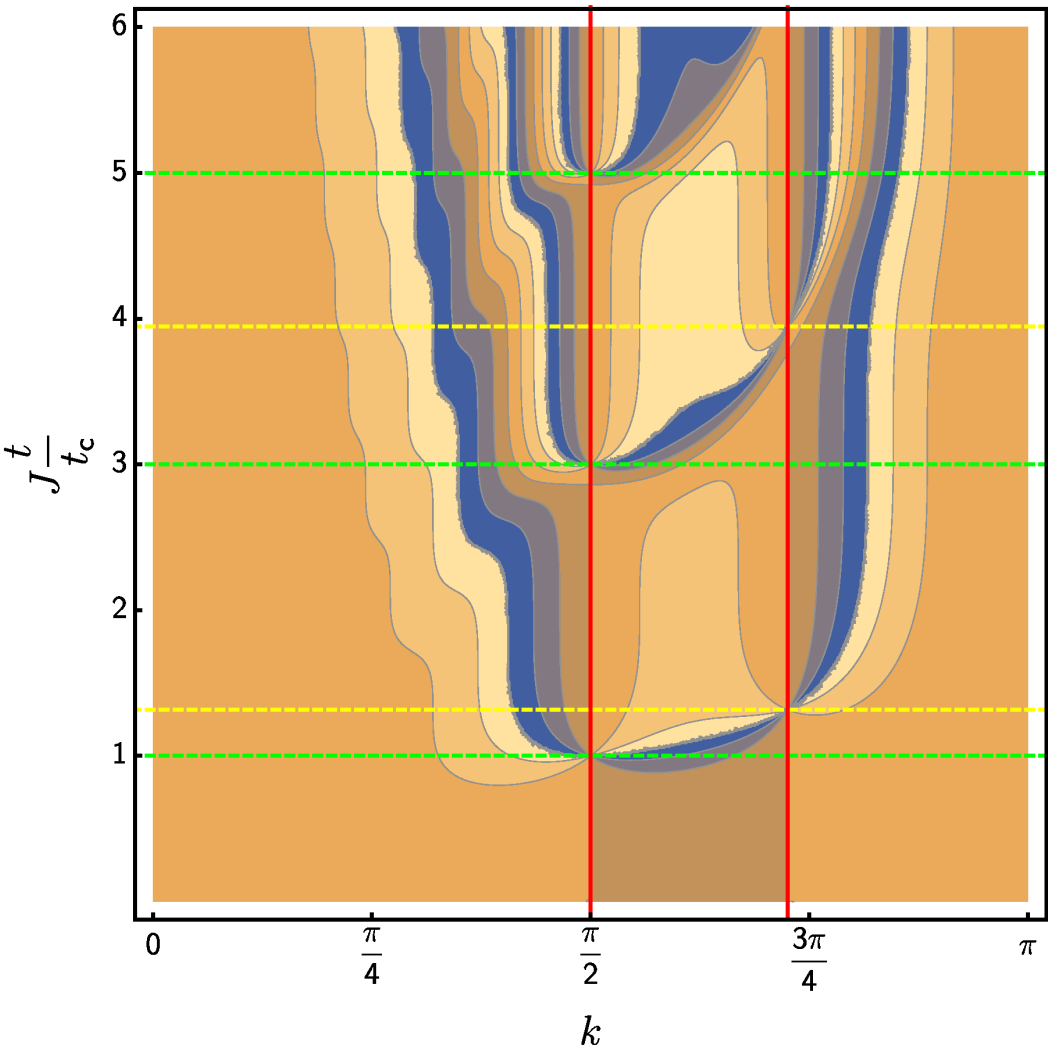

Figure III.9: In the contour plot of the geometric phase, the connection between a critical momentum and its critical time scale becomes visible.

III.A.4.i DTOP in the long-ranged Kitaev chain

In the periodic case, the LE is calculated as a sum of logarithms of sine and cosine terms. This structure allows the use of a graphics processing unit (GPU) to evaluate the LE, and it it possible to do calculations for $N = 5000$ to $N = 10000$ within minutes, which is significantly faster than using a parallel algorithm on 12 CPU cores.

The long-ranged (lr) Kitaev chain has a $\mathbb{Z}$ topological invariant, as opposed to the $\mathbb{Z}_2$ invariants in the SSH model and the nearest-neighbour Kitaev chain. In these systems, it has been shown that crossing a topological phase transition (TPT) causes a DPT (see theorem II.25). The question whether or not this holds for $\mathbb{Z}$ invariants is still open. In this section, we discuss simulations of various quenches between different topological phases. In general, these quenches are governed by more than one critical time scale. We evaluate the DTOP in these systems and examine its behaviour in these more complex systems.

The Hamiltonian of a lr Kitaev chain is given by eq. (II.B.49). In our simulations, we included up to three nearest neighbours, such that the parameter vectors of the Hamiltonian become [96]

$$\vec{d}_k^{\,\mathrm{i,f}} = \sum_{m=1}^{3} \begin{pmatrix} -2J_m^{\mathrm{i,f}} \cos(mk) - \mu^{\mathrm{i,f}} \\ 2\Delta_m^{\mathrm{i,f}} \sin(mk) \\ 0 \end{pmatrix}. \tag{III.A.10}$$

Here, the $J_m^{\mathrm{i,f}}$ and $\Delta_m^{\mathrm{i,f}}$ are entries of the vectors $\vec{J}^{\mathrm{i,f}}$ and $\vec{\Delta}^{\mathrm{i,f}}$, which represent the m-th neighbour hopping or pairing amplitude, respectively. $\mu^{\mathrm{i,f}}$ is the chemical potential. We simulated quenches between phases with different Chern numbers. In table III.1, we list the parameters of the Hamiltonians we used as the pre- and post-quench Hamiltonian. The system size for the simulations shown below was $N = 5000$.

In all our simulation which cross a TPT, we find also DPT, see figure III.10 and figure III.13. Of course a set of examples is not a proof, but the Vajna-Dóra theorem II.25 seems to hold in models with a integer Chern number in the sense that TPT imply DPT. The presence of DPT does however not imply that a TPT was crossed, as figure III.8 in the previous section shows.

Our simulations also show that the structure of the DTOP becomes more complex, and changing the direction of the quench does not simply relate to its behaviour, as one might assume from the definition, because

$$\vec{d}_k^{\,\mathrm{i}} \cdot \vec{d}_k^{\,\mathrm{f}} = \vec{d}_k^{\,\mathrm{f}} \cdot \vec{d}_k^{\,\mathrm{i}}. \tag{III.A.11}$$

This only means that the critical momenta remain the same, but the dispersion relation and therefore the critical times may change, and therefore the LE may look very differently.

Table III.1: Parameters of the Hamiltonians used as the pre- and post-quench Hamiltonian. For example, doing a quench from $\nu_{\mathrm{Ch}} = 3$ to $\nu_{\mathrm{Ch}} = 0$ means, that the parameters in the corresponding rows are used.

ν_{Ch}	μ	$J_m;\ m=$			$\Delta_m;\ m=$		
		1	2	3	1	2	3
3	1	1	−2	2	0.3	−0.6	0.6
2	−2.5	1	−2	2	0.3	−0.6	0.6
1	1	1	−2	2	1.3	−0.6	0.6
0	5	1	−0.5	0.5	0.3	−0.6	0.6
−1	1	1	−2	2	−1.3	0.6	−0.6
−2	1	1	−2	2	−0.3	0.6	−0.6

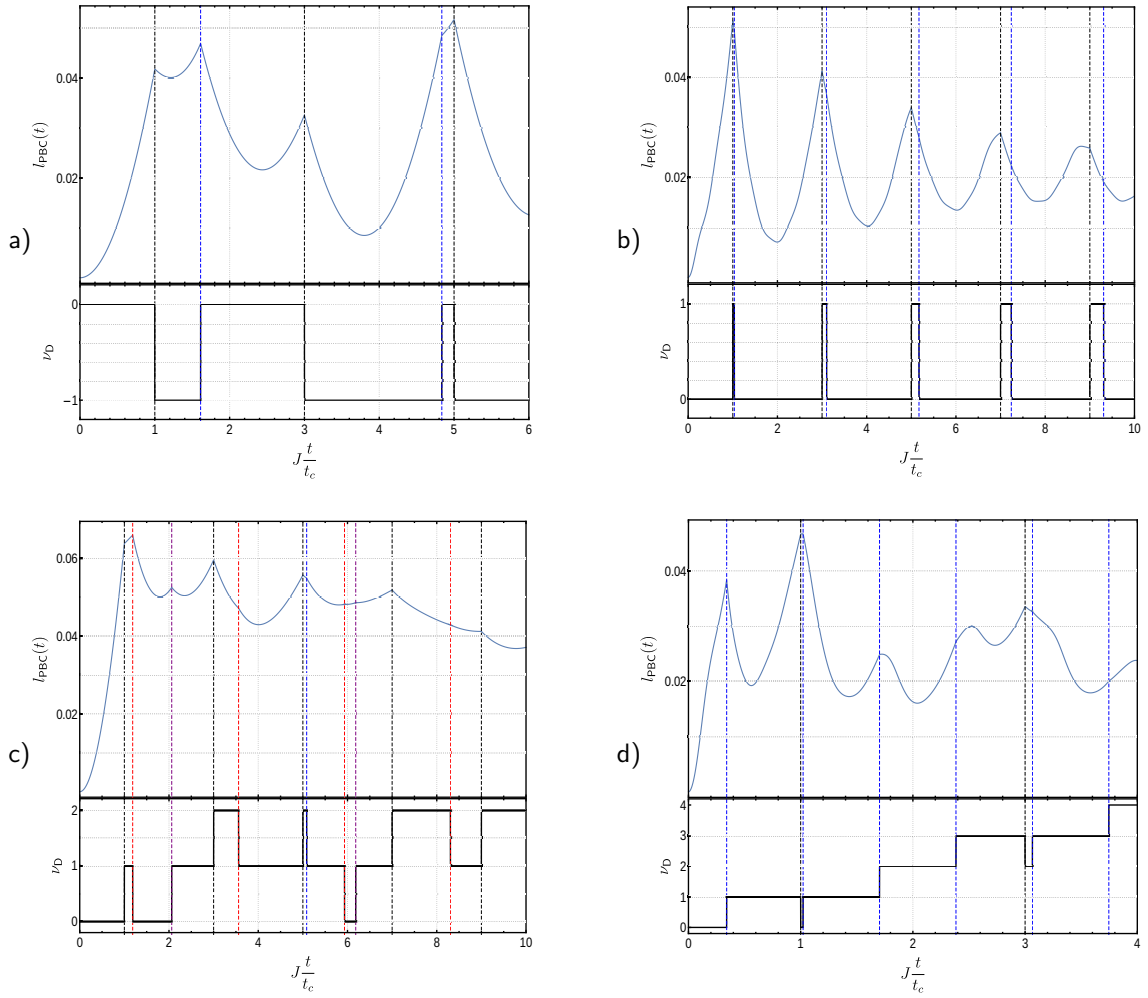

Figure III.10: LE after quenches in the lr Kitaev chain for various Chern numbers, see table III.1. We simulated quenches from the phase with $\nu_{\mathrm{Ch}} = 3$ to the phases with $\nu_{\mathrm{Ch}} = 0, 1, 2$ (panels (a)-(c)) and from $\nu_{\mathrm{Ch}} = 0$ to $\nu_{\mathrm{Ch}} = 3$ (panel (d)).

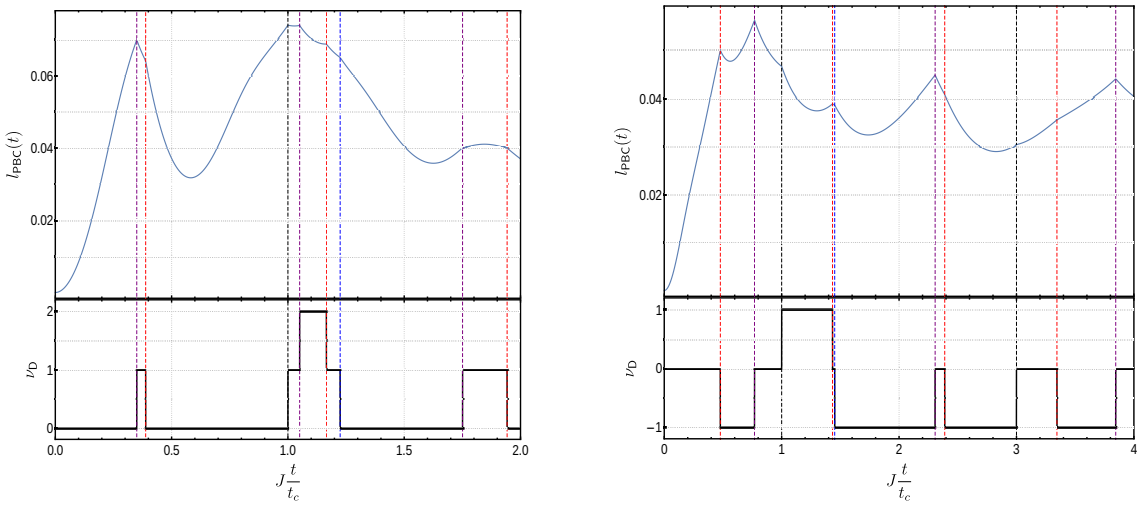

Figure III.11: LE after "symmetric" quenches in the Ir-Kitaev chain for various Chern numbers. Left panel: $\nu_{\mathsf{Ch}} = 1 \to -1$, right panel: $\nu_{\mathsf{Ch}} = 2 \to -2$

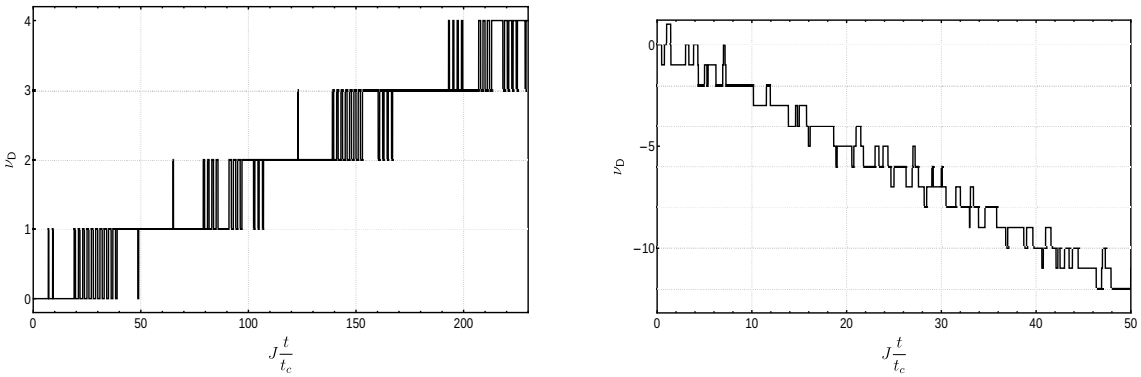

Figure III.12: DTOP for long times. Left panel: $\nu_{\mathsf{Ch}} = 3 \to 1$ right: $\nu_{\mathsf{Ch}} = 2 \to -2$

In "symmetric" quenches between phases with different Chern numbers, i.e. from ν_{Ch} to $-\nu_{\mathsf{Ch}}$, one might assume that nothing will happen, because ν_{Ch} changes its sign if one of the components of the parameter vectors changes its sign, and therefore, all the energy scales stay the same. In this case, the term $\hat{d}_k^{\mathrm{i}} \cdot \hat{d}_k^{\mathrm{f}}$is responsible for the non-trivial LE, because it does not simply change its sign, and therefore, the critical moments change. The results of our simulations are shown in figure III.11.

We also note that in either case, the DTOP never stays close to $\nu_{\mathsf{D}} = 0$, as some of the simulations might suggest. At long times, the DPT with small critical times will have occurred more often than the others. Therefore, the long-time behaviour of the DTOP is always determined by the shortest critical time scale in the system, which corresponds to the critical momentum with the largest energy. If this DPT lowers the DTOP, its long-time limit is

$$\nu_{\mathsf{D}}(t) \underset{t\to\infty}{\longrightarrow} -\infty, \tag{III.A.12}$$

if it raises the DTOP, it diverges to positive infinity, see figure III.12.

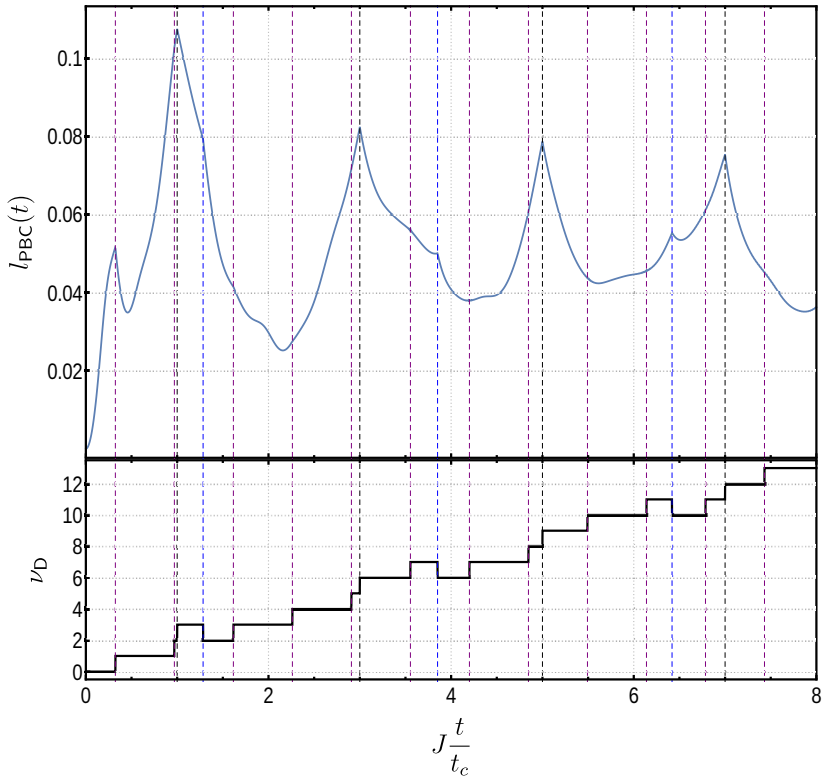

Figure III.13: LE after quenches in the lr-Kitaev chain from $\nu_{\mathrm{Ch}} = 3$ to $\nu_{\mathrm{Ch}} = 1$. In this case, $\hat{d}_k^{\mathrm{i}} \cdot \hat{d}_k^{\mathrm{f}}$has an odd number of zeros, and there are three critical time scales.

III.A.4.ii Pathological cases with three critical time scales

With specially tuned parameters of the Hamiltonian, it is possible to create a situation where $\vec{d}_k^{\,\mathrm{i}} \cdot \vec{d}_k^{\,\mathrm{f}}$ touches zero, i.e. has a double root at a certain $k = k_{00}$. As a starting point, we used the model described in section III.A.4 and varied the chemical potential μ such that we obtain the situation described above.

There are two possible situations. First, we can find a μ such that the only zero of $\vec{d}_k^{\,\mathrm{i}} \cdot \vec{d}_k^{\,\mathrm{f}}$ is a double zero. We find this situation at $\mu = 1.21125$. This situation is shown in the left panels of figure III.14 and figure III.15. The other possible case is that there is one ordinary zero and one double zero, as shown in the right panels of figure III.14 and figure III.15.

It look like it is not sufficient that $\vec{d}_k^{\,\mathrm{i}} \cdot \vec{d}_k^{\,\mathrm{f}}$ has a zero, but it must also change its sign. We can understand this in terms of the relation of ν_{D} to the sign of $\frac{\partial}{\partial k} \vec{d}_k^{\,\mathrm{i}} \cdot \vec{d}_k^{\,\mathrm{f}}$ eq. (III.A.7): When the sign of $\vec{d}_k^{\,\mathrm{i}} \cdot \vec{d}_k^{\,\mathrm{f}}$ does not change, the slope is zero, and the jump in ν_{D} is suppressed.

In both cases, the system does not cross a TPT, because $\vec{d}_k^{\,\mathrm{i}}$ and $\vec{d}_k^{\,\mathrm{f}}$ never become anti-parallel (i.e. $\vec{d}_k^{\,\mathrm{i}} \cdot \vec{d}_k^{\,\mathrm{f}}$=-1), and therefore there is a continuous map from the one to the other. Thus, they must be topologically equivalent [108].

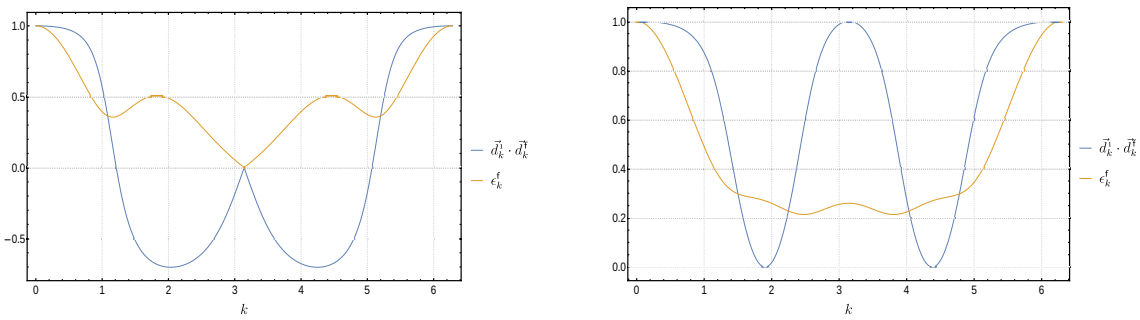

Figure III.14: Cosine of the Bogoljubov angle and normalized energy dispersion ($\epsilon_{\mathrm{max}} \equiv 1$) for $\mu = 0.3$ (left) and $\mu = 1.21125$ (right)

.

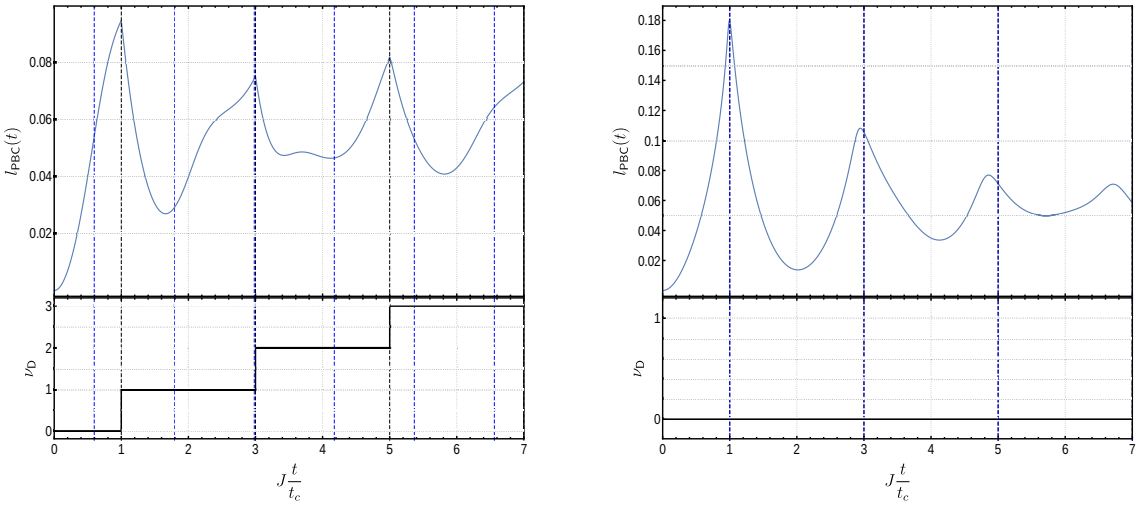

Figure III.15: LE and DTOP for $\mu = 0.3$ (left) and $\mu = 1.21125$. On the left panel, there are no singularities visible at all, because the two critical times where the DTOP is expected to jump up or down, respectively, coincide. On the right panel, there is only one critical time scale resulting from the ordinary zero. The double zero again does not cause a singularity.

III.B Edge contributions in the LE

In this section, we discuss the LE in FF with open boundary conditions. The discussion consists of two main parts: The limits of ED algorithms in OBC are addressed in section III.B.1, including a short discussion on the performance of arbitrary-precision algorithms. The second part of this section will concentrate on the edge contribution to the LE, which we extract by extrapolating the solution for finite systems towards the thermodynamic limit.

III.B.1 High-precision calculations in the SSH model

To resolve the eigenvalues of the edge modes in the SSH chain correctly, it is not sufficient to use double-precision arithmetics. We implemented the exact diagonalization algorithm in C++, using the multi-precision LAPACK implementation MPACK with the quad-double and the GMP backend [79]. The implementation of this algorithm was supported by Craig McRae. The calculations where performed on a HPC cluster at McGill University in Montréal, QC, and on the local HPC cluster at University of Manitoba.

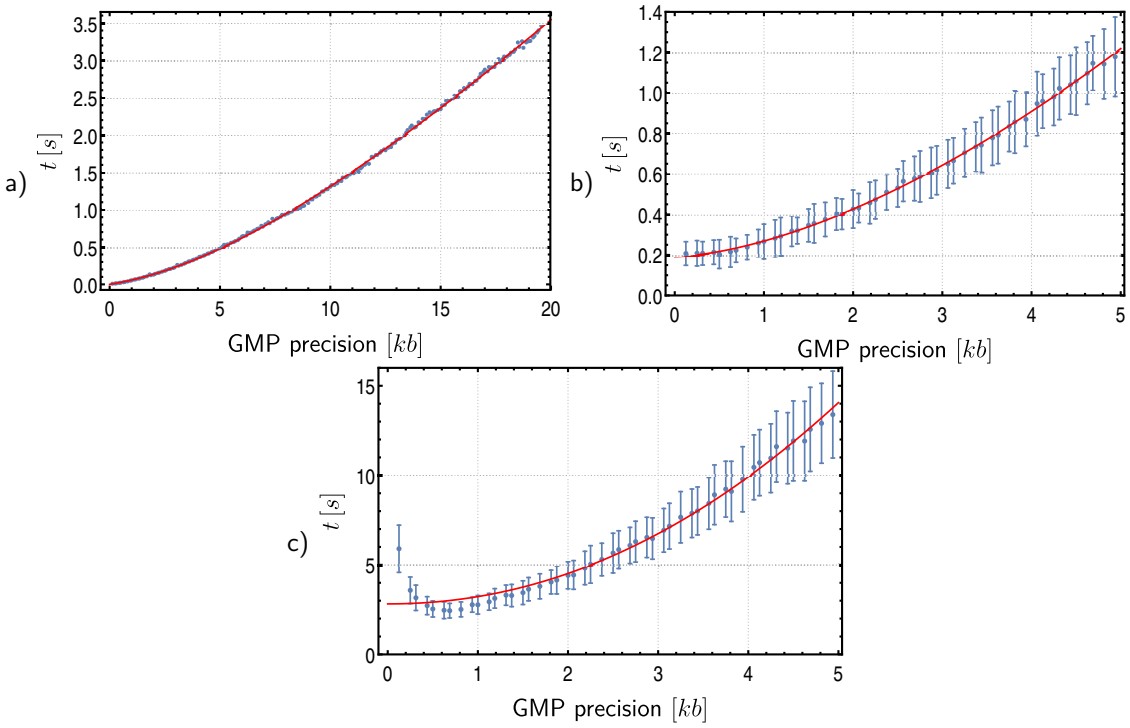

Figure III.16: Some benchmark calculations for the MPACK [79] algorithms. The red lines are best fitting curves. Details about the used models are explained in the text. Error bars are standard deviations. Top left: Multiplication of two random floating point numbers. Time was measured for 10000 multiplications, including the drawing of random numbers. Top right: Run time of the multiplication of two random hermitian 50×50 matrices. Bottom: Run time of the diagonalization of a random hermitian 50×50 matrix.

III.B.1.i GMP benchmarks

To perform calculations on HPC clusters, it is necessary to estimate the run time of a program as precisely as possible. We are not aware of any benchmarks we could rely on to do these estimates, so we performed a few test calculations ourselves. These covered only the algorithms we needed to use, i.e. multiplication and diagonalization of hermitian matrices, which are maybe the most important LAPACK algorithms for a physicist.

The code for these tests was written in C++ and compiled using Intel's C/C++ compiler. We ran the benchmarks on a desktop PC with a 4-core Intel i7-2600 CPU.

Float multiplication

We tested the run time of a floating point multiplication using GMP for a precision (i.e. number of bits used for a single number) up to 20000. In order to reach measurable times, we ran 10000 multiplications for each precision and measured the overall time, which is also why we have no standard deviations in figure III.16 (a). Another error we have in these measurements is the drawing of new random numbers for every multiplication, which also happens within the measured time.

The fit function we used is

$$t(p) = a\mathrm{e}^{-bp} + c + dp, \tag{III.B.1}$$

p being the precision in use. This function pictures the linear increase of run time at large precision as well as an exponentially decaying contribution which captures the relatively higher overhead at small precisions. The fit yielded $a = 2.28$, $b = 0.1007$, $c = -2.28$ and $d = 0.276$, and the function $f(p)$ reproduces the simulation well.

For matrix multiplication, we used matrices of dimension $n = 50$ and performed 100 multiplications. The points in figure III.16 (b) are the mean values, and the error bars the standard derivation for each precision. We fitted the data using a power laws eq. (III.B.2). The fit parameters are given in table III.2. The fit function is

$$t(x) = a \cdot x^b + c. \tag{III.B.2}$$

Here, x can mean precision p or matrix size n, and a, b and c are positive real parameters. We also checked

Table III.2: Fit parameters for the power law approximation to the run time dependency on the precision p or the matrix size N. The offset time c is only necessary if the precision is varied. For variable matrix size, it vanishes nearly exactly and was set to zero to fit the data.

	multiplication		**diagonalization**	
	p	N	p	N
a	0.077	$1.741 \cdot 10^{-6}$	0.407	$3.385 \cdot 10^{-6}$
b	1.612	2.897	2.061	3.145
c	0.192		2.820	

the performance of MPACK with varied matrix size. Usually, the problem of matrix multiplication is known to scale like n^2 in the matrix size n, and for diagonalization we expect a n^3 scaling. However, we find in both cases different leading exponents, see figure III.17 and table III.2. For both the multiplication and diagonalization, we could not find a well-fitting polynomial and instead used a power function eq. (III.B.2) to approximate the scaling behaviour. The fit paramters are given in table III.2.

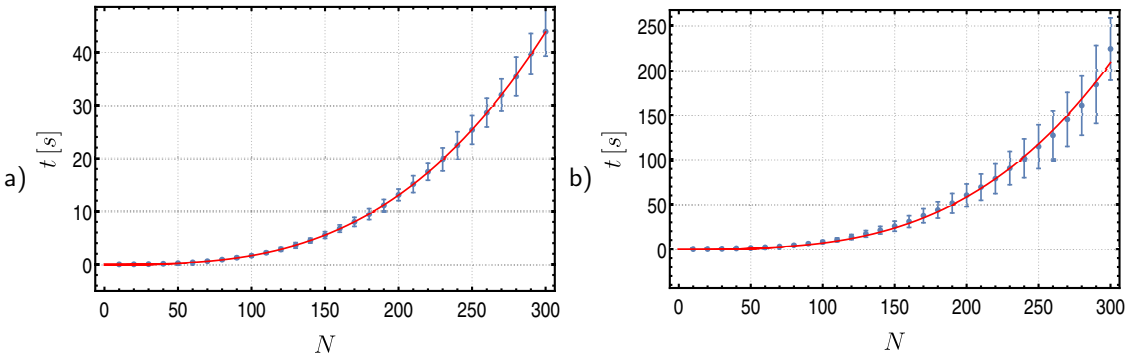

Figure III.17: Scaling of (a) multiplication and (b) diagonalization with the matrix size. The fit curves (red) are discussed in the text. Error bars are standard derivations.

III.B.1.ii Loschmidt echo

To estimate the precision we need to perform the ED calculations in larger systems, we tested the scaling of the eigenvalues of the edge states with the system size. This test was run at 50 decimal digits of precision, which roughly corresponds to 200 bits of GMP precision, for $\delta = 0.1$. We find the expected

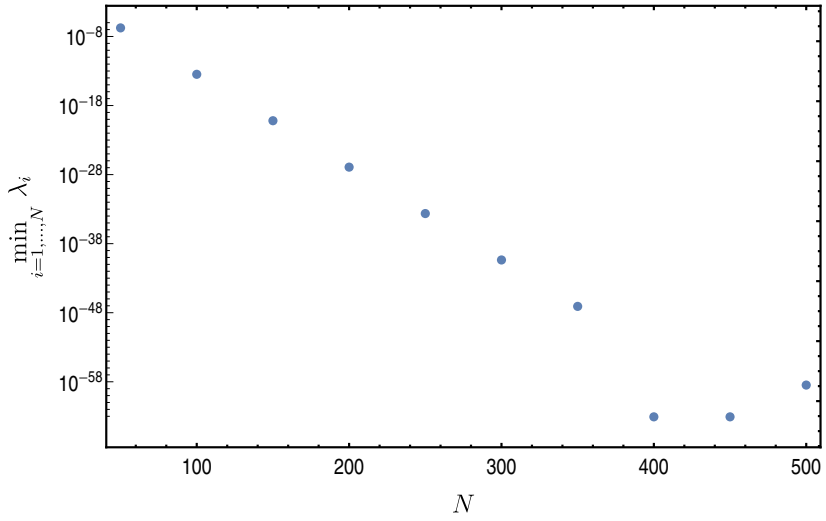

Figure III.18: Smallest positive eigenvalue of the SSH chain dependent on the number of lattice sites. We observe an exponential scaling until the precision barrier is hit. For larger systems, the eigenvalue is not resolved correctly, and thus we expect the ED algorithm to fail in these cases.

scaling as e^{-N}, as shown in figure III.18. Extrapolating from the data in this figure, at $N = 1000$, the smallest eigenvalue should be roughly of order 10^{-150}, thus we expect to be able to solve the system using a GMP precision of 1000 bits, i.e. about 250 decimal digits.

For symmetric quenches in the SSH chain, the critical time is given by

$$t_{\mathrm{c}}^{(n)} \approx \frac{\pi\sqrt{1+\delta^2}}{2J\sqrt{2}|\delta|}(2n+1), \tag{III.B.3}$$

rather than solving $\hat{d}_k^{\mathrm{i}} \cdot \hat{d}_k^{\mathrm{f}} = 0$. The Loschmidt return rate (LRR) after a symmetric quench from the topological to the topologically trivial phase, i.e. from $\delta < 0$ to $\delta > 0$, at different values of δ is shown in figure III.19.

If the system is quenched from the topologically trivial to the topological phase, the critical time scale is doubled, and DPT occur at $t = 2(2n+1)t_{\mathrm{c}}$, where $n \in \mathbb{N}_0$. This additional factor of 2 occurs due to the polarized nature of the state: The enlarged unit cell contains one dimer, i.e. two lattice site. This lines up with the ends of the chain in the topologically trivial phase, but in the topological phase, there is an additional half unit cell at the edges [107]. Further, the LRR $l(t) = -\frac{1}{N}\log|G(t)|$ takes much larger values, i.e. $G(t)$ is much closer to zero. This causes two numerical problems:

1. The energy of the edge modes is not resolved correctly.
2. The eigenvalues of the matrix in the determinant eq. (II.D.31) are not resolved correctly.

The first of these cases immediately causes the algorithm to fail, see figure III.20 (b). In the latter case, the problem occurs when diagonalizing the matrix inside the determinant and is only a problem for certain time steps, when $G(t)$ is very small. This is shown in figure III.20 (a) and figure III.21.

To see if the problems for this quench direction can be solved using higher precision, we ran the same calculation again with 2500 bits of precision. The results are shown in figure III.21. For small systems, we

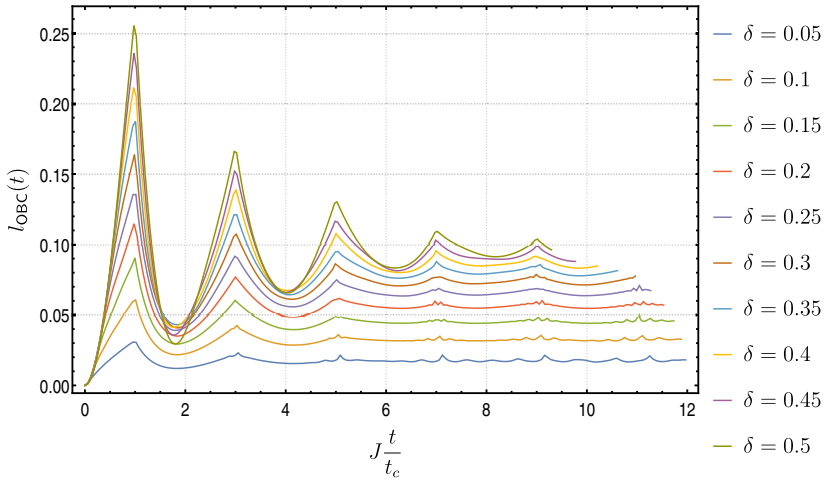

Figure III.19: LRR for symmetric quenches from the topological to the topologically trivial phase, i.e. from $\delta < 0$ to $\delta > 0$, over a range of $\delta = 0.05, ..., 0.5$. For small values of δ, finite size effects become visible quickly, because the velocity of sound for the quasi-particles in the chain is large [101].

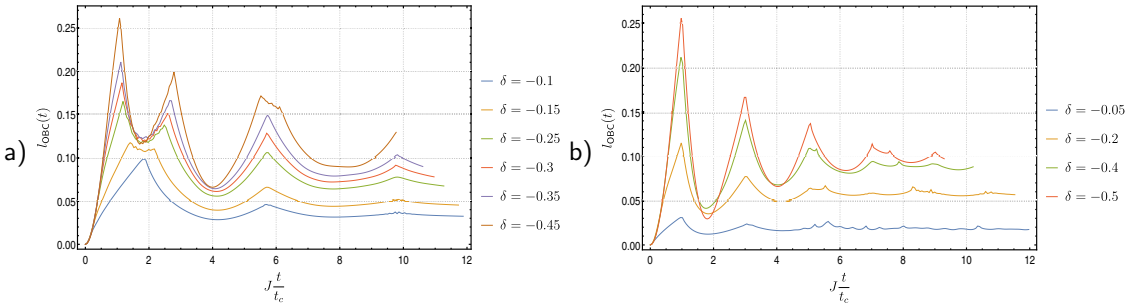

Figure III.20: LRR for symmetric quenches from the topologically trivial to the topological phase, i.e. from $\delta > 0$ to $\delta < 0$, over a range of $\delta = 0.05, ..., 0.5$. In the right panel, the algorithm resolved the edge modes correctly, although the evaluation of the LRR fails for certain times. The left panel shows the cases where the edge mode energy was determined to zero. Thus, the time evolution could not "see" them, and the critical time scale drops back to the critical time without any edge modes, when the system is in the trivial phase. For large times, finite size effects take over and make the data unusable.

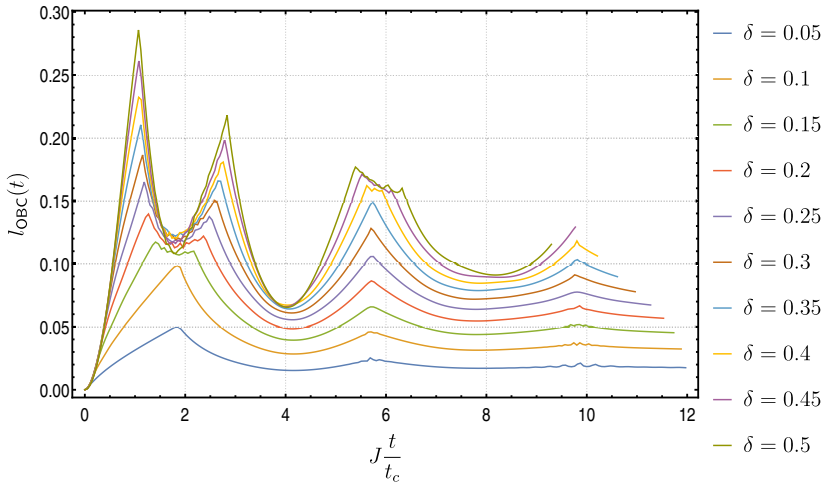

Figure III.21: Using a larger precision of 2500 bits solves the first of the above-mentioned problems. Still, the LRR is not evaluated correctly for some time steps. These are nearly the same as before, such that it is not clear if changing the precision to use really helps.

solved both issues by using a higher precision, so at some point it should also work for the large systems. It is not really clear to us what exactly goes wrong when evaluating the determinant, thus we can only guess what precision would be needed to get rid of this problem.

For a very high precision of 5000 bits, the eigenvalues are determined to a sufficient precision to be non-zero, such that the system behaves as expected in the topologically non-trivial phase for all calculation we ran. Still, for $\delta = -0.2$, the LE is not correctly resolved. At a value of $l(t) = 0.13$, the accuracy of the eigenvalues is not sufficient.

At this point,

$$l(t) = 0.13 \quad \Rightarrow \quad G(t) \approx 0.9 \cdot 10^{-1000}. \tag{III.B.4}$$

It is not obvious how to estimate which precision would be sufficient, but given the very slight changes on a range from 1000 bits to 5000 bits, it is safe to assume, that a precision much larger than 5000 bits would be required. At that high precision, our algorithm takes a very long time to run. At 5000 bits precision and $N = 1000$, the diagonalization of the Hamiltonian takes approximately one day. MPACK does not implement parallel execution by itself, and there fore, computational resources can not be used efficiently for these parameters. Both matrix products and diagonalization scale exponentially in the precision. Therefore, we decided to base this work on smaller systems, where the calculations can be done in Mathematica.

III.B.2 Bulk-Boundary correspondence

We calculate the edge contribution to the LE exploiting its scaling behaviour. Considering Anderson's orthogonality catastrophe (see section II.D.2), the LE itself will scale like e^{-N}, where N is the system

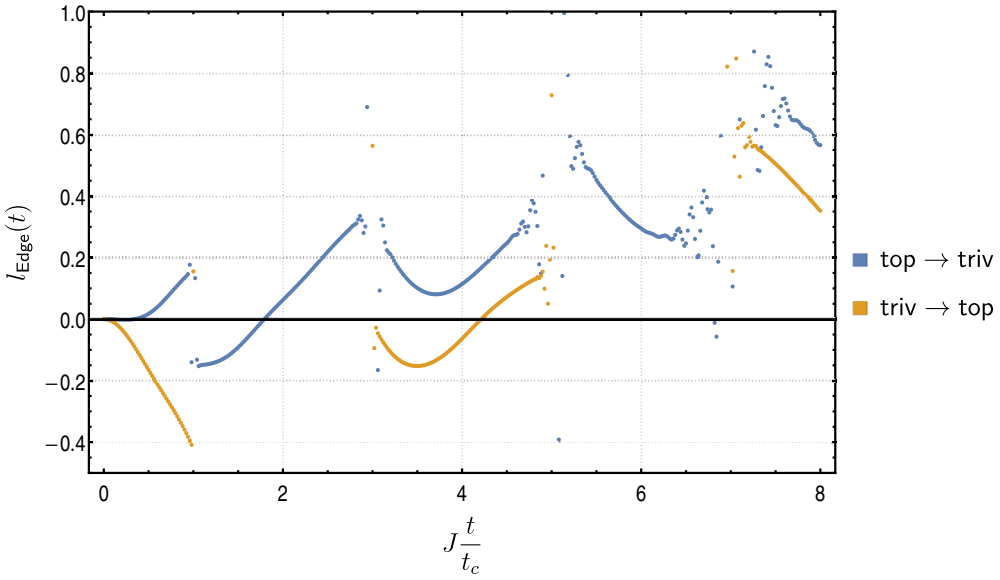

Figure III.22: Scaled LRR for symmetric quenches at $|\delta| = 0.3$. We observe singularities in the edge contribution whenever the LRR has a singularity as well. For the quench from the topological to the topologically trivial phase, the edge contribution stays near zero for all times. In the other direction, the edge contribution jumps to large values e.g. between $Jt = 1..3t_c$. These values are out of the scale of this graph, but shown in figure III.23

size. By definition, the Loschmidt return rate (LRR) scales constant in the system size,

$$l(t) = -\frac{1}{N}\log|G(t)|. \tag{III.B.5}$$

This eliminates the e^{-N} scaling. The edge contribution does not change dependent in N, and causes a constant contribution to the LE. Therefore, in the LRR, it contributes at order $\frac{1}{N}$,

$$l(t) = l_{\text{bulk}}(t) + \frac{1}{N}l_{\text{edge}}(t). \tag{III.B.6}$$

The bulk solution is given by the LE in PBC, eq. (III.A.1). Consequently, the edge contribution is

$$l_{\text{edge}}(t) = N\left[l(t) - l_{\text{bulk}}(t)\right]. \tag{III.B.7}$$

Thus, $l_{\text{edge}}(t)$ can be extracted by extrapolating $\frac{1}{N}$ towards $N \to \infty$. The results in this section were obtained doing this extrapolation from ED results. For the SSH model, we compare this data with results of ref. [96].

We find, that the edge contributions also have singularities which scale with the critical time. This behaviour raises the question whether there is a dynamical equivalent of bulk-boundary correspondence, which causes the edge modes to be singular when the bulk undergoes a DPT. Particularly for the quench from the trivial to the topological phase, the large jumps in the edge contribution seem to indicate, that these modes are only populated after every other DPT, and unpopulated otherwise. In order to gain a better understanding of these modes, we perform similar calculations for different models, namely the nearest-neighbour (nn) and the long-ranged (lr) Kitaev chain.

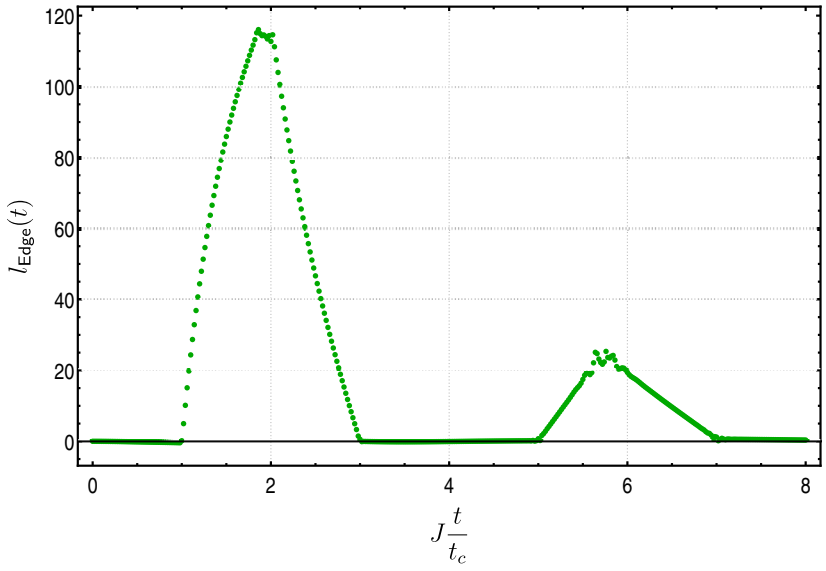

Figure III.23: Scaled LRR for symmetric quenches at $|\delta| = 0.3$ from the trivial to the topological phase. Because we are using an ED algorithm instead of the exact results, as ref. [96] does, we are limited in the accessible system size. We addressed this problem in section III.B.1. Therefore, the results we present here are not fully converged yet, but a behaviour similar to ref. [96] is already visible.

III.B.3 Kitaev chain - ED

The nn Kitaev chain has for positive pairing amplitudes $\Delta > 0$ one topological phase transition at $\mu = 2J$ [14], see also section II.B.5.ii. In section III.A, we investigated the bulk properties of the Kitaev chain, in particular, we calculated the Pancharatnam geometric phase and the dynamical topological order parameter (DTOP) for a number of different quenches.

Now, we focus on the edge contribution to the LRR in this model as well, which we obtain analogous to the previous section by extrapolating towards the thermodynamic limit $\frac{1}{N} \to 0$. We start with the quench from $\mu \approx 0$ to $\mu = 3$. We can not set $\mu = 0$ here, because this would cause the Hamiltonian to be singular and the diagonalization to fail, but we can chose a small non-zero value for μ. In this case, LRR and DTOP are nearly identical in open and periodic boundary conditions, see figure III.24.

The edge contribution to the LRR is plotted in figure III.24 for a quench from $\mu \approx 0$ to $\mu = 3$ and vice versa. Also in this case, we find a non-trivial behaviour at the critical times, but without the large jumps we have seen in the SSH chain. Instead, the edge LRR stays near zero for both quenches. Interestingly, at $\mu \approx 0$, the edge LRR looks like parabola segments around $\left(n + \frac{1}{2}\right) t_c$ where $n \in \mathbb{N}_0$.

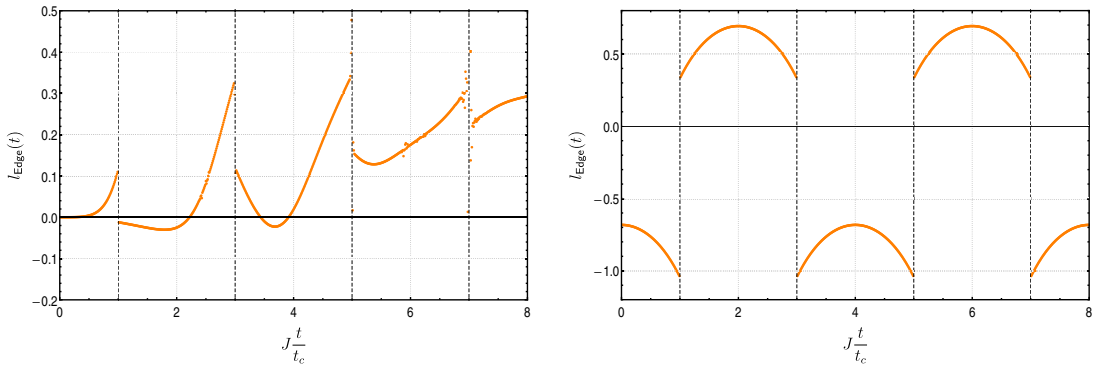

Figure III.24: Edge contribution in the LRR of a Kitaev chain after a quench from $\mu \approx 0$ to $\mu = 3$ (left) and vice-versa (right). In both direction, the presence of singularties at the critical times is clearly visible.

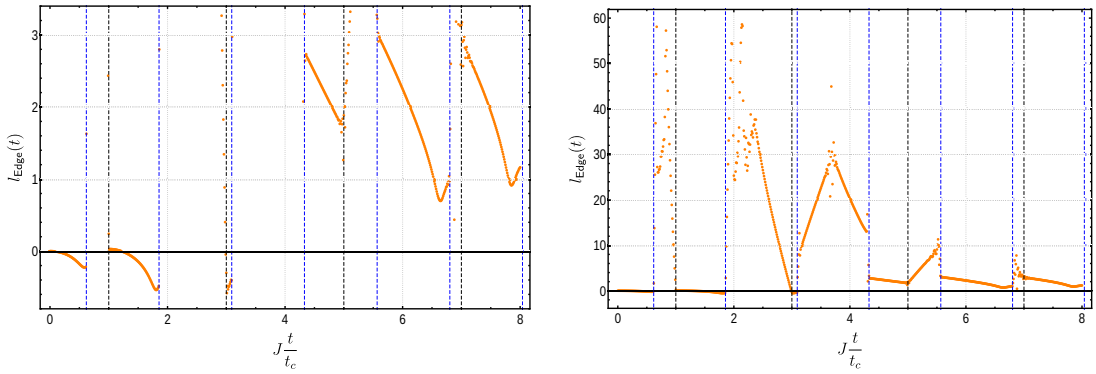

Figure III.25: Edge contribution in the LRR of a Kitaev chain after a quench from $\Delta = 4$ to $\Delta = -4$. Left panel: zoomed in picture, right panel: all values. In both directions, the presence of singularties at the critical times is clearly visible.

III.B.4 Long-ranged Kitaev chain - ED

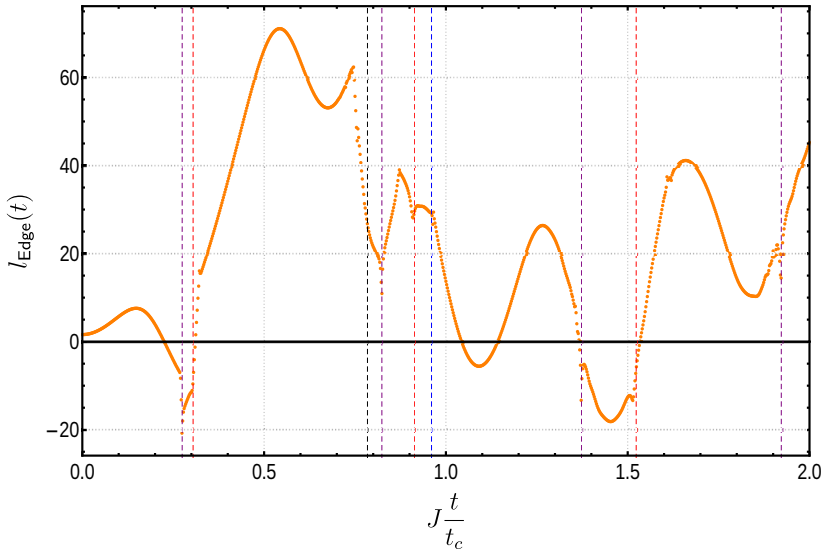

Figure III.26: Scaled edge contribution for a quench in the long-ranged Kitaev chain from the phase with $\nu_{\text{Ch}} = 1$ to the phase with $\nu_{\text{Ch}} = -1$.

We simulated quenches in the Kitaev chain for various combinations of μ, always chosen such that the TPT as $\mu = 2|J|$ is crossed (figure III.24), and several symmetric quenches in the pairing amplitude for Δ to -Δ (figure III.25). The same occurs in quenches in the lr Kitaev chain, which has an integer winding number. As an example, we show the edge contribution in the quench from the phase with $\nu_{\text{Ch}} = 1$ to the phase with $\nu_{\text{Ch}} = -1$ (figure III.26). The exact quench parameters are given in table III.1. In all cases we observe singularities at the critical times, at least for small t, where the numerics are converged, and no finite size effects are visible.

Together with the exact results from ref. [96] for the SSH model, we provide numerical data which suggests the presence of bulk-boundary correspondence for DPT over various models. This is not strictly speaking a proof, but rather a manifest assumption, which also fits into the Wick rotation picture of the correspondence of DPT and equilibrium phase transitions.

III.C Further investigation of edge modes

In this section, we discuss quantities which might be interesting towards a better understanding of dynamical phase transitions (DPT). So far, there are only numerical results available, but we hope, that it might be possible to calculate these quantities analytically at least in the SSH model, and thus to gain a deeper insight to the underlying physics.

III.C.1 Overlap with single-particle states

The Loschmidt echo (LE) is the overlap between to many-particle wave functions and thus a highly non-local quantity. If the edge modes of the topological phase are connected to DPT, it is natural to assume that something happens near the edge [96]. Because we know the time dependent correlation matrix $R(t)$, see also eq. (II.D.38), it is in principle possible to calculate any dynamical property of the system.

If we were considering a single-particle problem, the local density

$$\rho_j = \left\langle c_j c_j^\dagger \right\rangle \tag{III.C.1}$$

would be an interesting quantity. Here, we consider a problem with $\frac{N}{2}$ particles. We start in the ground state of the model, and $\langle\cdot\rangle$ indicates an expectation value. After the quench, the system is in a highly excited state, but due to space inversion symmetry, the overall density is $\rho_j = \frac{1}{2}$ for all times.

Instead of investigating the local density in real space basis, we can do the same calculation in the energy basis, where the initial Hamiltonian of the system is diagonal. Because the system evolves under the (non-diagonal) final Hamiltonian, we observe a non-trivial time evolution in this basis. We calculate the overlap with the single-particle states as

$$P_k(t) = \langle k| R(t) |k\rangle . \tag{III.C.2}$$

$|k\rangle$ denote the eigenstates of the initial Hamiltonian,

$$\langle k| \mathbf{H}^{\mathsf{i}} |k\rangle = \epsilon_k^{\mathsf{i}}. \tag{III.C.3}$$

We consider the SSH model at large values of $|\delta|$, because the edge modes are then strongly localized and it is sufficient to evaluate $P_{\frac{N}{2}}$ and $P_{\frac{N}{2}+1}$, which is shown in figure III.27.

Although there is still a significant coupling between the dimers, a DPT happens when both edge modes are equally populated. The energy difference between the edge modes is very small compared to the energy difference between the other modes. In the time average, there is always one particle in these two modes,

$$\frac{1}{t}\int_0^t \left(P_{\frac{N}{2}}(\tau) + P_{\frac{N}{2}+1}(\tau)\right) \mathrm{d}\tau = 0.5 \tag{III.C.4}$$

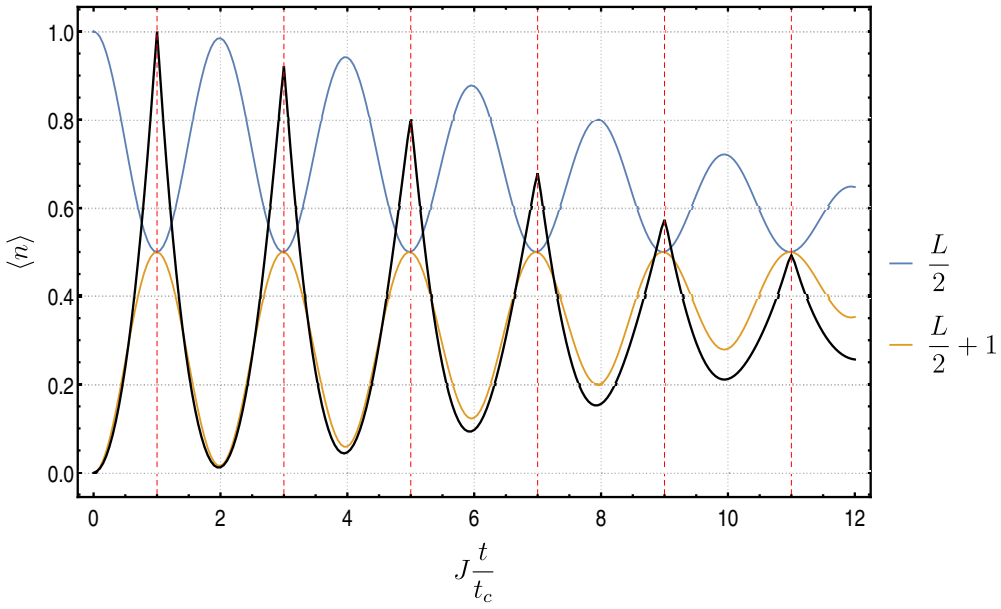

Figure III.27: Single-particle overlap in the edge modes, evaluated for a symmetric quench from the topological to the topologically trivial phase at $|\delta| = 0.8$ and $N = 200$ lattice sites. The solid black line is the normalized Loschmidt return rate (LRR), the red dashed lines indicate the critical times.

One can think of the edge modes as an effective two-level system which determines the DPT. In this picture, the single-particle overlap corresponds to a Rabi oscillation, and the DPT occur when the Bloch vector in this two-level system crosses the equator of the Bloch sphere. The Rabi-type oscillation we observe is bounded by $P_k(t) = 0.5$, i.e. there is no complete transfer of probability into the initially unoccupied mode as in usual Rabi oscillations.

Note this is not the same Bloch sphere as the construction in ref. [14]: Here, we fix an initial pair of states instead of a final one. Instead it is an effective model at large $|\delta|$ which only takes into account the two localized modes. One of those modes is occupied at $t = 0$ and it should be possible to describe the Rabi-type oscillations analytically. If one only considers the two edge states, it looks like one can read off when DPT occur from the points where they are equally populated.

In principle, one could also construct a Bloch sphere for pairs of bulk modes, because eq. (III.C.4) can be generalized due to particle-hole symmetry (PHS). In general, it reads

$$\frac{1}{t}\int_0^t \left(P_m(\tau) + P_{N-m+1}(\tau)\right) \mathrm{d}\tau = 0.5 \tag{III.C.5}$$

and holds for any $1 \leq m \leq \frac{L}{2}$. Away from $m = \frac{N}{2}$, the energy difference of these modes is of the same order of magnitude as for any other combination of modes, and the oscillation does not decouple from the rest of the system and is therefore meaningless to DPT. Its period is still similar to the critical time, but no longer equal.

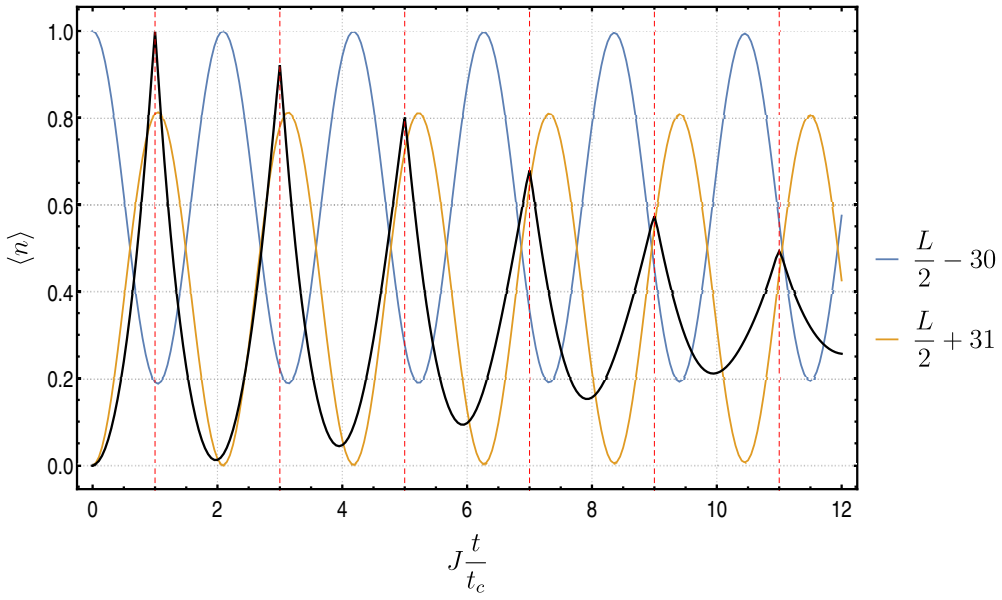

Figure III.28: Single-particle overlap in two bulk modes, evaluated for a symmetric quench from the topological to the topologically trivial phase at $|\delta| = 0.8$ and $N = 200$ lattice sites. The solid black line is the normalized LRR, the red dashed lines indicate the critical times. This behaviour is similar for other bulk modes. Frequency and Amplitude change as one compares different pairs of states.

III.C.2 Entanglement entropy

The von Neumann entanglement entropy (EE) of a bipartite system AB is

$$S_{\text{ent}} = -\text{Tr}\left\{\rho_A \log \rho_A\right\} = -\text{Tr}\left\{\rho_B \log \rho_B\right\}, \tag{III.C.6}$$

where ρ_A and ρ_B are the reduced density matrices of the subsystems A and B, respectively. Starting from the density matrix of the whole system ρ_{AB}. In our case, the subsystem A contains the first m sites of a chain of N sites, and B contains the remaining $N - m$ sites. Then, the reduced density matrices are

$$\rho_A = \text{Tr}_B\left\{\rho_{AB}\right\} = \sum_{i=m+1}^{N} \langle i|\, \rho_{AB}\, |i\rangle \tag{III.C.7}$$

for the first part and

$$\rho_B = \text{Tr}_A\left\{\rho_{AB}\right\} = \sum_{i=1}^{m} \langle i|\, \rho_{AB}\, |i\rangle \tag{III.C.8}$$

for the second part. $|i\rangle$ denote the Cartesian unit vectors, whose only non-zero component is a 1 at the i-th position.

For free systems, there is a simple relation between the relevant eigenvalues of the single-particle Hamiltonian and those of the many-particle Hamiltonian. Therefore, the EE can be calculated from the Fock space correlation matrix R, which is also used to calculate the LE [17; 81; 82; 85; 99]. The correlation

matrix of the subsystem we trace over R_m is then the $m \times m$ submatrix of the ground state correlation matrix R.

$$R_m = \begin{pmatrix} R_{11} & \cdots & R_{1m} \\ \vdots & \ddots & \vdots \\ R_{m1} & \cdots & R_{mm} \end{pmatrix}, \tag{III.C.9}$$

with R_{ij} being the entries of R. Let now

$$\mathrm{diag}(\lambda_1, ..., \lambda_m) = U R_m U^\dagger \tag{III.C.10}$$

be the diagonal matrix containing the eigenvalues of R_m for a certain unitary transformation U [17; 81]. Then,

$$S_{\mathsf{ent}} = \sum_i \left[\lambda_i \log(\lambda_i) + (1-\lambda_i)\log(1-\lambda_i)\right]. \tag{III.C.11}$$

The matrix R_m is highly singular: For the full correlation matrix R, all eigenvalues are either $\lambda_k = 1$ or $\lambda_k = 0$, because the mode is either populated or empty at $t = 0$. In both cases, one of the two logarithms in eq. (III.C.11) diverges in the ground state. We find that also in the submatrix R_m many eigenvalues are close enough to 0 or 1 to cause numerical problems in the time evolution.

The factor in front of the logarithms regularizes their divergence, because it is (up to a numerical error) identically zero in these cases. Still, to use the above equation numerically, we must sum only over those λ_i that are "different enough" from zero or one, respectively, in the sense, that the difference is two or three orders of magnitude above the numerical precision error. For double precision, that means it is larger than, say, 10^{-14}.

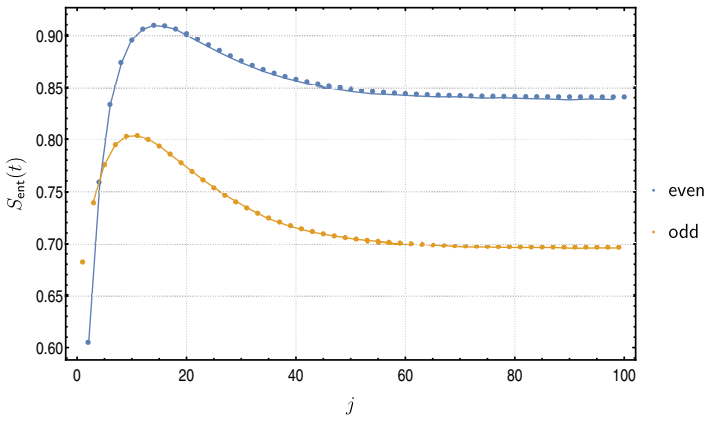

Figure III.29: Entanglement entropy (EE) at $t = 0$ for a chain containing $\frac{N}{2} + 1$ particles, with $N = 200$. We compare the ED results (dots) with data from ref. [99] (lines). We can reproduce their data, even though we consider a finite chain instead of a semi-infinite one. In the middle of the chain, i.e. near $j = \frac{N}{2} = 100$, the contribution from the edges already decayed completely, and thus only the bulk EE is present. Because of the staggered hopping, the EE behaves distinctly different for a cut at even or odd lattice sites j.

We calculated both the ground state EE S_{ent} in the SSH model for different values of δ. For $\delta = 0.04$ at $t = 0$, we checked our algorithm against data from ref. [99], and in figure III.29, we show that we obtain identical results up to the error of numerical precision.

In order to calculate the time evolution of the EE $S_{\mathsf{ent}}(t)$, we use the time dependent correlation matrix $R_m(t)$, which we obtain similar to eq. (III.C.9), except that it is a submatrix of the time-dependent

correlation matrix $R(t)$, which is given by eq. (II.D.38). We can not directly compare our results to previous works in this case, but we recognize a similar behaviour as in ref. [21; 82].

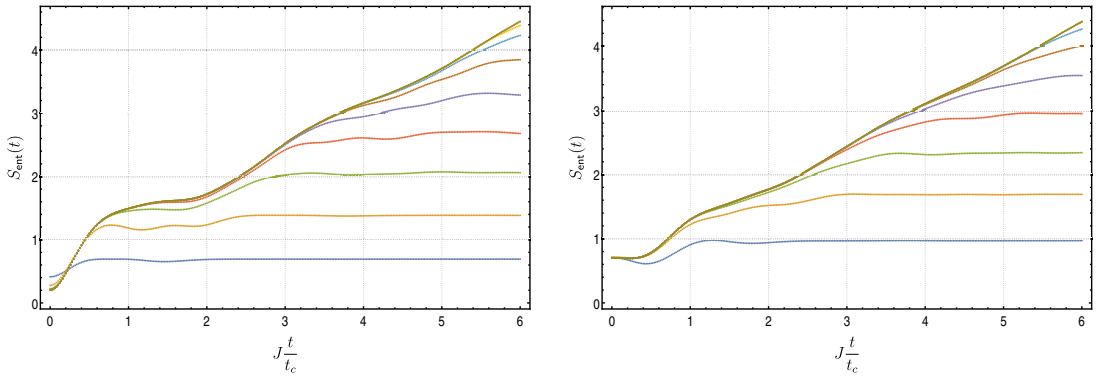

Figure III.30: Entanglement entropy (EE) of the first n sites of the chain with the remaining $N-n$ sites after a symmetric quench from the topological to the topologically trivial phase at $|\delta| = 0.3$. Left panel: odd $n = 1, 3, 5, \ldots$, right panel: even $n = 2, 4, 6, \ldots$. For larger n, the EE converges to the bulk EE. At small n and large t, there is a maximal EE depending on n. For odd n, the oscillations of $S_{\text{ent}}(t)$ are stronger than for even n, because in the trivial phase, odd n means that a strong bond is cut open.

In figure III.30, the chain was symmetrically quenched from the topological to the topologically trivial phase at $|\delta| = 0.3$, in figure III.31, the quench was in the opposite direction. The oscillations at small times are stronger if we cut a strong bond in both cases, because the entanglement between dimerized sites is much larger that between neighbouring dimers. For larger n, the EE seems to converge towards a bulk EE, which is independent of n.

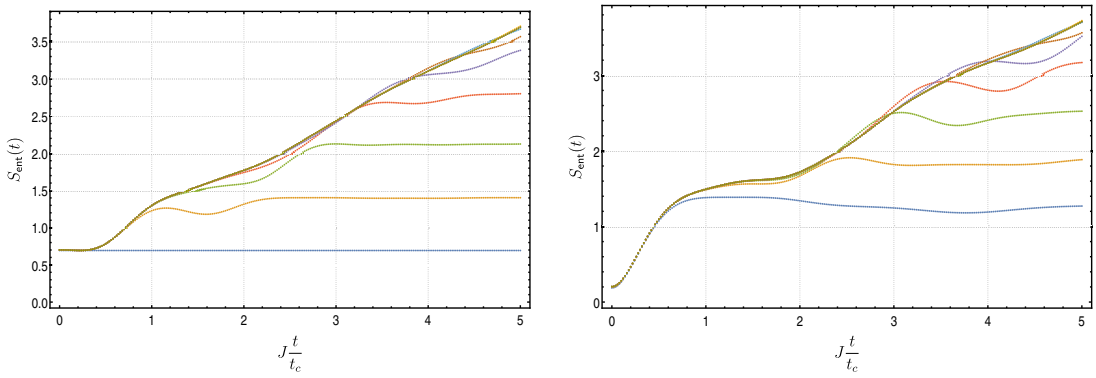

Figure III.31: EE of the first n sites of the chain with the remaining $N-n$ sites after a symmetric quench from the topologically trivial to the topological phase at $|\delta| = 0.3$. Left panel: odd $n = 1, 3, 5, \ldots$, right panel: even $n = 2, 4, 6, \ldots$. Here, we cut a strong bond if n is even, and therefore the oscillations at small t are larger for even n. The EE for $n = 1$ is constant in time at $S_{\text{ent},n=1}(t) \approx \log(2)$, which is a hint for a strong entanglement between the edge modes, because the neighbouring sites are weakly coupled.

In the topologically non-trivial phase, the edge modes are very close to each other in energy. It is known that the entanglement spectrum has a twofold degeneracy [33; 99], but it is unclear how strong the edge

modes are entangled. Spatially they are localized at the edges of the system, and thus we expect their effect on the EE to be visible for a cut anywhere in the chain. The case that is the easiest to handle is when the chain is cut in the middle, because the bulk-like behaviour of the contribution from all other modes is most distinct.

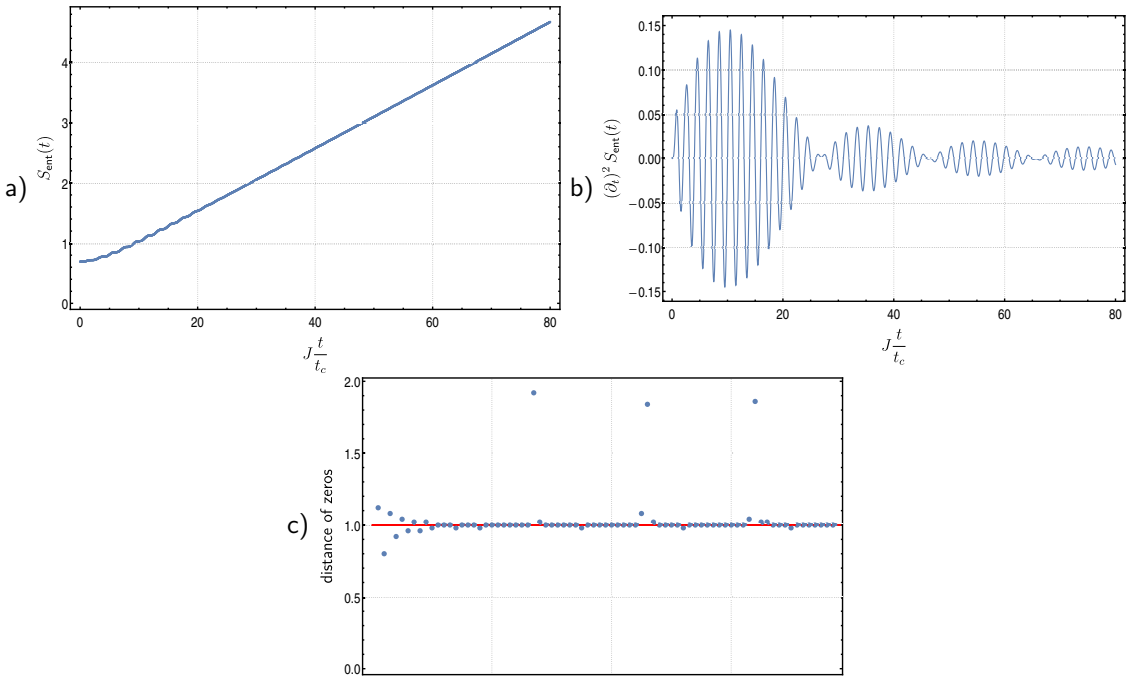

Figure III.32: EE when the chain is cut in half after a symmetric quench from the topological to the topologically trivial phase at $|\delta| = 0.9$ (a). The oscillations at small t decay slower for large $|\delta|$, and become visible in the second derivative of $S_{\text{ent}}(t)$ (b). It looks like there are two main frequencies of the oscillation, the shorter one being the inverse critical time. Panel (c) shows the distance between neighbouring zeros of $(\partial_t)^2 S_{\text{ent}}(t)$ in units of t_c, which is one for sufficiently large times except at the zeros of the envelope function.

We further assume the edge contribution to be best observable at large dimerizations, because the sound velocity in the system

$$v_{\text{snd}}(\delta) = \max_{k\in(0,\frac{\pi}{2})} \left(\frac{\partial \epsilon_k^{\text{f}}}{\partial k} \right). \tag{III.C.12}$$

Evaluating this expression and using eq. (II.B.42), we obtain

$$\epsilon_k^{\text{f}} = \sqrt{\vec{d}_k^{\text{f}} \cdot \vec{d}_k^{\text{f}}} = 2\sqrt{(\cos^2(k) + \delta^2 \sin^2(k))} \qquad \text{and thus} \tag{III.C.13}$$

$$\left(\frac{\partial \epsilon_k^{\text{f}}}{\partial k} \right) = 2\frac{(\delta^2 - 1)\sin(2k)}{\sqrt{\cos^2(k) + \delta^2 \sin^2(k)}}. \tag{III.C.14}$$

Close to $|\delta| = 1$, the denominator becomes one and the maximum is determined by the numerator. In this limit, the maximum is close to $\frac{3\pi}{4}$, and the speed of sound becomes

$$v_{\text{snd}}(\delta) = 2 - 2\delta^2 \underset{\delta\to 1}{\longrightarrow} 0. \tag{III.C.15}$$

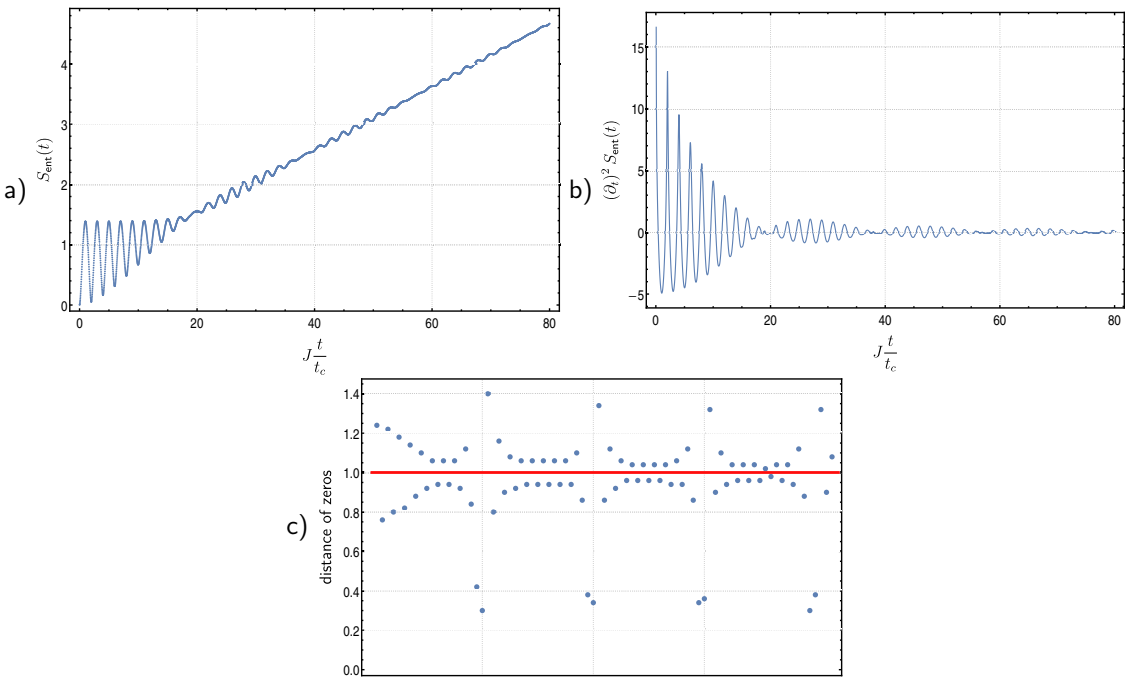

Figure III.33: EE when the chain is cut in half after a symmetric quench from the topologically trivial to the topological phase at $|\delta| = 0.9$ (a). In this case, the envelope function of the second derivative (b) clearly shows a different behaviour than for the quench in the opposite direction. Panel (c) shows again the distances between the zeros of $(\partial_t)^2 S_{\text{ent}}(t)$, which remain close to one but now oscillate between values slightly larger or smaller than one.

Therefore, there is few long-range entanglement between the bulk states, and the EE is mostly determined by the edge states.

Due to these considerations, we expect the EE to show an interesting behaviour at large $|\delta|$. Results of the first few calculations are shown in figure III.32 and figure III.33. The relation between the frequency of the faster oscillation and t_c holds over a wide range of $|\delta|$ and becomes more distinct as $|\delta|$ approaches one. It is distinctly visible for $0.6 \leq |\delta| < 1$. For smaller $|\delta|$, the envelope frequency is in the same order of magnitude, and causes a number of additional zeros in $(\partial_t)^2 S_{\text{ent}}(t)$, such that the mutual distance between the zeros below is no longer insightful for small t. However, even for $|\delta| = 0.3$, we find a periodicity of the zeros close one, because the envelope decays and the additional zeros vanish. The frequency f_{env} of the envelope function seems to scale roughly as

$$f_{\text{env}} \approx \frac{c}{v_{\text{snd}}} \tag{III.C.16}$$

for some constant c. It does not change dependent on the system size. Therefore, we assume that the envelope oscillation is related to the quasi-particles created by the quench. Similar oscillations of the EE in Fermi-gases have been observed [29], and it seems reasonable to expect a signature of all relevant time scales in the EE.

In panel (a) of figure III.33, the EE is limited by $2\log(2)$ for small times if we cut a strong bond. For large delta, there is nearly no long-range interaction between the dimers. One possible explanation for this value is, that there are two sources of EE playing a role in this case. There is a strong entanglement between

the two sites for the opened dimer. The other $\log(2)$ contribution might be causes by the entanglement of the edge modes.

Chapter IV

Conclusion and outlook

IV.A Review of main results

In the present thesis, we investigated the interplay of topological phase transition (TPT) and dynamical phase transitions (DPT) in free fermion (FF) systems. Previous studies in this field nearly exclusively considered FF in periodic boundary conditions (PBC), where momentum is a good quantum number and therefore, the Loschmidt echo (LE) is known analytically. However, open boundary conditions (OBC) are more interesting because real systems usually have OBC. In particular, characteristic edge modes are present in topologically non-trivial systems iff there is an open boundary.

IV.A.1 Dynamical topological order parameter

In PBC, one considers the phase of the LE to define, inspired by the Pancharatnam geometric phase (PGP) [80], a dynamical topological order parameter (DTOP) [14]. This parameter counts how often the wave function wraps the unit circle as the momentum k sweeps through the Brillouin zone.

Because it is unknown how general this formalism is, we applied it to different models with different topological properties. It is unclear, if a TPT always triggers a DPT. It was shown, that this holds in systems with a $\mathbb{Z}_2$ winding number. Numerically, we did not find a counterexample in the long-ranged Kitaev chain. We simulated a number of quenches between phases with different winding numbers, see section III.A.

For all the quenches we simulated, there are at least two critical time scales. Each time scale causes either a jump up or a jump down in the DTOP. Ordering the time scales by their critical times, the direction of the jump alternates. If for example the shortest critical time causes a jump up, the second shortest critical time must cause a jump down and so on, due to continuity and periodicity restrictions on $\hat{d}_k^{\mathrm{i}} \cdot \hat{d}_k^{\mathrm{f}}$. Therefore, the monotony of the DTOP known from systems with a $\mathbb{Z}_2$ winding number is necessarily lost in systems with more than one critical time scale.

In our simulations, we have not encountered a quench after which the LE is smooth for all times. Numerically, it looks like the crossing of a TPT still causes DPT in systems with an $\mathbb{Z}$ winding number. We stress that it might however be possible to construct a counterexample, so this question remains open.

IV.A.2 Dynamical bulk-boundary correspondence

Bulk-boundary correspondence (BBC) is a well-known equilibrium property of TI, see section II.A.1.iii. Due to the analogy of DPT and equilibrium phase transitions (EPT), the question whether there is a dynamical equivalent arises naturally. Based on an unpublished study of Sedlmayr [96], we examined the edge contribution of the LE, which we extract using an extrapolation to the thermodynamic limit.

The eigensystem of the SSH model is given analytically up to an implicit function, which has to be treated numerically. All calculations can be done based on this solution, and we can test numerical approaches against the semi-analytical solution. We implemented an algorithm based on exact diagonalization (ED) to calculate the LE in open boundary conditions, as described in section II.D.5.

The edge contribution of the LE has jumps at the critical times for all quenches we simulated in the SSH chain, the Kitaev chain and the long-ranged Kitaev chain, see section III.B.2. This indicates that something must happen in the edge modes. We found, that in the particle-hole symmetric (PHS) SSH model, the occurence of DPT lines up with the times where both edge modes are equally populated for large dimerization strengths, as we show in section III.C.1. In this limit, it should be possible to set up an effective Rabi-like model, which only takes into account the edge modes.

We calculated the von Neumann entanglement entropy (EE) after a quench in the SSH chain and researched the structure of the oscillations at small times, see section III.C.2. We essentially find two interfering oscillations. One of them has a period of two times the critical time of the DPT, the other

seems to be related to the inverse velocity of sound in the system. Concerning DPT, the first is clearly the more interesting one. At small times, if a strong bond of the chain is cut, the EE oscillates between 0 and $2\log 2$ and if a weak bond is cut, it remains nearly constant at $\log 2$. Because at large values of the dimerization the neighbouring dimers are nearly completely decoupled, this observation can only be explained by a strong entanglement between the edge modes.

All these results can be explained by dynamical BBC which seems to be present at least in the SSH model: If there is dynamical BBC, any change of topology in the bulk leads to singularities at the edges. Therefore, the edge contribution to a global quantity like the LE would be expected to be singular at critical times. It also makes sense to assume a strong entanglement between these modes, because they necessarily share mutual information across a long spatial distance.

IV.B Future work

We only started to understand how symmetry-protected edge modes influence the non-equilibrium time evolution of a FF system. In PBC, it is still unclear whether or not the relation between TPT and DPT holds in general, e.g. in systems which do not belong to the BDI symmetry class.

A more general approach than running simulations would require an analytical understanding of what is happening at the edges. A promising idea is to use the formalism of Fredholm determinants which is widely used in Bethe ansatz calculation and random matrix theory [27; 28].

Numerically, it might be interesting to calculate the EE in other systems than the SSH chain, which is only possible using the ED algorithm, since no analytic solutions are known for these systems in OBC. In the SSH chain, it should also be possible to derive an explicit expression for the EE, which would allow a more detailed understanding of the time scales of the oscillations. Further, one could search for an equivalent to the overlap with the initial state in systems without PHS, or to understand en effective model analytically.

Our ED algorithm uses only matrix multiplication on GPU so far. It would also be interesting to put more parts of the algorithm on coprocessors like graphics processing units (GPU) or Xeon Phi accelerators (XPA). These devices have a different memory mapping than usual processors and achieve their performance by combining many cores at lower clock frequencies instead of few cores at very high frequencies. Therefore, they are an ideal environment for of parallel algorithms. Many standard matrix operations such as multiplication or diagonalization are known to be highly parallelizable.

Most current GPU implementations only support single precision calculations, some also work with double precision. If this is sufficient, we can in principle implement most of our ED algorithm on a GPU. Sometimes, our algorithm needs higher precision, as pointed out in section III.B.1. Double-double and quad-double libraries are not available for GPU yet, but in principle they compile on XPA, which, unlike GPU, support the x86 command set nearly completely. Being able to perform simulations completely on GPU or XPA would cut the needed calculation time drastically and allow us to run simulations in a much larger range of models and parameters.

Chapter V

Acknowledgements

I would like to acknowledge my advisers, Dr. Jesko Sirker and Dr. Sebastian Eggert for their support throughout the thesis project. Further, I thank the department of physics and astronomy for the invitation to University of Manitoba, the hospitality, and for financial support. My stay in Winnipeg was partly financed PROMOS programme of the German academic exchange service (Deutscher Akkademischer Austauschdienst, DAAD).

The thesis project was also supported by NVidia Corp. by donating a Tesla K40 GPU which was used for some calculations, and by Compute Canada and WestGrid, and the Regionales Hochschulrechenzentrum Kaiserslauern (RHRK) by providing high-performance computing (HPC) resources. I specially acknowledge the support of Dr. Grigory Shamov, who provided support setting up the GPU and installing all drivers correctly, as well as compiling various libraries for the use on GREX, the local HPC cluster at University of Manitoba. The same goes for the Guillimin Support team at McGill university in Montréal, QC.

This thesis is partly based on previous works by two former group members, Dr. Nicholas Sedlmayr (now Michigan State University, US-MI) and Dr. Moitri Maiti (now Joint Institute for Nuclear Research, Dubna, RU). The development of the multi-precision exact diagonalization algorithm was supported by Craig McRae.

Further, I owe thanks to my colleagues Max Kiefer, Andrew Urichuk, Louis Chen, Amin Naseri, Laura Mihalceanu, Ellen Wiedemann, and Dr. Maxime Lanoy for many helpful discussions, and for their support during typesetting and proofreading this thesis. I also would like to thank Dr. Elroy Friesen and University of Manitoba Singers for keeping me in touch with the non-physics world throughout the year. Finally, I also would like to thank my family for supporting me during my programme and during the thesis project.

Eidesstattliche Erklärung

Hiermit erkläre ich, C. Philipp Jaeger, dass ich die Diplomarbeit selbstständig verfasst und keine anderen als die angegebenen Quellen und Hilfsmittel benutzt habe. Wörtlich oder sinngemäß übernommenes Gedankengut wurde als Entlehnung kenntlich gemacht. Die Arbeit wurde keinem Prüfungsamt vorgelegt und bisher nicht veröffentlicht.

C. Philipp Jaeger

Appendix A

Correlation functions

Correlation functions (CF) are a very basic and widely used concept in physics. In many-particle physics, they are particularly interesting, because they contain all information about how particles interact. In this appendix, we will briefly introduce this concept. We also discuss the Wick theorem, which provides an easy way to calculate higher-order correlations, and how to use CF to obtain local quantities such as, for example, the susceptibility. Later on, we show some simulations of CF in the Su-Schrieffer-Heeger (SSH) model.

A.1 Green's functions

In Quantum field theory (QFT), a common way of treating CF is the notion of Green's functions (GF). In general, a GF G is the inverse of a differential operator L,

$$Ly = f \tag{A.1.1}$$

with parameters y. The fundamental solution of this equation is given by a right-inverse operator G, which fulfills $LG = 1$, and therefore

$$y = Gf. \tag{A.1.2}$$

Then,

$$Ly = L(Gf) = (LG)f = f \tag{A.1.3}$$

To an arbitrary inhomogeneity f, the particular solution is then given by the convolution

$$y_{\mathsf{P}} = G * f \equiv \int \mathcal{G}(x - x')f(x')\mathrm{d}x'. \tag{A.1.4}$$

The function $\mathcal{G}(x)$ is called a *Green's function*. These functions are often used in QFT to calculate expectation values like for example CF.

DEFINITION A.1 *(Correlation function)*

Let $\hat{\phi}(\vec{x}_m)$ be a scalar field depending on the parameters $\vec{x}_m$. Then, the correlation function is

$$\left\langle \hat{\phi}(\vec{x}_1)...\hat{\phi}(\vec{x}_n) \right\rangle = \langle \mathsf{vac}|\, N\hat{\phi}(\vec{x}_1)...\hat{\phi}(\vec{x}_n)\, |\mathsf{vac}\rangle\,, \tag{A.1.5}$$

where N is the normal-ordering operator.

For example, for fermionic operators c_j, $c_j^\dagger$ on lattice sites j at $T = 0$, the two-point correlation

$$\langle c_i c_j^\dagger \rangle = \delta_{ij} \tag{A.1.6}$$

is only non-zero if i and j are identical.

At zero temperature, (two-point) GF are related to two-point CF by

$$\mathcal{G}(x - x') = -\mathrm{i}\langle \hat{\phi}(x)\hat{\phi}^\dagger(x')\rangle. \tag{A.1.7}$$

For a detailed discussion we refer to ref. [74].

A.1.1 Wick's Theorem

Writing the expectation value in definition A.1 as an integral, we find that it becomes tricky to evaluate even for small n. Luckily, it is possible to decompose higher-order CF into two-point CF relatively easily. Experimentally, one finds that higher-order CF are only non-zero if they contain the same number of creation and annihilation operators.

THEOREM A.2 *(Wick's Theorem)*

Let $\hat{\phi}(\vec{x}_m)$ be a scalar field depending on the parameters $\vec{x}_m$. Then

$$\left\langle \hat{\phi}(\vec{x}_1)...\hat{\phi}(\vec{x}_n) \right\rangle = \sum_{m=1}^{n} \sum_{l=1}^{n-m} \sigma(l) \left\langle \hat{\phi}(\vec{x}_m)\hat{\phi}(\vec{x}_{m+l}) \right\rangle, \tag{A.1.8}$$

where $\sigma(l)$ is the sign of the permutation of the field operators.

Evaluating the normal-ordering operator, we take into account all possible pairings of operators. For n operators, one consequently obtains $n!$ possible pairings. If the operators are fermionic, one has to keep track of the anti-commutators, and every other term must be counted with a negative sign. This is implemented by the function $\sigma(l)$.

With this theorem, we can evaluate any CF-based quantity relatively easily, because the correlation matrix R (see eq. (II.D.40)) is known, and its entries are all two-point correlations in the system. In the following section, we give an example how to use Wick's theorem evaluating the local susceptibility.

A.1.2 Susceptibility

In many-particle systems, it is often insightful to investigate correlation functions (CF). In this system, the density-density CF is given by the correlation matrix eq. (II.D.38), which contains all two-point correlations in real space.

Applying Wick's theorem A.2, also higher order CF are accessible. If DPT are related to the local occupation number, one would expect some non-trivial behaviour in the local compressibility, which measures the energy needed to insert an additional particle into the system or to remove one at some lattice site i. It is defined as

$$\chi_i = -\frac{\partial \langle n_i \rangle}{\partial \mu}, \qquad \text{where} \qquad n_i = \left\langle c_i^\dagger c_i \right\rangle . \tag{A.1.9}$$

We evaluate the derivative using the definition of the expectation value in the grand canonical ensemble. We are interested in the particle-hole symmetric case at half filling, and thus we evaluate the derivative at $\mu = 0$.

$$\langle n_i \rangle = \frac{\mathrm{Tr}\left\{ n_i \cdot \mathrm{e}^{-\beta(\mathbf{H}_0 - \mu N)} \right\}}{\mathrm{Tr}\left\{ \mathrm{e}^{-\beta(\mathbf{H}_0 - \mu N)} \right\}} \tag{A.1.10}$$

and thus

$$\chi_i = \left\langle n_i \sum_j n_j \right\rangle - \sum_j \langle n_i \rangle \langle n_j \rangle . \tag{A.1.11}$$

Further, $\langle n_i \rangle = 0.5$ for any site i, as we consider the SSH chain to be half-filled. This makes the second term trivial to evaluate. The first term is a four-point CF, which we treat applying Wick's theorem. As all operators in the bracket act at a single time, there are three possible orderings:

$$\left\langle n_i \sum_j n_j \right\rangle = \sum_j \left\langle c_i^\dagger c_i c_j^\dagger c_j \right\rangle \tag{A.1.12}$$

$$= \left\langle c_i^\dagger c_i \right\rangle \sum_j \left\langle c_j^\dagger c_j \right\rangle - \sum_j \left\langle c_i^\dagger c_j^\dagger \right\rangle \left\langle c_j c_i \right\rangle - \sum_j \left\langle c_i^\dagger c_j \right\rangle \left\langle c_i c_j^\dagger \right\rangle \tag{A.1.13}$$

$$= \frac{N}{4} - 0 + 1 - \sum_j R_{ij} R_{ji}. \tag{A.1.14}$$

The first term cancels with the remainder of χ_i. To evaluate the second term, we use the anti-commutation relation for the fermionic operators

$$\left[c_i^\dagger, c_j \right]_+ = \delta_{ij} \tag{A.1.15}$$

$$\Rightarrow c_i^\dagger c_j = \delta_{ij} - c_j c_i^\dagger \tag{A.1.16}$$

Using the fact that the correlation matrix $\mathbf{R}$ is hermitian, the final result is

$$\chi_i = \frac{N}{4} + 1 - \sum_j R_{ij} R_{ij}^\dagger - \frac{N}{4} = 1 - \sum_j |R_{ij}|^2 . \tag{A.1.17}$$

A.2 Simulations in the SSH chain

At $T = 0$, this is identically 0.5 at all times, because the Fermi distribution is a step function. Thus, for all i, j it is either $\left\langle c_i c_j^\dagger \right\rangle$ or $\left\langle c_i^\dagger c_j \right\rangle$. For finite systems, there is always a gap, because the eigenstates are discrete. If there is no temperature or chemical potential larger that this gap present, the CF of the type $\left\langle c_i c_j^\dagger \right\rangle \left\langle c_i^\dagger c_j \right\rangle$ are always trivial. To work around this problem, we can introduce either a finite chemical potential or a finite temperature larger than the finite size gap, as shown in figure I.1.

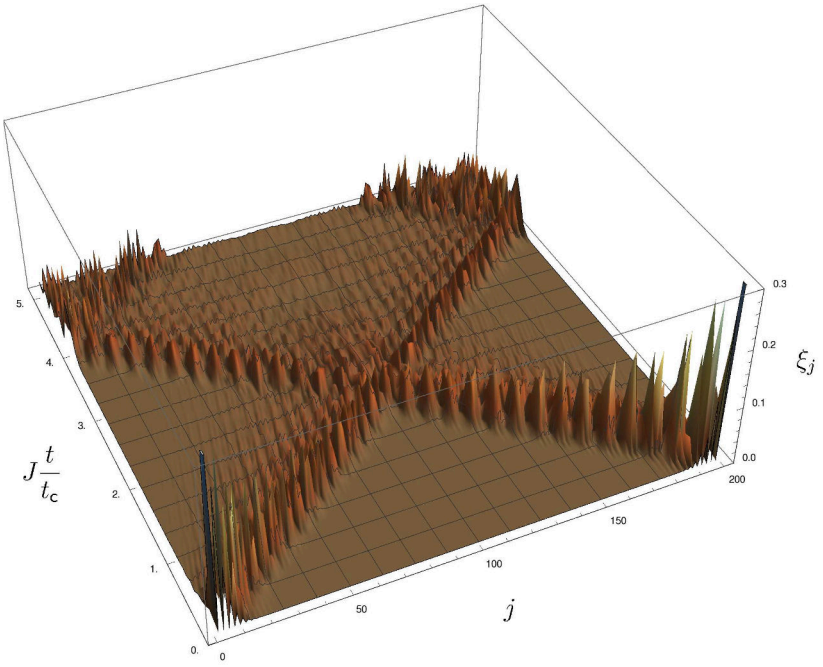

Figure I.1: Local susceptibility over time and lattice site. We evaluated the derivative $\left(\frac{\partial \langle n \rangle}{\partial \mu}\right)$ numerically at a finite value $\mu = 0.1 \to -0.1$, in order to circumvent finite-size gap. At the time of the quench, quasi-particles are generated in the system, which move in a light-cone shape [101]

When initially implementing the calculation of χ_i, we accidentally calculated instead the quantity

$$\tau_i = \left| \sum_j \left\langle c_i c_j^\dagger \right\rangle \right|^2 = \left| 1 - \sum_j R_{ij} \right|^2 , \tag{A.2.1}$$

which turns out to show an interesting behaviour. Physically it can be interpreted as the square of the sum over the tunnelling amplitudes from site i to j or vice versa, or as a total flow rate at site i from or to the rest of the chain. We calculated this CF using the semi-analytic solutions for the SSH model.

In the case where edge modes are present after the quench, the compressibility at the edges goes down to around 0.7 and stays there, whereas if there are no edge modes, it drops to 0 almost immediately at the boundaries.

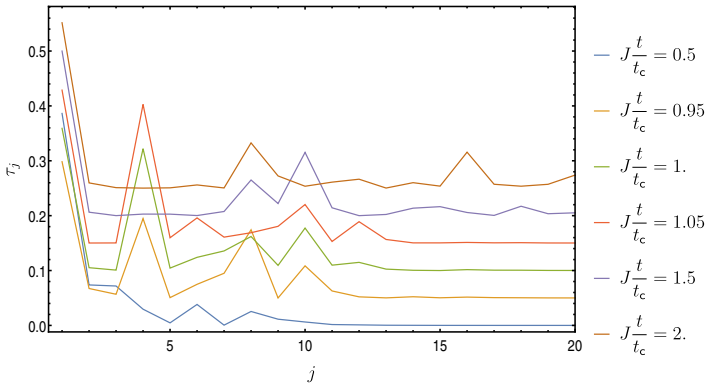

Figure I.2: Flow amplitudes on the first few lattice sites from the edge of the system at several times, evaluated for a SSH chain of length $N = 200$ with dimerization strength $\delta = 0.3$. The individual graphs are offset for the sake of clarity by multiples of 0.05.

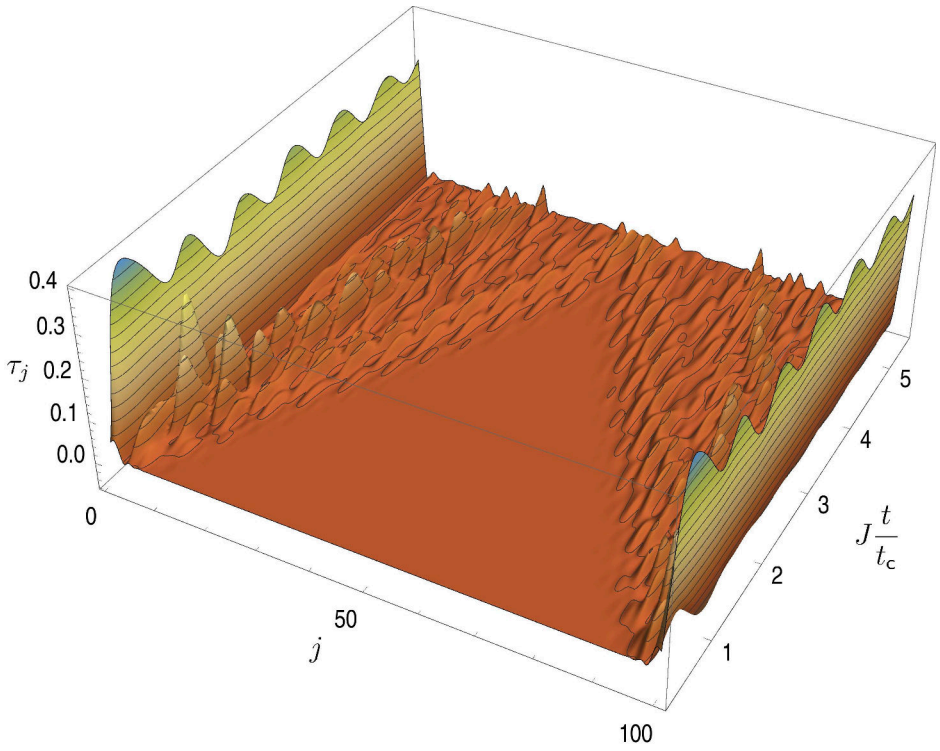

Figure I.3: Correlation landscape. The overall tunnelling rate is large near the edges, and numerically zero in the bulk for small times. At $t = 0$, quasi-particles are created at the edges [101], which propagate in a light-cone like shape into the bulk.

Appendix B

Programmes

In this appendix, we show some of the algorithms we used for our simulations. The code is cut to the most important lines due to readability. We omit most initialization of variables etc., because it is not really insightful.

B.1 GMP benchmark routines

As an example for the arbitrary precision algorithms, we show the benchmark code for matrix diagonalization using MPACK and GMP.

```
#include <iostream>
#include <mblas_gmp.h>
#include <mlapack_gmp.h>
#include <gmpxx.h>
#include <gmp.h>
#include <time.h>
#include <omp.h>

#define N 50

#define NUM_MAX 12
#define PREC_MIN 100
#define PREC_MAX 5000
#define PREC_STEP 100

#define mpc2int(mpc) (mpc.real().get_ui())

using namespace std;

float dt_msec(timespec t0, timespec t1)
{
    return (t1.tv_sec - t0.tv_sec) * 1000.0f + \
            (t1.tv_nsec - t0.tv_nsec) / 1000000.0f;
}

int main (void)
{
    for (long prec = PREC_MAX; prec >= PREC_MIN; prec-=PREC_STEP) {
        double sumdt = 0;
        double sumsquares = 0;
        long trueprec = 0;
        #pragma omp parallel for reduction (+:sumdt) reduction \
                (+:sumsquares) firstprivate (prec)
        for (int num =1; num <= NUM_MAX; num++) {
            timespec t1, t2;
            mpf_set_default_prec(prec);
            mpc_class *A = new mpc_class[N*N];
            mpc_class *work = new mpc_class[N*N];
            mpf_class *rwork = new mpf_class[3*N-2];
            mpf_class *D = new mpf_class[N];
            long info;
            gmp_randclass gen (gmp_randinit_default);
```

```
            for(long j = 0; j < N; j++) { //zeile
                for(long i = 0; i <= j; i++) { //spalte
                    mpf_class r = gen.get_f();
                    A[j*N+i]=r;
                    A[i*N+j]=r;
                }
            }
            clock_gettime(CLOCK_REALTIME, &t1);
            Cheev("V", "U", N, A, N, D, work, -1, rwork, &info);
            mpackint dim = mpc2int(work[0]);
            Cheev("V", "U", N, A, N, D, work, dim, rwork, &info);
            clock_gettime(CLOCK_REALTIME, &t2);
            //print prec and runtime in ms
            double dt = dt_msec(t1, t2);
            sumdt+=dt_msec(t1, t2);
            sumsquares+=dt*dt;  //ms^2
            trueprec=A[0].real().get_prec();
            //printMat(1, N, D, N);
            delete[]A;
            delete[]work;
            delete[]rwork;
            delete[]D;
        }
        double sd = sqrt( sumsquares/NUM_MAX - \
                sumdt*sumdt/NUM_MAX/NUM_MAX );
        cout<<trueprec<<" "<<sumdt/NUM_MAX<<" "<<sd<<endl<<flush;
    }

    return 0;
}
```

B.2 Mathematica notebooks

B.2.1 Loschmidt echo and DTOP

The following Mathematica code simulate the Loschmidt echo (LE) in an SSH model with dimerization d in periodic boundary conditions with length La.

```
In[1]:= tc = Pi Sqrt[(1 + d^2)/8]/d;
        di[k_] := {Cos[k], d Sin[k], 0};
        df[k_] := {Cos[k], -d Sin[k], 0};
        didf[k_] := di[k].df[k]/Sqrt[di[k].di[k]]/Sqrt[df[k].df[k]];
        eps[k_] := Sqrt[df[k].df[k]];
        G[k_, t_] := Cos[ t eps[k]] + I didf[k] Sin[ t eps[k]];

In[2]:= ledat = ParallelTable[{t, -Sum[
             Log[Abs[G[2 Pi n/La, t tc]]], {n, 1, ParticleFilling}]/
           La}, {t, Range[0, tmax, dt]}];
```

The dynamical topological order parameter (DTOP) can be calculated from the definition II.26 or from the slope of $\hat{d}_k^{\mathrm{i}} \cdot \hat{d}_k^{\mathrm{f}}$,

```
In[3]:= PhiG[k_, t_] :=
        ArcTan[Im[G[k, t] Exp[-I t eps[k] didf[k]]]/
          Re[G[k, t] Exp[-I t eps[k] didf[k]]]];

In[4]:= nuD[t_] := (nudtmp =
          Table[PhiG[2 Pi (n + 1)/La, t] - PhiG[2 Pi n/La, t] /.
            x_ /; Abs[x] > 1 → Null, {n, 1, La/4}];
         tofix = Position[nudtmp, Null];
         For[i = 1, i ≤ Length[tofix], i++,
          nudtmp[[
            tofix[[i]]]] = (nudtmp[[tofix[[i]] - 1]] +
              nudtmp[[tofix[[i]] + 1]])/2
          ];
         Total[nudtmp]/2/Pi);
        nuddat = ParallelTable[{t, nuD[t tc]}, {t, Range[0, tmax, dt]}];
```

In[5]:=
```
s[k_] = Sign[Evaluate[D[0.5 (1 - didf[k]), k]]];
jumps = ;
Clear[t];
For[i = 1, i ≤ Length[tclist], i++, j = 1;
While[(j - 2) tclist[[i]]/tc < tmax,
 AppendTo[jumps,
  s[k /. kc[[i]]] HeavisideTheta[t - j tclist[[i]]/tc]];
 j = j + 2];];
nuD[t_] := Total[jumps];
```

B.2.2 LE in open BC

For the Kitaev chain, we show how to build the correlation matrix and how to calculate the LE using theorem II.22. The variable `Hk` contains the $2N \times 2N$ Bogoliubov-de-Gennes Hamiltonian of the system, as shown in section II.B.2. We diagonalize the initial and the final Hamiltonian and build the correlation matrix `R` and the basis transformation `U` according to section II.D.5.

```
In[6]:= Hki = Evaluate[vv = vi; Delta = Deltai; mu = mui; Hk];
        ESfulli = Transpose[Eigensystem[N[Hki]]];
        ESposi = Sort[Select[ESfulli, #[[1]] > 0 &], #1[[1]] > #2[[1]] &];
        gi = ESposi[[All, 2, ;; L]];
        hi = ESposi[[All, 2, L + 1 ;;]];
        R = KroneckerProduct[{{1, 0}, {0, 0}}, Transpose[hi].hi] +
         KroneckerProduct[{{0, 1}, {0, 0}}, Transpose[hi].gi] +
         KroneckerProduct[{{0, 0}, {1, 0}}, Transpose[gi].hi] +
         KroneckerProduct[{{0, 0}, {0, 1}}, Transpose[gi].gi];

In[7]:= Hkf = Evaluate[vv = vf; Delta = Deltaf; mu = muf; Hk];
        ESfullf = Transpose[Eigensystem[N[Hkf]]];
        ESposf = Sort[Select[ESfullf, #[[1]] > 0 &], #1[[1]] > #2[[1]] &];
        Ekf = ESposf[[All, 1]];
        gf = ESposf[[All, 2, ;; L]];
        hf = ESposf[[All, 2, L + 1 ;;]];
        U = N[KroneckerProduct[{{1, 0}, {0, 1}}, gf] +
          KroneckerProduct[{{0, 1}, {1, 0}}, hf]];
```

Then, we combine the Eigenvalues in the correct order and apply theorem II.22.

```
In[8]:= LE[t_] := Abs[Det[IdentityMatrix[2 L] - R +
           R.Transpose[U].
           MatrixExp[-I*DiagonalMatrix[Join[Ekf, -Ekf]]*t].U]];
        data = ParallelTable[{t, -Log[LE[t tc]]/2/L}, {t, trange}];
```

B.2.3 Calculation of the entanglement entropy

The example below shows how to calculate the (reduced) time-dependent correlation matrix (rTDCM) and the entaglement entropy (EE) in the SSH model. First, we diagonalize the initial Hamiltonian.

```
In[9]:= ESfull = Transpose[ Eigensystem[Hsshi]];
        ES = Sort[ESfull, #1[[1]] < #2[[1]] &];
```

Here, we define the rTDCM `Rt1[l,t]` for the first `l` lattice sites and the EE `Sent1[i,t]`.

```
In[10]:= Rt1[l_, t_] := (
          U1 = (MatrixExp[-I*Hsshf*t tc].Transpose[
               ES[[1 ;; ParticleFilling, 2]]])[[1 ;; l]];
          U1.ConjugateTranspose[U1]);
         Sent1[i_, t_] := (
          ev = Re[Eigenvalues[Rt1[i, t]]];
          -Re[Sum[
             If[And[10^-10 ≤ ev[[j]], ev[[j]] ≤ 1 - 10^-10],
              N[ev[[j]] Log[ev[[j]]] + (1 - ev[[j]]) Log[1 - ev[[j]]], 200],
              0], j, 1, i]]
          );
```

Bibliography

[1] Altland, A. and M. R. Zirnbauer
1997. Nonstandard symmetry classes in mesoscopic normal-superconducting hybrid structures. *Physical Review B (Condensed Matter)*, 55(2):1142–1161.

[2] Anderson, P. W.
1967. Infrared Catastrophe in Fermi Gases with Local Scattering Potentials. *Physical Review Letters*, 18(24):1049–1051.

[3] Andraschko, F., T. Enss, and J. Sirker
2014. Purification and many-body localization in cold atomic gases. *Physical Review Letters*, 113(21):1–5.

[4] Andraschko, F. and J. Sirker
2014. Dynamical quantum phase transitions and the Loschmidt echo: A transfer matrix approach. *Physical Review B*, 89(12):125120.

[5] Aoki, H., N. Tsuji, M. Eckstein, M. Kollar, T. Oka, and P. Werner
2014. Nonequilibrium dynamical mean-field theory and its applications. *Reviews of Modern Physics*, 86(2):779–837.

[6] Avron, J. E., D. Osadchy, and R. Seiler
2003. A topological look at the Quantum Hall effect. *Physics Today*, 56(8):38–42.

[7] Bañuls, M. C., J. I. Cirac, and M. B. Hastings
2011. Strong and Weak Thermalization of Infinite Nonintegrable Quantum Systems. *Physical Review Letters*, 106(5):050405.

[8] Barmettler, P., M. Punk, V. Gritsev, E. Demler, and E. Altman
2010. Quantum quenches in the anisotropic spin-1/2-Heisenberg chain: different approaches to many-body dynamics far from equilibrium. *New Journal of Physics*, 12(12):55017–55017.

[9] Basko, D. M., I. L. Aleiner, and B. L. Altshuler
2006. Metal–insulator transition in a weakly interacting many-electron system with localized single-particle states. *Annals of Physics*, 321(5):1126–1205.

[10] Bernevig, B. A., T. L. Hughes, and S.-C. Zhang
2006. Quantum Spin Hall Effect and Topological Phase Transition in HgTe Quantum Wells. *Science*, 314(December):1757–1762.

[11] Berry, M. V.
1984. Quantal Phase Factors Accompanying Adiabatic Changes. *Proceedings of the Royal Society A: Mathematical, Physical and Engineering Sciences*, 392(1802):45–57.

[12] Bogoljubov, N. N.
1958. On a new method in the theory of superconductivity. *Il Nuovo Cimento*, 7(6):794–805.

[13] Boltzmann, L.
1877. Über die Beziehung eines allgemeine mechanischen Satzes zum zweiten Haupsatze der Wärmetheorie. *Sitzungsberichte der Akademie der Wissenschaften*, II(75):67–73.

[14] Budich, J. C. and M. Heyl
2016. Dynamical topological order parameters far from equilibrium. *Physical Review B*, 93(8):085416.

[15] Cartan, É.
1926. Sur une classe remarquable d'éspaces de Riemann, I. *Bulletin de la Société Mathématique de France*, 54:114–134.

[16] Cartan, É.
1927. Sur une classe remarquable d'éspaces de Riemann, II. *Bulletin de la Société Mathématique de France*, 54:214–216.

[17] Casini, H. and M. Huerta
2009. Entanglement entropy in free quantum field theory. *Journal of Physics A: Mathematical and Theoretical*, 42(50):504007.

[18] Chandran, A., V. Khemani, C. R. Laumann, and S. L. Sondhi
2014. Many-body localization and symmetry-protected topological order. *Physical Review B*, 89(14):144201.

[19] Chen, X., Z.-C. Gu, and X.-G. Wen
2011a. Classification of gapped symmetric phases in one-dimensional spin systems. *Physical Review B*, 83(3):035107.

[20] Chen, X., Z.-X. Liu, and X.-G. Wen
2011b. Two-dimensional symmetry-protected topological orders and their protected gapless edge excitations. *Physical Review B*, 84(23):235141.

[21] Chung, M.-C. and I. Peschel
2001. Density-matrix spectra of solvable fermionic systems. *Physical Review B*, 64(6):064412.

[22] Das, T.
2016. A pedagogic review on designing model topological insulators. *arXiv preprint*, P. 32.

[23] de Gennes, P. G.
1966. *Superconductivity of Metals and Alloys*. New York, Amsterdam: W. A. Benjamin, Inc.

[24] Demmel, J.
1990. LAPACK: a portable linear algebra library for supercomputers. In *IEEE Control Systems Society Workshop on Computer-Aided Control System Design*, Supercomputing '90, Pp. 1–7, Los Alamitos, CA, USA. IEEE.

[25] Deutsch, J. M.
1991. Quantum statistical mechanics in a closed system. *Physical Review A*, 43(4):2046–2049.

[26] Dynkin, E. B.
1947. Calculation of the coefficients in the Campbell–Hausdorff formula (Original in Russian). *Doklady Akademii Nauk SSSR*, 57:323–326.

[27] Eisert, J., M. Cramer, and M. B. Plenio
2010. Colloquium : Area laws for the entanglement entropy. *Reviews of Modern Physics*, 82(1):277–306.

[28] Eisert, J., M. Friesdorf, and C. Gogolin
2015. Quantum many-body systems out of equilibrium. *Nature Physics*, 11(2):124–130.

[29] Eisler, V.
2013. Universality in the Full Counting Statistics of Trapped Fermions. *Physical Review Letters*, 111(8):080402.

[30] Essin, A. M. and V. Gurarie
2011. Bulk-boundary correspondence of topological insulators from their respective Green's functions. *Physical Review B*, 84(12):125132.

[31] Euler, L.
1767. Récherches sur la courbure des surfaces. *Mémoires de l'academie des sciences de Berlin*, 16:119–143.

[32] Fehske, H., R. Schneider, and A. Weiße
2008. *Computational Many-Particle Physics*, volume 739 of *Lecture Notes in Physics*. Berlin, Heidelberg: Springer Berlin Heidelberg.

[33] Fidkowski, L.
2010. Entanglement Spectrum of Topological Insulators and Superconductors. *Physical Review Letters*, 104(13):130502.

[34] Fisher, M. E.
1965. The Nature of Critical Points. In *Lectures in Theoretical Physics, Vol. VIIc*, W. E. Brittin, ed. Boulder: The University of Colorado Press.

[35] Fisher, M. P. A., P. B. Weichman, G. Grinstein, and D. S. Fisher
1989. Boson localization and the superfluid-insulator transition. *Physical Review B*, 40(1):546–570.

[36] Fläschner, N., D. Vogel, M. Tarnowski, B. S. Rem, D.-S. Lühmann, M. Heyl, J. C. Budich, L. Mathey, K. Sengstock, and C. Weitenberg
2016. Observation of a dynamical topological phase transition. *arXiv preprint*, (1):1608.05616.

[37] Fließbach, T.
2010. *Statistische Physik*, 5 edition. Heidelberg: Spektrum Akademischer Verlag Heidelberg.

[38] Gaba, E.
2006. Minimal_surface_curvature_planes-en.svg.

[39] Gauss, C. F.
1900. Allgemeine Flächentheorie (Disquisitiones generales circa superficies curvas 1827). Deutsch herausgegeben von A. Wangerin. Zweite revidirte Auflage. Leipzig: Wilh. Engelmann. 64 S. (Ostwald's Klassiker No. 5) (1900).

[40] Gebert, M., H. Küttler, and P. Müller
2013. Anderson's orthogonality catastrophe. *arXiv preprint*.

[41] Gergs, N. M., L. Fritz, and D. Schuricht
2016. Topological order in the Kitaev/Majorana chain in the presence of disorder and interactions. *Physical Review B*, 93(7):075129.

[42] Goldman, N., J. Beugnon, and F. Gerbier
2012. Detecting Chiral Edge States in the Hofstadter Optical Lattice. *Physical Review Letters*, 108(25):255303.

[43] Goldman, N., J. C. Budich, and P. Zoller
2016. Topological quantum matter with ultracold gases in optical lattices. *Nature Physics*, 12(7):639–645.

[44] Greiner, M., O. Mandel, T. Esslinger, T. W. Hänsch, and I. Bloch
2002. Quantum phase transition from a superfluid to a Mott insulator in a gas of ultracold atoms. *Nature*, 415(6867):39–44.

[45] Grisins, P. and I. E. Mazets
2011. Thermalization in a one-dimensional integrable system. *Physical Review A*, 84(5):053635.

[46] Guan, X.-W., M. T. Batchelor, and C. Lee
2013. Fermi gases in one dimension: From Bethe ansatz to experiments. *Reviews of Modern Physics*, 85(4):1633–1691.

[47] Gyarmati, I.
1970. *Non-equilibrium Thermodynamics*, Ingenieurwissenschaftliche Bibliothek / Engineering Science Library. Berlin, Heidelberg: Springer Berlin Heidelberg.

[48] Haldane, F. D. M.
1988. Model for a Quantum Hall Effect without Landau Levels: Condensed-Matter Realization of the "Parity Anomaly". *Physical Review Letters*, 61(18):2015–2018.

[49] Hasan, M. Z. and C. L. Kane
2010. Colloquium : Topological insulators. *Reviews of Modern Physics*, 82(4):3045–3067.

[50] Heyl, M., A. Polkovnikov, and S. Kehrein
2013. Dynamical Quantum Phase Transitions in the Transverse-Field Ising Model. *Physical Review Letters*, 110(13):135704.

[51] Hickey, J. M., S. Genway, I. Lesanovsky, and J. P. Garrahan
2012. Time-integrated observables as order parameters for dynamical phase transitions in closed quantum systems. *Physical Review B*, 87(18):184303.

[52] Hosur, P. and X. Qi
2013. Recent developments in transport phenomena in Weyl semimetals. *Comptes Rendus Physique*, 14(9-10):857–870.

[53] Huang, Z. and A. V. Balatsky
2016. Dynamical Quantum Phase Transitions: Role of Topological Nodes in Wave Function Overlaps. *Physical Review Letters*, 117(8):086802.

[54] Ib Munk-Nielsen, M.
2014. *Geometric phases in classical mechanics*. Bachelor's thesis, University of Copenhagen.

[55] Inc., W. R.
2016. Mathematica 10.4.

[56] Jain, J. K.
1989. Composite-fermion approach for the fractional quantum Hall effect. *Physical Review Letters*, 63(2):199–202.

[57] Jänich, K.
1996. *Topologie*, Springer-Lehrbuch. Berlin, Heidelberg: Springer Berlin Heidelberg.

[58] Kane, C. L. and E. J. Mele
2005. Z2 Topological Order and the Quantum Spin Hall Effect. *Physical Review Letters*, 95(14):146802.

[59] Kilch, I.
2003. An elementary derivation of Levitov's Formula. In *Quantum Noise in mesoscopic Physics*, Y. V. Nazarov, ed., P. 397. Dordrecht: Springer Netherlands.

[60] Kitaev, A. Y.
2000. Unpaired Majorana fermions in quantum wires. *Physics-Uspekhi*, 44(10S):131–136.

[61] Klitzing, K. V., G. Dorda, and M. Pepper
1980. New Method for High-Accuracy Determination of the Fine-Structure Constant Based on Quantized Hall Resistance. *Physical Review Letters*, 45(6):494–497.

[62] Kollath, C., A. M. Läuchli, and E. Altman
2007. Quench Dynamics and Nonequilibrium Phase Diagram of the Bose-Hubbard Model. *Physical Review Letters*, 98(18):180601.

[63] König, M., H. Buhmann, L. W. Molenkamp, T. L. Hughes, C.-X. Liu, X.-L. Qi, and S.-C. Zhang
2008. The Quantum Spin Hall Effect: Theory and Experiment. *Journal of the Physical Society of Japan*, 77(3):031007.

[64] Korepin, E. V., N. N. Bogoljubov, and A. G. Izergin
1997. *Quantum inverse scattering method and correlation functions*, Cambridge Monographs on Mathematical Physics, cup edition. Cambridge University Press.

[65] Kuzemsky, a. L.
2015. Variational principle of Bogoliubov and generalized mean fields in many-particle interacting systems. *International Journal of Modern Physics B*, 29(18):1530010.

[66] Laughlin, R. B.
1981. Quantized Hall conductivity in two dimensions. *Physical Review B*, 23(10):5632–5633.

[67] Laughlin, R. B.
1983. Anomalous Quantum Hall Effect: An Incompressible Quantum Fluid with Fractionally Charged Excitations. *Physical Review Letters*, 50(18):1395–1398.

[68] Lee, T. D. and C. N. Yang
1952. Statistical Theory of Equations of State and Phase Transitions. II. Lattice Gas and Ising Model. *Physical Review*, 87(3):410–419.

[69] Leggett, A. J.
2015. The Bogoliubov–de Gennes and Andreev Equations: Andreev Reflection.

[70] Levitov, L. S., H. Lee, and G. B. Lesovik
1996. Electron counting statistics and coherent states of electric current. *Journal of Mathematical Physics*, 37(10):4845–4866.

[71] Levitov, L. S., H. Lee, and G. B. Lesovik
2003. *Quantum Noise in Mesoscopic Physics*. Dordrecht: Springer Netherlands.

[72] Li, J., R.-L. Chu, J. K. Jain, and S.-Q. Shen
2009. Topological Anderson Insulator. *Physical Review Letters*, 102(13):136806.

[73] Loschmidt, J.
1876. Über den Zustand des Wärmegleichgewichts eines Systems von Körpern mit Rücksicht auf die Schwerkraft. *Sitzungsberichte der Akademie der Wissenschaften*, II(73):128–142.

[74] Mahan, G. D.
2000. *Many-Particle Physics*, Physics of Solids and Liquids. Boston, MA: Springer US.

[75] Metzner, W., M. Salmhofer, C. Honerkamp, V. Meden, and K. Schönhammer
2012. Functional renormalization group approach to correlated fermion systems. *Reviews of Modern Physics*, 84(1):299–352.

[76] Moore, J. E.
2010. The birth of topological insulators. *Nature*, 464(7286):194–198.

[77] Mourik, V., K. Zuo, S. M. Frolov, S. R. Plissard, E. P. a. M. Bakkers, and L. P. Kouwenhoven
2012. Signatures of Majorana Fermions in Hybrid Superconductor-Semiconductor Nanowire Devices. *Science*, 336(6084):1003–1007.

[78] Muralidharan, S., K. Lochan, and S. Shankaranarayanan
2016. Generalized thermalization for integrable system under quantum quench. *arXiv preprint*.

[79] Nakata, M.
2012. The MPACK (MBLAS/MLAPACK); a multiple precision arithmetic version of BLAS and LAPACK.

[80] Pancharatnam, S.
1956. Generalized theory of interference, and its applications. *Proceedings of the Indian Academy of Sciences - Section A*, 44(5):247–262.

[81] Peschel, I.
2003. Calculation of reduced density matrices from correlation functions. *Journal of Physics A: Mathematical and General*, 36(14):L205–L208.

[82] Peschel, I. and V. Eisler
2009. Reduced density matrices and entanglement entropy in free lattice models. *Journal of Physics A: Mathematical and Theoretical*, 42(50):504003.

[83] Polkovnikov, A., K. Sengupta, A. Silva, and M. Vengalattore
2011. Colloquium : Nonequilibrium dynamics of closed interacting quantum systems. *Reviews of Modern Physics*, 83(3):863–883.

[84] Pollmann, F., S. Mukerjee, A. G. Green, and J. E. Moore
2010a. Dynamics after a sweep through a quantum critical point. *Physical Review E*, 81(2):020101.

[85] Pollmann, F., A. M. Turner, E. Berg, and M. Oshikawa
2010b. Entanglement spectrum of a topological phase in one dimension. *Physical Review B*, 81(6):064439.

[86] Qi, X.-L. and S.-C. Zhang
2010. The quantum spin Hall effect and topological insulators. *Physics Today*, 63(1):33.

[87] Qi, X.-L. and S.-C. Zhang
2011. Topological insulators and superconductors. *Reviews of Modern Physics*, 83(4):1057–1110.

[88] Rechtsman, M. C., J. M. Zeuner, Y. Plotnik, Y. Lumer, D. Podolsky, F. Dreisow, S. Nolte, M. Segev, and A. Szameit
2013. Photonic Floquet topological insulators. *Nature*, 496(7444):196–200.

[89] Remmert, R. and G. Schuhmacher
2007. *Funktionentheorie 2*, Springer-Lehrbuch, 3 edition. Berlin, Heidelberg: Springer Berlin Heidelberg.

[90] Rigol, M., V. Dunjko, and M. Olshanii
2008. Thermalization and its mechanism for generic isolated quantum systems. *Nature*, 452(7189):854–858.

[91] Rigol, M., V. Dunjko, V. Yurovsky, and M. Olshanii
2007. Relaxation in a Completely Integrable Many-Body Quantum System: An Ab Initio Study of the Dynamics of the Highly Excited States of 1D Lattice Hard-Core Bosons. *Physical Review Letters*, 98(5):050405.

[92] Rossini, D., T. Calarco, V. Giovannetti, S. Montangero, and R. Fazio
2006. Decoherence induced by interacting quantum spin baths. *Physical Review A - Atomic, Molecular, and Optical Physics*, 75(3):1–16.

[93] Ryu, S., A. P. Schnyder, A. Furusaki, and A. W. W. Ludwig
2010. Topological insulators and superconductors: tenfold way and dimensional hierarchy. *New Journal of Physics*, 12(6):065010.

[94] Schnyder, A. P., S. Ryu, A. Furusaki, and A. W. W. Ludwig
2008. Classification of topological insulators and superconductors in three spatial dimensions. *Physical Review B*, 78(19):195125.

[95] Schwabl, F.
2006. *Statistische Mechanik*, Springer-Lehrbuch. Berlin/Heidelberg: Springer-Verlag.

[96] Sedlmayr, N.
2016. Dynamical phase transitions in topological insulators and superconductors. *Unpublished*.

[97] Sharma, S., U. Divakaran, A. Polkovnikov, and A. Dutta
2016. Slow quenches in a quantum Ising chain; dynamical phase transitions and topology. *Physical Review B*, 93(14):144306.

[98] Simon, B.
2010. *Trace Ideals and Their Applications*, volume 120 of *Mathematical Surveys and Monographs*. Providence, Rhode Island: American Mathematical Society.

[99] Sirker, J., M. Maiti, N. P. Konstantinidis, and N. Sedlmayr
2014. Boundary Fidelity and Entanglement in the symmetry protected topological phase of the SSH model. *Journal of Statistical Mechanics: Theory and Experiment*, 2014(10):P10032.

[100] Sirker, J., R. G. Pereira, and I. Affleck
2011. Conservation laws, integrability, and transport in one-dimensional quantum systems. *Physical Review B - Condensed Matter and Materials Physics*, 83(3):1–22.

[101] Su, W. P., J. R. Schrieffer, and A. J. Heeger
1979. Solitons in Polyacetylene. *Physical Review Letters*, 42(25):1698–1701.

[102] The Royal Swedish Accademy of Sciences
2016. Topological Phase Transitions and Topological Phases of Matter. Technical report, The Royal Swedish Accademy of Sciences, Stockholm.

[103] Thouless, D. J., M. Kohmoto, M. P. Nightingale, and M. den Nijs
1982. Quantized Hall Conductance in a Two-Dimensional Periodic Potential. *Physical Review Letters*, 49(6):405–408.

[104] Trotzky, S., Y.-A. Chen, A. Flesch, I. P. McCulloch, U. Schollwöck, J. Eisert, and I. Bloch
2012. Probing the relaxation towards equilibrium in an isolated strongly correlated one-dimensional Bose gas. *Nature Physics*, 8(4):325–330.

[105] Tsui, D. C., H. L. Stormer, and A. C. Gossard
1982. Two-dimensional magnetotransport in the extreme quantum limit. *Physical Review Letters*, 48(22):1559–1562.

[106] Vajna, S. and B. Dóra
2014a. Disentangling dynamical phase transitions from equilibrium phase transitions. *Physical Review B*, 89(16):161105.

[107] Vajna, S. and B. Dóra
2014b. Supplementary material for "Disentangling dynamical phase transitions from equilibrium phase transitions".

[108] Vajna, S. and B. Dóra
2015. Topological classification of dynamical phase transitions. *Physical Review B*, 91(15):155127.

[109] Vodola, D., L. Lepori, E. Ercolessi, A. V. Gorshkov, and G. Pupillo
2014. Kitaev Chains with Long-Range Pairing. *Physical Review Letters*, 113(15):156402.

[110] von Klitzing, K.
1986. The quantized Hall effect. *Reviews of Modern Physics*, 58(3):519–531.

[111] Wilson, K. G.
1971a. Renormalization Group and Critical Phenomena. I. Renormalization Group and the Kadanoff Scaling Picture. *Physical Review B*, 4(9):3174–3183.

[112] Wilson, K. G.
1971b. Renormalization Group and Critical Phenomena. II. Phase-Space Cell Analysis of Critical Behavior. *Physical Review B*, 4(9):3184–3205.

[113] Wisniacki, A.
2012. Loschmidt echo. *Scholarpedia*, 7(8):11687.

[114] Xia, Y., D. Qian, D. Hsieh, L. Wray, A. Pal, H. Lin, A. Bansil, D. Grauer, Y. S. Hor, R. J. Cava, and M. Z. Hasan
2009. Observation of a large-gap topological-insulator class with a single Dirac cone on the surface. *Nat Phys*, 5(6):398–402.

[115] Xu, S.-Y., I. Belopolski, N. Alidoust, M. Neupane, G. Bian, C. Zhang, R. Sankar, G. Chang, Z. Yuan, C.-C. Lee, S.-M. Huang, H. Zheng, J. Ma, D. S. Sanchez, B. Wang, A. Bansil, F. Chou, P. P. Shibayev, H. Lin, S. Jia, and M. Z. Hasan
2015. Discovery of a Weyl fermion semimetal and topological Fermi arcs. *Science*, 349(6248):613–617.

[116] Zhang, H., C.-X. Liu, X.-L. Qi, X. Dai, Z. Fang, and S.-C. Zhang
2009. Topological insulators in Bi2Se3, Bi2Te3 and Sb2Te3 with a single Dirac cone on the surface. *Nat Phys*, 5(6):438–442.

[117] Zhao, E., N. Bray-Ali, C. J. Williams, I. B. Spielman, and I. I. Satija
2011. Chern numbers hiding in time-of-flight images. *Physical Review A*, 84(6):063629.

[118] Zhao, Y., F. Andraschko, and J. Sirker
2016. Entanglement entropy of disordered quantum chains following a global quench. *Physical Review B*, 93(20):205146.